The role of microtubule plus-end binding protein TACC3 during axon outgrowth and guidance:

Author: Burcu Erdogan

The role of microtubule plus-end binding protein TACC3 during axon outgrowth and guidance

Burcu Erdogan

A dissertation submitted to the
Faculty of the Department of Biology
in partial fulfillment of the requirement for the degree of
Doctor of Philosophy

Boston College
Morrissey College of Arts and Science
Graduate School

June 2019

THE ROLE OF MICROTUBULE PLUS-END BINDING PROTEIN TACC3 DURING AXON OUTGROWTH AND GUIDANCE

Burcu Erdogan

Advisor: Laura Anne Lowery, PhD

Abstract

Axon guidance is a critical process in forming the connections between a neuron and its target. Development of a properly functioning nervous system relies heavily on how accurately an axon is guided to the right target. Defects in the guidance machinery may result in neurological disorders. The growth cone that is formed at the tip of a growing axon is responsible for navigating axons to their final targets. The growth cone steers the growing axon towards the appropriate direction by integrating extracellular guidance cues received by membrane-associated receptors at the growth cone periphery. Upon receiving guidance cues, a number of intracellular signal transduction pathways are initiated downstream of the guidance receptors, that can promote or halt growth cone advance. The growth cone generates these responses by remodeling its cytoskeletal components, which are actin network in the periphery and microtubules in the growth cone center.

In this thesis, we focus on understanding the role of microtubule dynamics regulation within the growth cone as it makes guidance decisions. Specifically, we examine the role of TACC3 as a microtubule plus-end binding protein during axon outgrowth and guidance. We show that TACC3 localizes at microtubule plus-ends in embryonic *Xenopus laevis* growth cones and regulates microtubule growth parameters. We also show that TACC3 is important for promoting axon outgrowth in cultured neural tube explants. Furthermore, our data suggests that TACC3 affects axon guidance *in vivo* and *ex vivo*.

Examination of embryos depleted of TACC3 revealed guidance defects in the spinal cord neurons, while TACC3-overexpressing cultured spinal neurons showed increased resistance to Slit2-induced growth cone collapse. Finally, in an attempt to delineate the mechanism behind TACC3-mediated axon guidance under Slit2, we studied the importance of tyrosine phosphorylation induced by Abelson tyrosine kinase. We find that retaining phosphorylatable tyrosines within the TACC domain is important for its microtubule plus-end tracking behavior and its impact on microtubule dynamics regulation, axon outgrowth and guidance. Together, this thesis contributes new insights to the understanding of the role of TACC3 as a microtubule plus-end binding protein and identifies TACC3 as a potential regulator of axon outgrowth and guidance during *Xenopus laevis* embryonic development.

Acknowledgements

This thesis would not have been completed without the help and support of many individuals. I would like to thank everyone who has helped me along the way.

First and foremost, I would like to express my deepest gratitude to my advisor Laura Anne Lowery. There was not a single day that I don't think how lucky and grateful I am for being able to work with the most amazing advisor that I could imagine. You were not only an advisor but also a friend and one of the biggest supporters of me in both my scientific and personal life. You have never stopped supporting and believing in me even in moments that I doubted myself. It was your endless and unconditional love, trust and encouragement that made me able to see the light at the end of the tunnel today. I will always be your "B-2".

I would like to thank my PhD committee chair Dr. Eric Folker for giving me the chance to do one of my rotations in his lab and image for long hours in the freezing microscope room and for serving on my committee for all these years. You have always stimulated me with your questions to make me think more critically about my work. As a graduate student who has come from where academic hierarchy is deeply felt and endorsed, I will never forget the email you sent me to address you by your first name instead of "Dr. Folker" which I appreciated in terms of the equality you try to create.

I would like to thank Dr. Sarah McMenamin for agreeing to serve on my committee right as she joined the department. Thank you for all the valuable discussions and questions you proposed during my committee meetings. Finally, thank you both for always being so flexible and understanding with arranging our meetings.

I would like to thank my readers Dr. Bryan Ballif and Dr. Alicia Ebert from University of Vermont. To Dr. Ballif, thank you for agreeing to read my thesis and also for coming and talking

to me at my first NESDB conference, which was my first scientific networking experience. This was the conference which also planted the seeds of our collaboration and led to the creation of the work mentioned in Chapter 4 of this thesis. To Dr. Alicia Ebert, thank you for agreeing to take the time to read my thesis and coming all the way from Vermont.

To the legendary past and present members of Lowery Lab; Sangmook, Paula, Micaela, Garrett and Beth. I couldn't survive without your endless and unconditional support you provided me. We laughed, danced and ran together. We suffered the annoying beeping sound of micromanipulators, cursed together clogged needles with morpholinos or to the embryos that did not fertilize or western blots that didn't show a band or did show a band. We reminded each other that "We Can Do It" and we can do it together. It was your immediate support I felt nearby every single day. You all were beyond just being a lab mate; you were my second family. I couldn't have come this far without your support. Thank you so much for everything.

I would also like to thank the Biology Office, Peter Marino, Dina Goodfriend, Colette McLaughlin, and Diane Butera. From the very first day I started at BC, they have been a tremendous help with everything to make sure we do not deal with anything else other than our research. Thank you so much for solving every little and big problem and making our lives much easier.

I would also like to thank Prof. Larry Benowitz from Boston Children's Hospital whom I worked with as an intern when I first moved to Boston. It was the initial support and opportunity he gave me that led me to open this chapter of my life in Boston.

Speaking of opening a new chapter, Zeynep deserves the biggest shout out. Zeynep, I will never forget the time you came to pick me up from the airport, brought me home and made me some Turkish tea. Although I was super excited for coming to the heart of science, I was quite

nervous leaving home too, but you made me feel at home from the very first second you opened your doors. It was your encouragement that made me stay in Boston and work in Laura Anne's lab. You always tried to show me the best way and presented me the best options by sharing your experiences. Thank you for your patience with me and for your never-ending support.

To my ageless gypsy Ayca Teyze, thank you for making me a member of your family. You always lifted up my soul with your laughter along with a large coffee filled all the way to the top and a Napoleon. Keep your doors open and Napoleon ready, this journey hasn't ended.

To my friends I left in Turkey, you have been always with me during this journey. I grew up with you and I carry a piece from every single one of you and those pieces kept me together during the hardest times. Thank you for staying up all night and spending that one day I could see you every summer. I love you all so much and cannot wait to see you again in two weeks.

Here comes the man, to my biggest supporter for 14 years, ever since we loaded a gel together. He is the one who relentlessly and tirelessly listens to my complaints on my rides back home, who tells me that everything is going to be alright, who reminds me that I can do it and it is ok if I can't. Ugur, you are my best friend and we have a long way to run and ride together. Looking forward to the new adventures awaiting us.

Finally, I would like to express my deepest gratitude to my family who have supported me constantly with every single step I take in my life. It has been challenging all these years to be separated but you have never stopped supporting my decisions and have encouraged me to pursue the path I choose. Looks like we will have more skype dates for a little while longer.

Table of Contents

List of Figures

Chapter 1

Introduction

Part of the content in this chapter was adapted from:

Bearce E.A., Erdogan B., Lowery L.A. TIPsy tour guides: how microtubule plus-end tracking proteins (+TIPs) facilitate axon guidance
Front Cell Neurosci. 2015 30:9:241

Erdogan B., Ebbert P.T., Lowery L.A. Using *Xenopus laevis* retinal and spinal neurons to study mechanisms of axon guidance *in vivo* and *in vitro. Semin. Cell Dev. Biol.* 2016 51:61-72

1.1 Axon guidance is critical during embryonic nervous system development

The neuron is one of the most fundamental working units of the brain and the nervous system. Neurons connect one another and other cells in the body to relay information necessary for normal functioning of the brain and the body. The connection between a neuron and its targets is made via projections called axons. During embryonic development, neurons extend their axons in search of their targets. Connecting to the right target requires accurate navigation of growing axons. During its navigation, growing axons are guided by cues presented to them by the environment they travel through. These guidance molecules can act either as attractive or repellent, depending on the developmental time and the space at which the axon travels. Furthermore, it is the integration and correct interpretation of these guidance signals that directs the growing axon towards the right direction.

Since the time Cajal first proposed the chemotrophic effectors of axon guidance, efforts have been put towards identification of these chemotropic cues (Dickson, 2002; Huber et al., 2003). With the advent of high-resolution imaging techniques, we now investigate the interaction between these extracellular guidance signals, their receivers on the cell surface, and intracellular downstream response generators. The growth cone is the main subject for studying how extracellular cues are received and translated to direct axon growth to the right direction.

During embryonic development, problems may emerge due to mutations in genes involved in axon guidance. These mutations may perturb navigation of axons to their targets which may result in defects in neuronal connections and ultimately cause the development of neurological disorders. Therefore, understanding how axons are correctly navigated to their targets is of critical importance.

1.2 The growth cone navigates the growing the axon to its target

The growth cone is a specialized structure that is formed at the growing end of an axon during nervous system development. Its highly dynamic and motile nature gives the growth cone the ability to continuously probe the extracellular terrain in search for guidance signals. It is the growth cone that interacts with these signals via the receptors that reside at the growth cone periphery and directs the growing axon into certain directions as it grows (Kolodkin and Tessier-Lavigne, 2011). Interpretation and translation of these signals into movement is generated by reorganization of the cytoskeletal components within the growth cone (Fig. 1.1).

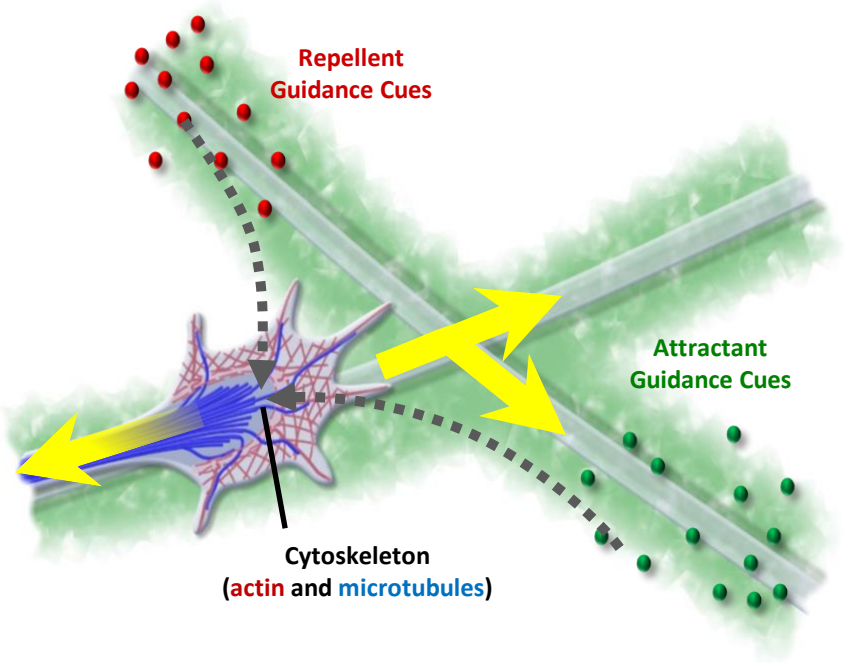

Figure 1.1 The growth cone responds to guidance signals as it navigates the growing axon

The two major cytoskeletal components of the growth cone are the actin network in the growth cone periphery and microtubules positioned majorly at the central domain. It is the communication and cooperation between these two cytoskeletal polymers that determine growth cone's movement decision (Dent et al., 2011; Lowery and Van Vactor, 2009).

1.3 The growth cone cytoskeleton is important for growth cone motility

1.3.1 Actin dynamics in growth cone motility

The growth cone peripheral domain is composed of two distinct actin-rich architectures: a sheet-like veil called lamellipodia and thin finger-like extensions called filopodia (Fig. 1.2).

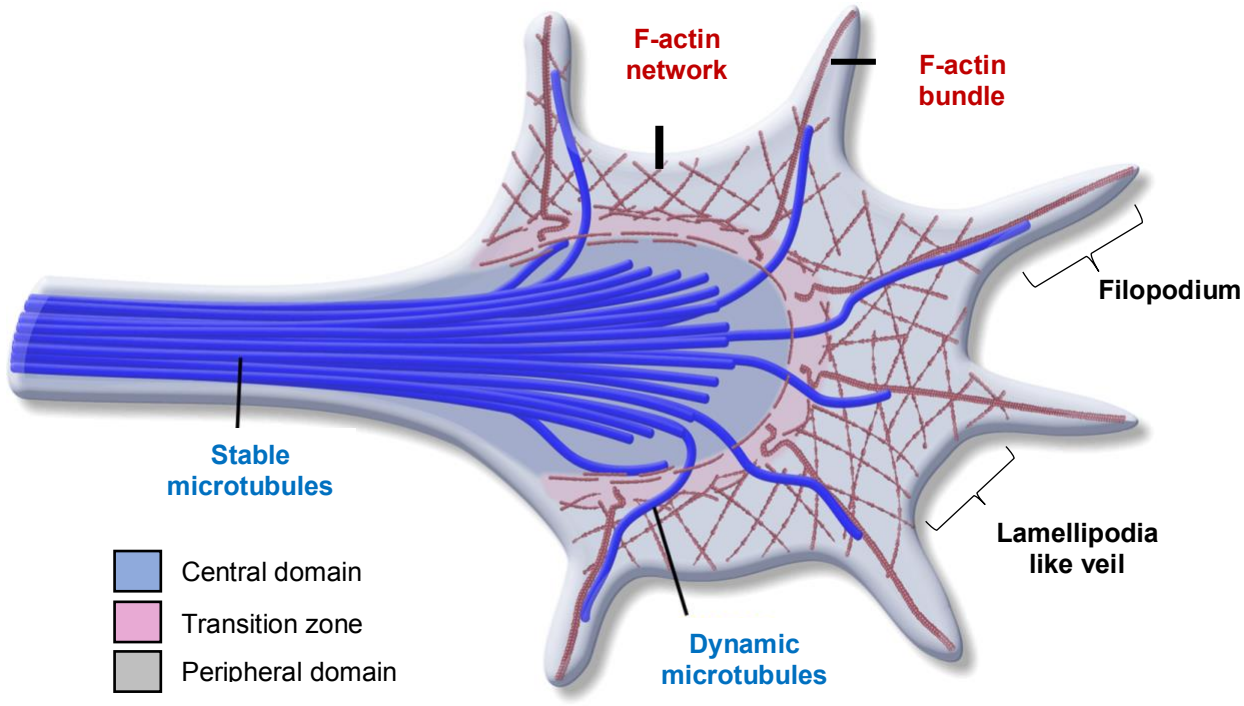

Figure 1.2 Cartoon showing the cytoskeletal organization within the growth cone

The growth cone is divided into 3 domains; the central domain is dominated by stable microtubules (blue rods); the transition zone, where actin arcs are located, forms a barrier between the central domain and actin (red rods) rich peripheral domain. The actin cytoskeleton in the periphery forms a branched network in the lamellipodia-like veil and bundles in the finger-like protrusions called filopodia (image courtesy of Laura Anne Lowery)

The veil-like lamellipodia is composed of branched filamentous actin (F-actin) networks while finger-like filopodia are invaded by parallel F-actin bundles (Fig.1.2). Filopodia act as guidance sensors as the growth cone navigates through the environment. The interaction between the extracellular environment and filopodia is crucial to determine the direction of growth cone movement (Kerstein et al., 2015; Myers et al., 2011). The forward movement of the growth cone

relies on membrane protrusion mediated by pushing forces generated by actin polymerization (Gomez and Letourneau, 2014). In the growth cone, actin polymerization happens at the actin plus ends (or barbed ends) which point toward the growth cone periphery, while depolymerization happens at the minus ends that point toward the transition zone (Fig.1.2). Dissociated actin monomers at the transition zone can be transported back to the leading edge at the peripheral domain to sustain actin filament polymerization (Zicha et al., 2003) (Fig. 1.3.A).

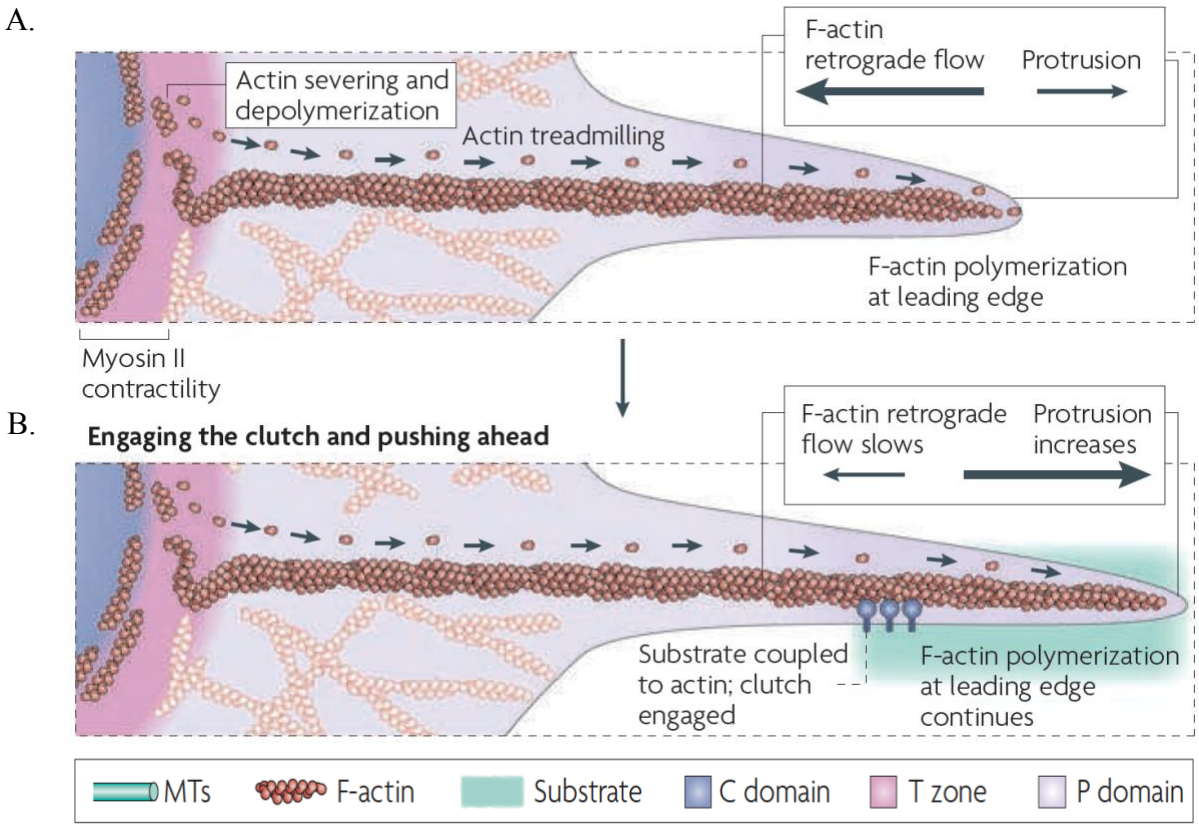

Figure 1.3 Actin dynamics in the growth cone filopodia

Actin dynamics within the filopodia regulates growth cone motility and advance. **(A)** Filopodia protrusion is mediated by actin polymerization. Actin monomers generated upon actin severing and depolymerization at the transition zone are transported back to leading edge to sustain actin polymerization. **(B)** F-actin bundles experience retrograde flow generated by pulling forces applied by myosin II at the transition zone. Adhesions made by integrin receptors with the underlying extracellular matrix form "molecular clutches" which link F-actin bundles to integrin and attenuates retrograde flow. Filopodia extension depends on the difference between actin polymerization and retrograde flow rates (image, Lowery and Van Vactor, 2009).

While the balance between actin assembly and disassembly is important, forces that mediate membrane protrusions for the growth cone to advance are not limited to the actin assembly rate. Actin filaments in the growth cone periphery are subjected to pulling forces, called F-actin retrograde flow (Forscher and Smith, 1988), generated by myosin-II motor proteins (Lin et al., 1996; Medeiros et al., 2006) (Fig. 1.3.B). Therefore, growth cone advance happens when actin polymerization exceeds the rate of both actin depolymerization and retrograde flow, while membrane retraction occurs when the rate of polymerization fails to exceed these forces.

Myosin-II generated actin retrograde flow can be interfered by coupling actin bundles to the underlying substrate via adhesion receptors, which is a phenomenon called the "molecular clutch" (Fig 1.3.B) (Mitchison and Kirschner, 1988). Clutching actin bundles to the underlying substrate via receptors happens at sites of adhesions, also known as point contacts (in growth cones), made between receptors and the extracellular matrix (ECM). Engagement of receptors with the underlying substrate initiates assembly of point contacts by recruiting adaptor and signaling proteins (Kerstein et al., 2015; Myers et al., 2011). The assembly and disassembly rates and the number of these point contacts determines the strength of the clutch and therefore the rate of retrograde flow and ultimately growth cone advance or retraction (Kerstein et al., 2015).

Point contact formation and turnover are modulated based on the surface that the growth cone interacts with, which underlies the mechanism of directed growth cone motility. While permissive surfaces promote point contact formation, non-permissive surfaces will not favor adhesion (Robles and Gomez, 2006), which will result in reduced "molecular clutch" formation and an increased rate of F-actin retrograde flow that, altogether, will halt growth cone advance and enforce the growth cone to steer away from that non-permissive environment.

The actin network plays an essential role in the regulation of growth cone steering events in response to extracellular cues. Early studies have shown that while impairing actin polymerization can retain neurite extension (Marsh and Letourneau, 1984), loss of filopodia due to actin cytoskeleton disruption induced by a low concentration of cytochalasin-B treatment (which only causes loss of F-actin in the filopodia) perturbs growth cone steering in response to guidance cues (Bentley and Toroian-Raymond, 1986; Zheng et al., 1996). Although the presence of filopodia is important for the growth cone to respond to guidance cues, what generates growth cone steering is the asymmetric modulation of filopodial dynamics that is essential to determine the direction of movement.

1.3.2 Microtubule dynamics in growth cone motility

While actin indeed plays an important role in regulating growth cone motility, it is actually the crosstalk between the actin and microtubules that intricately regulates growth cone motility and steering in response to extracellular stimuli.

Microtubules in the growth cone are positioned in two distinct domains; a relatively stable subset of microtubules, positioned at the growth cone central domain, and a highly dynamic subset that extends into the growth cone periphery. While the centrally positioned microtubules are majorly responsible for consolidation of growth cone advance to promote axon extension, microtubules that invade the growth cone periphery participate in growth cone directional movement by interacting with guidance signal machinery together with actin (Lowery and Van Vactor, 2009). Microtubules that extend into the growth cone peripheral domain are highly dynamic. They alternate between polymerization and depolymerization phases, a process that is known as “dynamic instability” (Mitchison and Kirschner, 1984).

The dynamicity of these microtubules is essential to maintain neurite extension and selection of the direction of growth (Tanaka et al., 1995). Rapid transition between growth and shrinkage is key to microtubules' explorative behavior within the growth cone periphery. With this dynamic nature, they can modulate their growth behavior spatiotemporally depending on the extracellular stimuli that the growth cone is exposed.

The spatiotemporal organization of peripheral dynamic microtubules within the growth cone is important for the distribution of signals carried by microtubules too. For example, microtubule-based anterograde transport of vesicle associated membrane protein2 (VAMP2) has been implicated to be important for steering the growth cone towards attractant cues. Several cytoskeletal components, such as actin, tubulin, RAC1, CDC42 and Arp2/3, have been identified to associate with VAMP2- positive vesicles, suggesting that the selected delivery of these cytoskeleton-associated proteins can promote cytoskeletal polymerization on one side of the growth cone, thereby inducing growth cone advance or steering. Not only do these vesicles contribute to the transport of cytoskeletal elements, but they also contribute to membrane remodeling. VAMP-2 dependent exocytosis facilitates the expansion of the growth cone plasma membrane which is necessary for protrusion activity. Moreover, receptors, such as integrin, that are carried within the vesicles, will be incorporated into the membrane, which will be followed by activation of focal adhesion kinases and modulation of the adhesion dynamics between the extracellular matrix and the growth cone. This will eventually contribute to clutch formation and attenuation of actin retrograde flow to promote growth cone advance. (Tojima et al., 2011)

The spatiotemporal organization of dynamic microtubules within the growth cone periphery is essential for creation of this asymmetry, and a crosstalk between microtubules and actin is required to achieve this regulation.

1.3.3 Microtubule – actin interaction is important for growth cone motility

As individual dynamic microtubules extend into the growth cone periphery, they often follow the F-actin bundle tracks (Challacombe et al., 1996). The extension of microtubules into the growth cone periphery, however, does not *depend* on the F-actin bundles as microtubules can still extend into the periphery when peripheral actin is abolished with low levels of actin depolymerizing drugs. However, presence of F-actin is essential to ensure a more organized distribution of microtubules (Burnette et al., 2007; Schaefer et al., 2002; Zhou et al., 2002). While F-actin tracks guide growing microtubules into the growth cone periphery, the extent of their interaction may differentially regulate microtubule advance (Challacombe et al., 1996). Microtubules follow F-actin tracks by transiently coupling to them, which is mediated by microtubule-actin crosslinking proteins (Cammarata et al., 2016). While this coupling can guide microtubule growth, it can also constrain microtubules from extending further due to the retrograde flow that actin filaments are subjected to (Schaefer et al., 2002; Schaefer et al., 2008). As it was discussed in the previous section, retrograde flow is attenuated at adhesion sites due to the molecular clutch formed between the F-actin bundles and the receptors that are tethered to extracellular matrix (Suter and Forscher, 1998; Suter and Forscher, 2000). Adhesions made on the side of cues that are translated as attractant will be stronger, and they will be weaker at sites where signals are read as repellent. This bias will affect actin polymerization dynamics and hence microtubule distribution, accordingly (Schaefer et al., 2008; Suter and Forscher, 2000). Net actin growth will be favored at sites of attractant signals, which will also facilitate microtubule invasion to those sites, for signal exchange necessary to modulate adhesion dynamics and initiate growth cone advance or steering towards that direction. From this perspective, it sounds as if F-actin dynamics determine the direction of movement, while microtubules play a supporting role by

following actin bundles to further consolidate the movement. However, there are studies showing that microtubules can also play an instructive role in determining the direction of movement.

Studies have shown that global perturbation of microtubule dynamicity with microtubule specific drugs can abolish growth cone directionality (Tanaka et al., 1995) or steering away from the repellent substrate border (Challacombe et al., 1997; Tanaka and Kirschner, 1995). Additionally, other studies have shown that attractive or repulsive turning can be induced by modulating microtubule stability locally on one side of the growth cone with low levels of taxol or nocodazole application, respectively (Buck and Zheng, 2002). Although these studies show that microtubules can be more than a supporting element and actually instruct growth cone directionality, they do not rule out the involvement of actin. Perturbing actin polymerization with low levels of cytochalasin D (20nM) abolishes growth cone turning induced with local taxol (5μM) application, suggesting that microtubule-initiated growth cone turning requires actin polymerization in the growth cone periphery (Buck and Zheng, 2002). These cytoskeletal drug experiments indicate that an interplay between the actin cytoskeleton and microtubules is essential for the directional movement of the growth cone, and generation of directionality requires the involvement of dynamic microtubules specifically.

These observations bring the question of how the interplay between actin cytoskeleton and microtubules is coordinated, and what are the regulators of microtubule dynamics that mediate asymmetric distribution and regulation of microtubule dynamics to control growth cone directional movement. Microtubule-associated proteins are key factors in regulating microtubule dynamic behavior as well as mediating interaction between microtubules and actin cytoskeleton, and the next section will explore the function of these proteins.

1.3.2.1 Microtubule plus-end tracking proteins regulate microtubule dynamics

Microtubules are polar structures with their relatively more dynamic ends are oriented towards the growth cone periphery. This more dynamic end is called the "plus-end" and it is the site where microtubules undergo frequent cycles of growth, shrinkage and pausing also known as "dynamic instability" (Mitchison and Kirschner, 1984). Among many microtubule-associated proteins (MAPs) that can regulate microtubule behaviors, one group of proteins come to the forefront for their role in regulating microtubule plus-end dynamics, due to their localization to these dynamically unstable plus-ends (Akhmanova and Hoogenraad, 2005; Akhmanova and Steinmetz, 2008). These plus-end tracking proteins (+TIPs) can interact with microtubules as well as with each other, creating a hub at the microtubule plus-end to control microtubule dynamic behavior and microtubule interaction with other cellular components such as actin (Cammarata et al., 2016). +TIPs can be divided into distinct groups based on the way that they interact with microtubules and the structural domain that they possess (Akhmanova and Steinmetz, 2010).

While some +TIPs are capable of binding to microtubules autonomously, some tracks plus-ends non-autonomously. The majority of non-autonomous plus-end tracking proteins utilize end-binding (EB) plus-end proteins to track the microtubule ends. EB protein family members are able to track microtubule plus-ends autonomously and they function as scaffolding proteins by interacting with many +TIPs that possess SxIP (serine/threonine- any amino acid -isoleucine-proline) or CAP-Gly (cytoskeletal associated protein glycine rich domain) binding motifs. +TIPs that do not possess any of these EB binding motifs often track plus-ends autonomously via different mechanisms (Akhmanova and Hoogenraad, 2005). Additionally, some +TIPs only bind to growing MT ends like EB proteins (Maurer et al., 2012), while some can bind both polymerizing and depolymerizing MT ends, such as the microtubule polymerase, XMAP215 (Brouhard et al.,

2008). This preference likely arises due to recognition of different structural features that are exposed as microtubules grow or shrink.

In addition to accumulating at the distal plus-end (in a 0.5 – 2μm range), some +TIPs can also bind microtubules outside of that region, which is called "lattice binding". In some cases, switching between plus-end binding and lattice binding depends upon post-translational modifications such as phosphorylation. This change in localization on microtubules could be promoted in different subcellular compartments due to distinct signaling events that the cell experiences. This could also influence the distribution and the function of that +TIP in conjunction with microtubule dynamics regulation in these specific regions of the cell.

A good example of such differential regulation comes from studies on CLASP (cytoplasmic linker associated protein). In epithelial cells, while CLASP localizes at the microtubule plus-ends in the cell body, its affinity is shifted toward the microtubule lattice in the leading edge, which is shown to be reduced upon phosphorylation by GSK3 kinase (Wittmann and Waterman-Storer, 2005). Although phosphorylation-dependent CLASP localization does not change microtubule growth, this phosphorylation-dependent local modulation has been shown to play a role in stabilization and attachment of MTs to the cell cortex as well as in the regulation of focal adhesion dynamics (Kumar et al., 2009).

These studies emphasize the importance of the regulation of +TIP – microtubule association under signals to control microtubule behavior in a spatially restricted manner to polarize the distribution and the function of the microtubules in order to mediate directed cell movement. As discussed earlier, such asymmetric regulations of microtubule dynamics mediated by +TIPs become particularly important for growth cones to determine their direction of movement

as they encounter guidance signals. In fact, many +TIPs have been studied for their potential role in mediating such responses during axon guidance (Bearce et al., 2015).

1.3.2.2 Microtubule plus-end binding proteins during axon growth and guidance

Microtubules within the growth cone are oriented with their plus-ends pointing towards the growth cone periphery. Due to their localization at microtubule distal ends, +TIPs bear a great potential in receiving guidance signals downstream of guidance receptors that reside at the growth cone periphery. As discussed earlier, guidance signals may not be homogenously presented to the growth cone, and the growth cone might need to process multiple signals at the same time which necessitates asymmetric reorganization of cytoskeletal polymers.

Similar to cells, differential regulation of microtubule dynamics induced by phosphorylation-dependent CLASP localization has been studied in growth cones too. Hur et al. showed that, while the lattice binding activity of CLASP, induced by inhibition of GSK3 kinase, perturbs microtubule extension into the growth cone periphery and impairs axon outgrowth, plus-end binding is favored by moderate phosphorylation and supports axon outgrowth by stabilizing microtubules (Hur et al., 2011). This phosphorylation-dependent microtubule interaction and resulting microtubule stability come in handy to generate the response to guidance signals. For example, GSK3 has been shown to be inhibited by Slit2 repellent cue-induced phosphorylation in dorsal root ganglion neurons, which results in perturbation of axon growth (Byun et al., 2012). Combining the findings from these studies, one can hypothesize that when a growth cone receives Slit2 signal on one side, GSK3 activity will be reduced, leading to CLASP localization along the microtubule lattice, which will impede microtubule extension into the growth cone periphery, while on the other side of the growth cone (where there is no Slit2 signal), microtubules will be freely extending into the growth cone periphery to promote extension toward that direction.

A similar hypothesis was drawn between CLASP and Abelson tyrosine kinase under the Slit2 pathway by Lee et al. A genetic screen performed in *Drosophila* identified Orbit/*mast* (the Drosophila ortholog of CLASP) as a genetic interactor of Abelson tyrosine kinase, and loss-of-function mutants of CLASP and Abelson demonstrated similar midline crossing defects (Lee et al., 2004). Like CLASP, other microtubule plus-end binding proteins have been implicated to be involved in axon outgrowth and guidance regulation by exerting various impacts on microtubule dynamics regulation. For example, local accumulation and localization of APC to microtubules on permissive substrate contact sites was suggested to be important for growth cone steering (Koester et al., 2007). This could be achieved by an increase in microtubule stability, as binding of APC to microtubules has been shown to enhance microtubule stability, which is judged by the maintenance of the number and the length of the microtubules despite the presence of nocodazole, a microtubule depolymerizing agent (Zumbrunn et al., 2001). Moreover, similar to CLASP, binding of APC is shown to be controlled by its phosphorylation status. Axon elongation induced by NGF appears to be mediated by inactivation of GSK3 activity, which results in increased APC-microtubule association, due to reduced APC phosphorylation (Zhou et al., 2004).

In addition to CLASP and APC, other +TIPs have also been implicated in various functions involved in growth cone steering events. For example, $p150^{Glued}$ has been shown to be involved in membrane trafficking (Valetti et al., 1999; Watson and Stephens, 2006) and CLIP-170 has been implicated in endosome motility (Pierre et al., 1992), which suggest a role for them in local membrane remodeling that is essential for membrane protrusion and hence growth cone advance.

Localization of +TIPs spatially and selectively in response to guidance signals is therefore important for asymmetric modulation of microtubule dynamics, thus distributing signals that would remodel the cytoskeleton and determine the direction of movement. However, microtubules

cannot act alone. An interaction between microtubules and actin is essential for that asymmetric distribution (Dent et al., 1999; Schaefer et al., 2002; Zhou et al., 2002) and for local modulation of microtubule dynamics to fine tune the growth cone's directional movement. +TIPs in that sense can mediate the necessary communication between the two polymers. In fact, there are some +TIPs that have been identified to serve as microtubule – actin crosslinkers to mediate this interaction (Cammarata et al., 2016), and a well-studied microtubule polymerase XMAP215 has recently been shown to be one of them and is of particular interest to the focus of this thesis (Slater et al., 2019).

1.3.2.2.1 *Xenopus* microtubule associated protein - 215 (XMAP215)

XMAP215 is the frog orthologue of human ch-TOG (colonic and hepatic tumor-overexpressed gene, also known as CKAP5) and was first identified as a microtubule growth promoting factor from *in vitro* studies performed with *Xenopus* egg extracts (Gard and Kirschner, 1987). Subsequent studies performed by reconstituting physiological microtubule dynamics using purified tubulin and XMAP215 identified this protein as a processive microtubule polymerase, meaning that it catalyzes addition of tubulin dimers to the growing microtubule plus-end (Brouhard et al., 2008).

XMAP215, unlike the majority of other +TIPs, can autonomously track microtubule plus-ends and bind to the outermost distal plus-ends; hence, its accumulation precedes the EB1 comet. In addition to its distinct plus-end localization, XMAP215 can also be seen along microtubule lattice at low levels. While 5 TOG domains positioned at the N-terminus are responsible for its plus-end tracking, the C-terminus mediates its lattice binding. XMAP215/ch-TOG family is present in every eukaryotic organism investigated (Gard et al., 2004) and its absence or reduction perturbs microtubule dynamics and morphology significantly in various cellular events, ranging

from shorter or disorganized mitotic spindle formation to reduced microtubule growth rates (Kinoshita et al., 2002).

More recently, growth cone specific functions for XMAP215 have been identified (Lowery et al., 2013). Manipulation of XMAP215 levels in *Xenopus laevis* embryonic spinal neuron cultures identified that XMAP215 knockdown (KD) impairs normal axon growth length. Since microtubule growth is essential for growth cone motility and advance, formation of shorter axons as a result of reduced levels of a microtubule growth promoting factor thereby is not surprising. However, high resolution live imaging of ectopically-expressed EB1-GFP in *Xenopus laevis* embryonic growth cones identified that XMAP215 KD leads to faster moving EB1-GFP comets. It was proposed that this enhanced EB1-GFP comet velocity could be due to increased microtubule translocation in the anterograde direction, which could arise due to more frequent transient decoupling from actin filaments' retrograde flow. As discussed earlier, actin filament coupling can guide growing microtubules and align their growth along a linear trajectory. However, in XMAP215 KD growth cones, there appeared to be multiple non-colinear trajectories, suggesting an increase microtubule decoupling from actin filaments. These observations were later supported by more recent findings by Slater et al (Slater et al., 2019). Sedimentation assays with purified F-actin and XMAP215 identified a direct interaction between actin and XMAP215. Moreover, super resolution imaging of microtubule and F-actin organization within the growth cone identified that XMAP215 KD leads to more random distribution of microtubules within the growth cone periphery, which led to a reduction in microtubule penetration into the peripheral domain and, ultimately, in reduction of microtubule penetration into filopodia, all of which might be occurring as a result of reduced microtubule/ F-actin coupling (Slater et al., 2019).

+TIP localization, confined to a very narrow region at the microtubule plus-ends, creates a protein hub which promotes interaction among these proteins and their participation in similar cellular processes. While work from Lowery *et al* and Slater *et al* are the first to propose a specific growth cone function for XMAP215, it may not be surprising to see the involvement of this protein in the regulation of microtubule dynamics within the growth cone. CLASP, which was identified to interact with the *Drosophila* ortholog of XMAP215, has also been shown to be involved in regulating microtubule behavior within the growth cone (Lowery et al., 2013). Another candidate that is worth exploring in that regard is TACC3, which was extensively studied for its interaction with XMAP215 in non-neuronal systems and has been shown to have great influence on XMAP215's function. Studies performed in *Drosophila* embryos showed that presence of D-TACC (the fly orthologue of TACC3) is important for efficient localization of Msps (the fly orthologue of XMAP215) to centrosomes and spindle microtubules, which also correlated with the number and the length of the microtubules that formed as a result (Lee et al., 2001). This was not the only study showing the close interaction between these two proteins. There were others reporting similar observations in various organisms, which suggests that the interaction is conserved throughout evolution (Peset and Vernos, 2008). These observations therefore suggested a potential function for TACC3 as a microtubule plus-end tracking protein and begged the question to explore its potential role within the growth cone.

1.3.2.2.2 Could TACC3 be a microtubule plus-end binding protein?

TACC3 is a member of the transforming acidic coiled-coil (TACC) protein family, named for their highly acidic composition and also the coiled-coil domain at their C-terminus (known as the TACC domain). TACC3 is present in organisms ranging from yeast to mammals and shows sequence similarity particularly in their highly conserved 200 amino acid-long TACC domain,

which has shown to be important for its centrosome localization (Bellanger and Gonczy, 2003; Gergely et al., 2000a; Lee et al., 2001; Srayko et al., 2003)

Studies regarding TACC3 and its impact on microtubule regulation were initially characterized during cell division (Gergely et al., 2000b; Peset et al., 2005). It has been shown that reducing levels of TACC3 results in formation of shorter spindle microtubules in worms (Bellanger and Gonczy, 2003; Le Bot et al., 2003; Srayko et al., 2003), destabilization of spindle microtubule in flies (Gergely et al., 2000b), and reduction in number and length of astral MTs in *Xenopus* egg extracts (Kinoshita et al., 2005; O'Brien et al., 2005; Peset et al., 2005), while its over expression results in longer spindle microtubules (Gergely et al., 2000a; Peset et al., 2005). The impact of TACC3 on microtubule stability, number and length have long been attributed to its interaction with XMAP215 (*Xenopus laevis* ortholog of human ch-TOG), a well characterized microtubule polymerase (Brouhard et al., 2008) discussed in the previous section. The major function of TACC3 had been proposed to bring XMAP215 to the centrosomes and also increase its affinity for microtubules (Kinoshita et al., 2005). XMAP215, as a microtubule polymerase, exerts its impact mainly on microtubule plus-ends and the TACC3/XMAP215 complex was proposed to indirectly increase the stability of microtubule plus-ends (Barros et al., 2005; Lee et al., 2001; Srayko et al., 2003). Therefore, it is intriguing to investigate whether TACC3 interacts with XMAP215 directly at microtubule plus-ends.

In fact, live imaging of D-TACC during cell division performed in *Drosophila* embryos had demonstrated small dots emerging from the centrosome (Lee et al., 2001). This further raised the possibility that TACC3 could track microtubule plus-ends, which is one of the questions that is aimed to be explored in this thesis. Additionally, the majority of the studies which looked at TACC3's function in regulation of microtubules have been performed in dividing cells. However,

microtubules play critical roles in other cellular processes by providing structural support or functioning as a railway for cellular trafficking, all of which are important for polarization or migration of cells or, in our case, growth cone motility. The possibility of TACC3 being involved in regulation of microtubules in the growth cone becomes an important question in regards to its enriched expression in developing nervous system (Tessmar et al., 2002) and its role implied in neuronal differentiation (Sadek et al., 2003) and maintenance of neural progenitor pools (Xie et al., 2007; Yang et al., 2012). Moreover, a growth cone function of its close interactor XMAP215 has been identified in embryonic spinal cord neuron cultures isolated from *Xenopus laevis* (Lowery et al., 2013; Slater et al., 2019), further raising the interest in exploring TACC3's function on microtubules in contexts other than during cell division. To explore the interaction of TACC3 with microtubules within the growth cone, we use *Xenopus laevis* as a model organism.

1.4 Xenopus laevis as a model organism to study axon growth and guidance

The complexity of neuronal networks has been a long-standing puzzle that has challenged scientists for centuries. Unveiling how this complex wiring is established in the mammalian brain has, in large part, relied on examination of simpler organisms with comparatively less intricate networks. For example, Ramón y Cajal's work on the chick brain produced the first description of the growth cone and Harrison's work with frogs established for us the first neuronal culture (Harrison, 1959). Furthermore, Sperry's pivotal experiment on frog retinal neuron regeneration explained the chemo-specificity of connections (Sperry, 1963), which has been refined by further studies in systems such as *Xenopus* (Fraser and Hunt, 1980).

Xenopus as a whole offers an advantageous complementary vertebrate model, with a multitude of benefits. First of all, recently sequenced genomic data from *Xenopus* shows high similarity with the human genome (Hellsten et al., 2010). There are several species of the *Xenopus*

genus, but two have become increasingly popular in research. The diploid western-clawed *Xenopus tropicalis* offers advantages in genomic studies due to its smaller genome. On the other hand, despite its large allotetraploid genome and longer maturation time, the African clawed frog *Xenopus laevis* provides numerous advantages which make it a gold standard for studying axon guidance in development.

The use of *Xenopus laevis* in axon guidance research is advantageous for multiple reasons. Frog husbandry is relatively straightforward, and female frogs can be easily stimulated to produce eggs by simply injecting chorionic gonadotropin hormone. Eggs are comparatively large in diameter, 1-2 mm, and are produced in large quantities. Fertilization occurs *ex utero* and provides the opportunity to track and manipulate embryonic development at desired stages. Furthermore, embryos can tolerate extensive surgical manipulations varying from microinjection to cell and tissue transplantation. Based upon the given developmental stage and the known fate map of *Xenopus laevis,* it is possible to target specific cell types. For instance, microinjecting mRNA at stages as early as the 1-4 cell stage results in global alteration of gene levels. Alternatively, injecting embryos at later stages, for example 16-64 cell, allows the restriction of gene manipulations to a more specific tissue (Moody, 1987a; Moody, 1987b).

Compared to other systems, *Xenopus laevis* neurons can be simply isolated and maintained at room temperature, permitting easy manipulation of live neurons as high resolution images are acquired, forgoing the need for strict incubation conditions such as those provided by CO_2 imaging chamber (Lowery et al., 2012) (Fig. 1.4). The primary benefit of *Xenopus laevis* for these studies, however, is its large growth cones, which can be up to 10 to 30 microns in diameter and are perfect for clear and detailed analysis of subcellular cytoskeletal structures and dynamics. There may be

no other vertebrate model system with growth cones as large and as easy to culture, manipulate, and image as *Xenopus laevis*.

Delivery of molecules such as DNA, mRNA, antibodies, or fluorescent dextrans to modify expression of a particular gene or label a specific tissue is available via approaches such as microinjection or electroporation (Bestman et al., 2006; Eide et al., 2000; Haas et al., 2002). Genetic knockdown can be achieved via a variety of methods, the most common of which has been microinjection of antisense morpholino (MO) oligonucleotides. With the use of standard controls (Eisen and Smith, 2008), MOs are advantageous tools to manipulate gene products (Blum et al., 2015) and have been widely used for *Xenopus* gene knockdown since 2000 (Heasman et al., 2000).

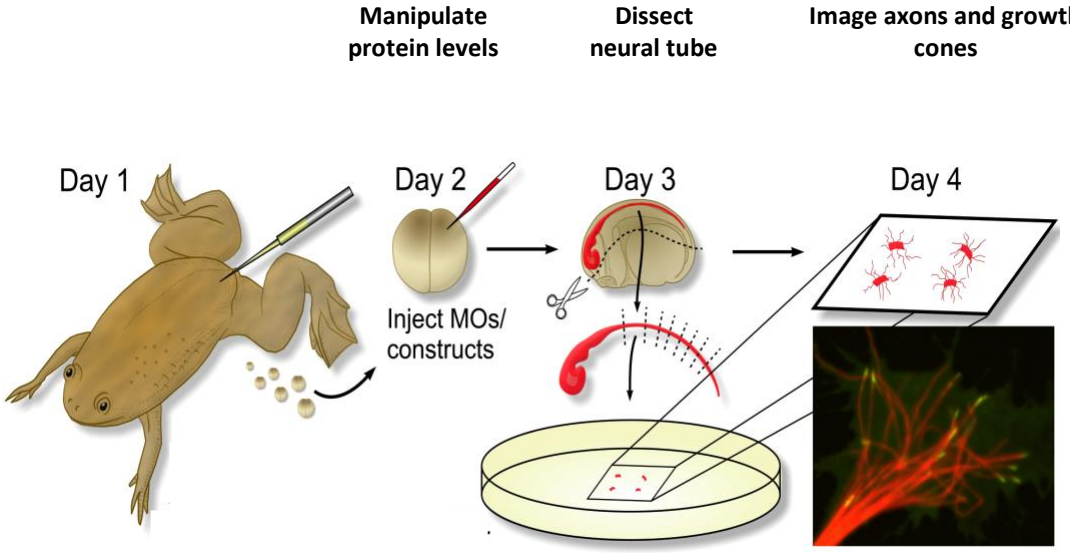

Figure 1.4 *Xenopus laevis* neural tube dissection and cytoskeletal imaging in the growth cone

(Day 1) Female frogs are injected with chorionic gonadotropin (CG) 12-18 h before egg collection. Eggs are collected and maintained in a salt solution and fertilized with minced testes. Owing to its *ex utero* development, Nieuwkoop and Faber (NF) based developmental stages can be tracked as the development proceeds at room temperature and manipulation of protein levels can be performed at desired stages. (Day 2) Morpholinos (MO; antisense oligonucleotide) for knock-down strategies and/or mRNA of protein of interest can be injected as early as 2-cell stage. (Day 3) Neural tube can be dissected the next day at stage20. Cultured explants can be kept at room temperature on bench. (Day 4) Cytoskeletal dynamics imaging can be performed the next day (adapted from Lowery et al., 2012)

In addition to microinjection, electroporation allows manipulation of genes in later stage tissue and can be advantageous over other delivery methods. For instance, if the molecule of interest takes part in neuronal development as well as earlier stages of embryonic development, manipulation of its levels at blastomeric stages may result in lethality or embryonic abnormalities. Therefore, the cell autonomous role of a particular protein during axon guidance is better examined if its function or level is manipulated at stages 20-40 when axonogenesis and brain wiring are still in progress (Falk et al., 2007).

With respect to axon guidance studies, the developing *Xenopus* nervous system provides a valuable working space. In particular, retinal and spinal neurons have been extensively used to decipher aspects of axon guidance machinery. Modern approaches have been developed for both systems to monitor mechanisms of axon guidance *in vitro* and *in vivo*.

Xenopus spinal neurons have been central to the examination of the interaction between extracellular guidance cues (Ming et al., 2002), their receptors (Hong et al., 1999; Stein and Tessier-Lavigne, 2001) and cytoplasmic secondary signals (Ming et al., 1997; Song et al., 1998; Song et al., 1997) in growth cone turning events. Axon guidance mechanisms that operate during development can be studied in vitro with cultured spinal neurons prepared at the time (stage 20) that the neural tube closes and axon outgrowth just begins. Modulation of intracellular signals, extracellular matrix and adhesion dynamics and cytoskeletal arrangements during axon guidance can be studied with isolated and cultured spinal neurons.

1.4.1 *Xenopus laevis* growth cones to assess cytoskeletal rearrangements during guidance

Examination of the growth cone in detail is difficult in an intact tissue, as it travels in a 3D environment, and this makes it challenging to track the moving growth cone without losing focus of its cytoskeletal features. Although recently developed imaging approaches have begun to make

in vivo growth cone cytoskeleton examination possible (Kleele et al., 2014), most of our knowledge on the structural organization of the growth cone comes from *in vitro* studies (Schaefer et al., 2002; Tanaka and Kirschner, 1991). In this regard, with their large growth cones, *Xenopus laevis* neurons provide an ideal system to study cytoskeletal dynamics. With the advance of protein labeling and high-resolution imaging techniques, it is possible to track fluorescently tagged proteins to gain insights into the motility dynamics of the growth cone during axon growth and guidance.

Tracking labeled microtubules revealed, for example, that spatial stabilization of microtubules via FLIP-released taxol can mediate growth cone turning (Buck and Zheng, 2002). Thus, mechanisms that promote microtubule growth have gained further attention. Microtubule binding proteins, particularly plus-end tracking proteins (+TIPs), have become a focus of study as they directly regulate microtubule plus-end dynamics (Akhmanova and Steinmetz, 2008), and tracking and quantitative analysis of fluorescently-tagged +TIPs in cultured *Xenopus* growth cones has provided new insights into how microtubule dynamics are regulated in the growth cone (Lowery et al., 2013; Nwagbara et al., 2014). Furthermore, acquisition of high-resolution live images of fluorescently-labeled known +TIPs, such as EB1, in cultured *Xenopus* growth cones can be used to measure parameters of microtubule growth dynamics *ex vivo* (Stepanova et al., 2003). There is open-source software, such as *plusTipTracker*, available for automated detection and analysis of these tagged +TIPs (Applegate et al., 2011; Stout et al., 2014) (Fig. 1.5). Additionally, tools such as quantitative fluorescent speckle microscopy (QFSM) or kymography are also commonly used to extract quantitative information regarding cytoskeletal dynamics from high-resolution microscopy images of growth cones.

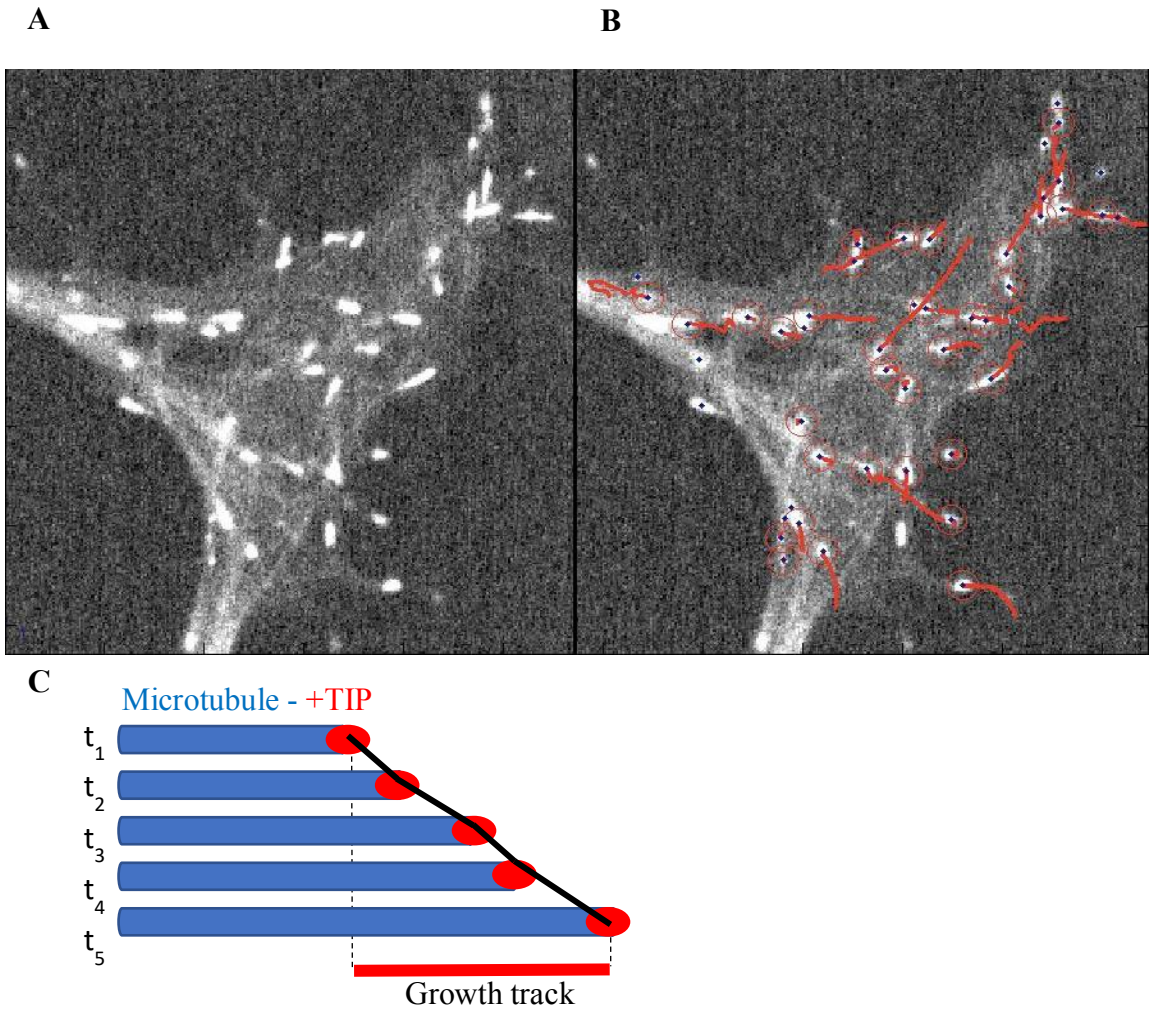

Figure 1.5 *plusTipTracker* is used to assess microtubule dynamics within the growth cone

(A) Still image of a growth cone expressing fluorescently labelled +TIP end-binding 1 (EB1) protein to mark growing microtubule ends. (B) Same growth cone shown in A is analyzed with plusTipTracker software. Red lines showing microtubule growth tracks generated over 1 min long time lapse recording with 2 sec intervals. (C) Cartoon depicting tracking system employed by plusTipTracker. Growth track is generated by tracking microtubule over time.

.

1.5 Remaining questions

Although TACC3 and its misexpression has been a subject for studies focusing on cell division, due to its involvement in tumor progression, its role outside of cell division remained largely unexplored. Considering the characterization of growth cone-specific function of its well - studied partner XMAP215, it is intriguing to test whether TACC3 could also regulate microtubule behavior within the growth cone.

Therefore, this work aims to address an unexplored function for TACC3 by first characterizing its interaction with microtubules in vertebrate neuronal growth cones and investigating its growth cone-specific function during *Xenopus laevis* nervous system development.

This thesis starts with characterization of TACC3 as a microtubule plus-end binding protein within the embryonic neuronal growth cones and explores its impact on microtubule growth dynamics and axon elongation as a microtubule plus-ends binding protein (Chapter 2). In the next chapter, we further investigate the mechanism by which TACC3 regulates axon outgrowth and ask whether it is involved in regulation of axon guidance during embryonic development (Chapter 3). In the last chapter, we test whether TACC3 could be a potential target for kinase signals downstream of axon guidance cues. We ask whether its phosphorylation status would alter its binding capacity to microtubules, thereby affecting its impact on regulation of axon outgrowth and guidance (Chapter4).

Chapter 2:

TACC3 is a microtubule plus-end tracking protein that promotes axon elongation and also regulates microtubule plus-end dynamics in multiple embryonic cell types

The content in this chapter was adapted from:

Nwagbara B.U., Faris A.E., Bearce E.A., Erdogan B., Ebbert P.T., Evans M.F., Rutherford E.L., Enzenbacher T.B., Lowery L.A. TACC3 is a microtubule plus-end tracking protein that promotes axon elongation and also regulates microtubule plus-end dynamics in multiple embryonic cell types. *Mol. Biol. Cell*, 2014, 25(21):3350-3362

2.1 Introduction

Microtubule (MT) plus-end dynamics are regulated by a conserved family of proteins called 'plus-end-tracking proteins' (+TIPs) (Akhmanova and Steinmetz, 2008). The regulation of MT plus-end dynamics by +TIPs is critical to multiple aspects of embryonic development, including within the neuronal growth cone during axon outgrowth (Lowery and Van Vactor, 2009; Tanaka et al., 1995). Despite their importance, few studies have examined how +TIPs affect MT dynamics in vertebrate growth cones (e.g. (Lowery et al., 2013; Marx et al., 2013; van der Vaart et al., 2012). Additionally, it remains unclear how the multitude of +TIPs interact with MTs and each other to control MT behaviors in these and other embryonic cell types.

The centrosome-associated protein TACC3, a member of the transforming acidic coiled coil (TACC) domain family, is strongly implicated in regulating MT stability during mitosis (Gergely et al., 2000a; Peset and Vernos, 2008). TACC3 was first identified as a MT-binding protein after immunostaining demonstrated its colocalization with MTs on centrosomes and mitotic spindles (Groisman et al., 2000). Reports have shown that reducing levels of TACC3 leads to shorter astral and spindle MTs in worms (Bellanger and Gonczy, 2003; Le Bot et al., 2003; Srayko et al., 2003), flies (Gergely et al., 2000b), and vertebrate cells (Kinoshita et al., 2005; O'Brien et al., 2005; Peset et al., 2005), while over-expressing TACC3 leads to longer spindle MTs (Gergely et al., 2000a; Peset et al., 2005). As a result of these studies, TACC3 has been called a MT growth-promoting or stabilizing factor, at least in the context of MTs during mitosis (Gergely et al., 2000a; Peset and Vernos, 2008).

Yet, an unanswered question in the TACC3 field is how a protein that is primarily localized to the centrosome can have such a strong effect on MT length. It has been suggested that a primary function of TACC3 is to recruit the microtubule polymerase, XMAP215, to the centrosome (Peset

and Vernos, 2008). The interaction between TACC3 and XMAP215 has been well-documented in multiple systems (Kinoshita et al., 2005; Lee et al., 2001; O'Brien et al., 2005; Peset et al., 2005), where it is apparent that TACC3 localizes XMAP215 to the centrosome, and that normal mitotic spindle assembly requires their interaction. However, despite the well-known localization of XMAP215 at growing MT plus-ends (Brouhard et al., 2008), it has remained unclear whether vertebrate TACC3 interacts with XMAP215 specifically at plus-ends during interphase.

There has been some evidence that TACC proteins, in other systems, may bind to and regulate the plus-ends of MTs (Peset and Vernos, 2008). While the single TACC ortholog in *Drosophila* (called D-TACC) is highly concentrated at centrosomes *in vivo* (Gergely et al., 2000b), green fluorescent protein (GFP)-tagged D-TACC was also observable as small puncta that emanate from the centrosome, likely corresponding to growing MT plus-ends (Lee et al., 2001). Furthermore, knockdown of D-TACC results in reductions in MT growth parameters in cultured fly cells, and *d-tacc* genetically interacts with the +TIP, *CLASP*, during the development of normal fly eye morphology (Long et al., 2013). However, time-lapse imaging of fluorescently-tagged TACC3 has not yet been examined in any vertebrate context, which would be necessary to determine if TACC3 does, indeed, track MT plus-ends. Additionally, the mechanism by which vertebrate TACC3 regulates MT plus-end dynamics is not known.

In addition to a general cellular role in the regulation of MT dynamics, there are also indications that TACC3 may play a specific role during neuronal development. TACC3 upregulation occurs when PC12 cells are in the process of differentiating into neurons (Sadek et al., 2003), and TACC3 is also involved in the maintenance of the neural progenitor pool during neocortical development (Xie et al., 2007; Yang et al., 2012). Moreover, *Xenopus* TACC3 expression is enriched in the developing embryonic nervous system (Tessmar et al., 2002).

However, a definite role for TACC3 within the embryonic neuronal growth cone during axonal outgrowth has not yet been elucidated.

In this chapter, we begin to investigate the potential function of TACC3 within the vertebrate developing nervous system by analyzing axon outgrowth parameters of cultured embryonic *Xenopus laevis* neurons after TACC3 manipulation. Additionally, we utilize live imaging of +TIP and MT behaviors in order to explore the effects of TACC3 manipulation on MT plus-end dynamics within living growth cones as well as within other embryonic cell types. Finally, we examine the interaction of TACC3 with XMAP215, on the plus-ends of MTs in interphase embryonic cells. These analyses highlight new insights into the function of TACC3 and how it regulates MT plus-end dynamics.

2.2 Results

2.2.1 TACC3 protein is expressed within embryonic neuronal growth cones and promotes axon outgrowth

We first performed immunostaining of fixed cultured embryonic neural crest cells and neuronal growth cones, using an antibody specific to *Xenopus laevis* TACC3. Within neural crest cells, we observed punctate staining throughout the entire cell (Fig. 2.1 A-C), as well as staining at the centrosome (Fig. 2.1 A'-C'), consistent with previous reports of TACC3 localization (Gergely et al., 2000b; Groisman et al., 2000). We also observed strong labeling within axons and growth cones (Fig. 2.1 D-F), which has not been previously reported, and we confirmed TACC3 presence in neural tissue by Western blot of axon lysates (not shown). These results suggest that TACC3 may play a role within the growth cone during axon outgrowth.

To investigate whether TACC3 functions during axonal development, we examined the extent of axon outgrowth of cultured neurons following manipulation of TACC3 levels. An

antisense morpholino oligonucleotide (MO) directed against the TACC3 start site inhibited TACC3 expression (Fig. 2.1 G) and reduced both axonal number and axonal length (Fig. 2.1 H-K). TACC3 over-expression (OE) did not affect axonal number but did result in significant increase in axonal length (Fig. 2.1 L-P). Thus, our findings suggest that TACC3 may play a critical role during embryonic nervous system development and indicate that normal levels of TACC3 are required for proper axonal outgrowth.

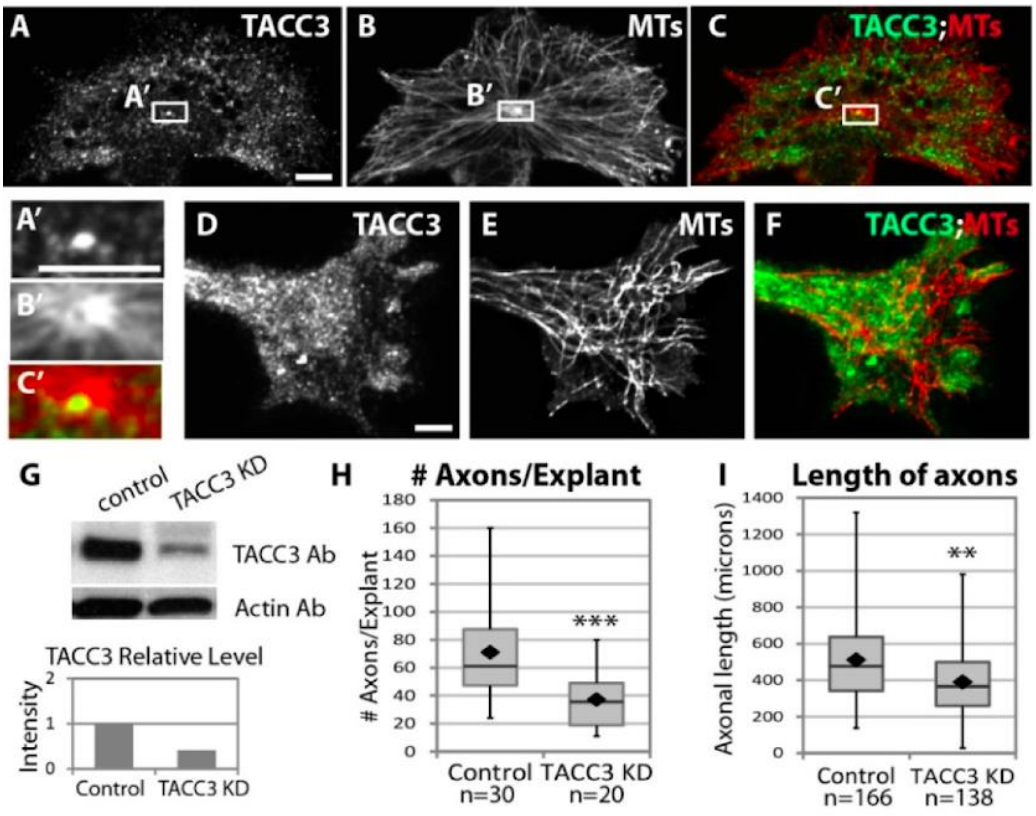

Figure 2.1 TACC3 is expressed within the embryonic cells and neuronal growth cones and promotes axon outgrowth

(A-F) Immunostaining with antibodies to TACC3 (A) and tubulin (B) showing localization of TACC3 as a punctate in cultured embryonic neural crest cells (note that TACC3 is enriched at the centrosome (C, A'-C')) and in growth cones (D-F). Scale bar, 5 µm. (G) Western blot showing that a morpholino (MO) targeted against TACC3 results in 50% knockdown (KD) by 2 days post fertilization. (H) The numbers of axons per neural tube explant were counted from a total of three independent experiments. (I) Axon outgrowth length was measured in cultured control and TACC3 KD explants after 24h conditions. (J-K) Representative phase contrast microscopy images of axons from control and TACC3 KD.

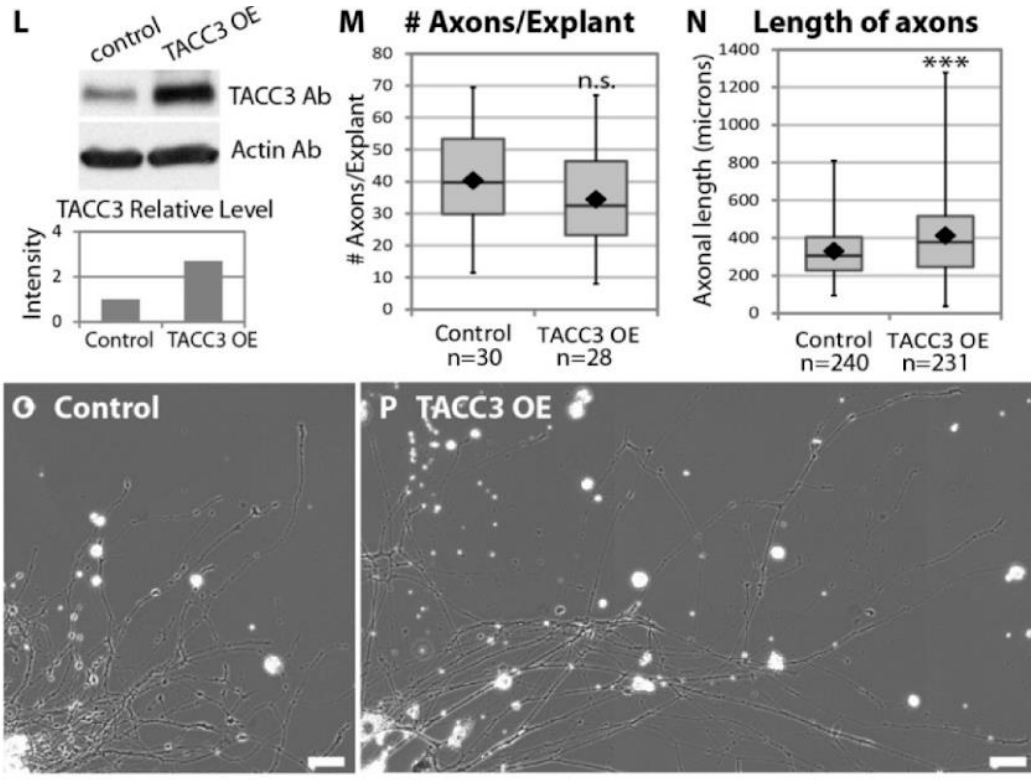

Figure 2.1 (contn'd) (L) Western blot showing that TACC3 levels are increased (overexpressed, OE) 2 days after injecting embryos with TACC3 mRNA. Quantification represents this blot, however, similar results were obtained with over 10 individual Western blots (not shown). Note that the TACC3 blot in L was exposed for a shorter amount of time than the one in G, which explains the fainter control band in L. (M-N) Axon outgrowth parameters after 18 hours in culture were quantified in control and TACC3 OE conditions. (O-P) Representative phase contrast microscopy images of axons from control and TACC3 OE. Box-and-whisker plots indicate the mean (diamond), median, extrema and quartiles. An unpaired t-test was performed to assess significance between conditions. **$p<0.01$, ***$p<0.001$. n.s. not significant. Bar is 50 μm for (J-K, O-P).

2.2.2 TACC3 regulates MT plus-end dynamics in growth cones and other cell types

Axon outgrowth is, in large part, regulated by MT dynamics within the neuronal growth cone, which is the dynamic structure at the tip of the growing axon (Lowery and Van Vactor, 2009; Tanaka et al., 1995). Thus, we sought to examine whether MT plus-end dynamics were specifically disrupted within growth cones after TACC3 manipulation. To test this, we acquired high-resolution live images of tagged EB1, which binds all growing MT plus-ends (Stepanova et al., 2003), and we then quantified parameters of MT polymerization dynamics using the Matlab-

based open-source software plusTipTracker (Applegate et al., 2011). This software program has been previously validated for accurate tracking of EB1-GFP comets in *Xenopus* laevis growth cones, using identical imaging conditions to those used in this current study (Stout et al 2014). EB1-GFP comet number and morphology were similar in control, TACC3 KD, and TACC3 OE growth cones (Fig. 2.2 A-C, Supplemental Movie 1). However, compared to controls, EB1-GFP comet velocity was reduced by 11% upon TACC3 KD, and increased by 11% upon TACC3 OE (Fig. 2.2 D). MT growth track lifetime (which measures the number of seconds of MT polymerization in a given growth track before pausing or catastrophe) was not affected by TACC3 manipulation (Fig. 2.2 E). Conversely, MT growth track length (which measures the distance of persistent MT polymerization growth before pausing or catastrophe) was significantly decreased in KD and increased in OE. TACC3 KD led to a 14% reduction in MT growth track length, while TACC3 OE led to an 18% increase in MT growth track length (Fig. 2.2 F). To summarize, although the time persistence of MT polymerization is independent of TACC3, the velocity and length of MT forward progression trend with the level of TACC3, suggesting that TACC3 promotes more efficient MT polymerization.

To determine if TACC3 regulation of MT dynamics is specific to neuronal growth cones, we also examined the effect of TACC3 manipulation in cultured embryonic neural crest cells. In these cells, we saw a similar effect to that which occurred within growth cones. There were reductions in MT growth velocity and length with TACC3 KD and increases in velocity and length with TACC3 OE (Fig. 2.2 G, I), while there was no effect on MT growth lifetime (Fig. 2.2 H). Altogether, our results demonstrate that TACC3 regulates MT plus-end dynamics in motile vertebrate interphase cells.

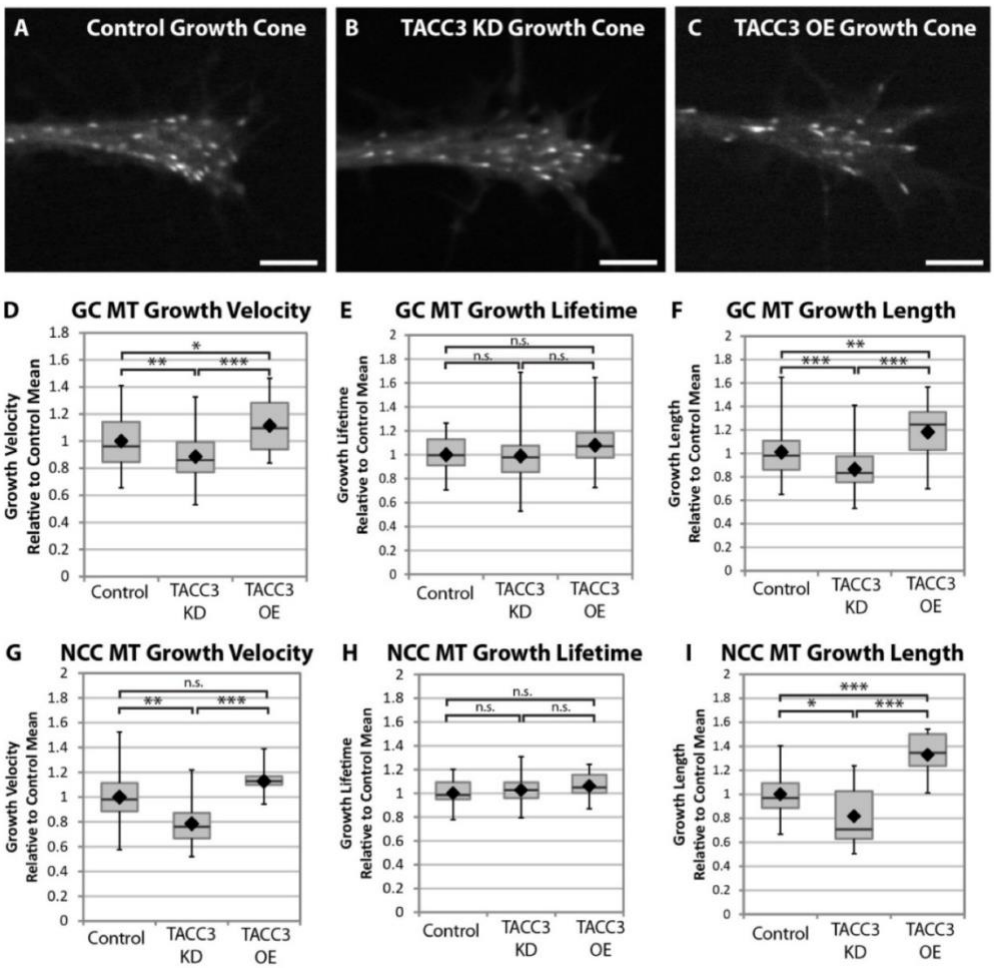

Figure 2.2- TACC3 regulates MT dynamics in *Xenopus laevis* growth cones and neural crest cells
(A-C) Representative micrographs of EB1-GFP comets in control (A), TACC3 KD (B), and TACC3 OE (C) conditions. See Figure 2 Movies 1-4. Bar is 5 µm. (D-F) Quantification of MT growth track parameters in cultured embryonic neuronal growth cones (GC) after TACC3 manipulation. EB1-GFP localizes to the ends of growing MTs and is thus a marker for MT polymerization. Automated tracking of EB1-GFP comets calculate MT growth track velocity (D), MT growth track lifetime (E) and MT growth track length (F). Examples of actual mean values for a single experiment: GC MT velocity - control 6.4 µm/min, TACC3 KD 5.7 µm/min, TACC3 OE 7.1 µm/min; GC MT lifetime - control 12.6 sec, KD 13.3 sec, OE 14.1 sec; GC MT length - control 1.4 µm, KD 1.3 µm, OE 1.7 µm; NCC MT velocity - control 7.5 µm/min, KD 6.0 µm/min, OE 8.5 µm/min; NCC MT lifetime - control 11.4 sec, KD 13.0 sec, OE 12.1 sec; NCC MT length - control 1.3 µm, KD 1.3 µm, OE 1.8 µm. For each independent experiment (six were performed in total), measurements of MT parameters were normalized to their respective experimental control means, due to the significant day-to-day fluctuations in control MT dynamics (in part, due to room temperature changes). Control data represents the means of 44 growth cones, representing a total of 1228 analyzed tracks; TACC3 KD represents 49 growth cones with 964 tracks; TACC3 OE represents 24 growth cones with 524 tracks. (G-I) Quantification of MT growth track parameters in cultured embryonic neural crest cells. Control data represents the means of 20 neural crest cells, representing a total of 2876 analyzed tracks; TACC3 KD represents 13 cells with 1313 tracks; TACC3 OE represents 10 cells with 1386 tracks. Box-and-whisker plots indicate the mean (diamond), median, extrema and quartiles. An unpaired t-test was performed to assess significance between conditions. *$p<0.05$, **$p<0.01$, ***$p<0.001$. ns not significant.

2.2.3 TACC3 can act as a +TIP in neuronal growth cones and other primary embryonic cell types

In order to gain further insight into how TACC3 mechanistically affects MT plus-end behaviors, we examined the sub-cellular dynamics of TACC3 within living embryonic cells. Thus, we tagged full-length TACC3 with GFP and examined its localization within both growth cones and neural crest cells (Fig. 2.3 A-C, G-I, Supplemental movies 2-4).

GFP-tagged TACC3 strongly localized to the growing plus-ends of MTs in both cell types (Fig. 2.3 A-C, G-I). In growth cones, the mean length of the GFP-TACC3 plus-end accumulation was approximately 0.70 μm (Fig. 2.3 D-E, data measured from 70 MTs). GFP-TACC3 was primarily detected on MT plus-ends that either appeared to be advancing forward or paused, with 100% of growing MTs displaying detectable GFP-TACC3 plus-end localization (Fig. 2.3F). 77% of paused MTs still showed GFP-TACC3 localization, while 25% of shrinking MTs also had observable GFP-TACC3 localization. These observations were similar in neural crest cells, although the GFP-TACC3 comets were shorter, with a mean length of 0.53 μm (Fig. 2.3J-K, data measured from 64 MTs). GFP-TACC3 accumulation was detectable on 100% of growing MTs, 69% of paused MTs, and 25% of shrinking MTs (Fig. 2.3L). Thus, we find that GFP-TACC3 robustly tracks plus-ends of MTs in vertebrate growth cones and neural crest cells.

Plus-end tracking of GFP-TACC3 was not restricted to neural-derived cells, as fibroblasts isolated from mesodermal somite tissue also showed clear plus-end tracking (Fig. 2.4A-C, Supplemental Movie 5-6). We additionally observed, on several occasions, that shrinking MTs paused concurrently with obvious accumulation of GFP-TACC3 (Fig. 2.4D). This was most apparent in the mesodermal and neural crest cells, as these had greater numbers of MTs to examine.

The plot profiles and distribution of GFP-TACC3 on MT plus-ends in fibroblasts was similar to that of the neural cell types, with mean length of GFP-TACC3 plus-end accumulation being 0.67 μm (Figure 2.4E, F, data measured from 55 MTs). GFP-TACC3 accumulation was detectable on 100% of growing MTs, 70% of paused MTs, and 25% of shrinking MTs (Figure 2.4G) for example of GFP-TACC3 on shrinking MT). Measuring fluorescence intensity values of GFP-TACC3 localized at the tips of MTs demonstrated that while GFP-TACC3 was observable on a quarter of shrinking MTs (Fig. 2.4G), mean GFP intensities were approximately 40% less on shrinking MTs than on growing MTs.

Additionally, the maximum intensity of GFP-TACC3 fluorescence on shrinking MTs (106 fluorescence units, the top whisker in Figure 4H box-plot) was close to half that of the maximum intensity of fluorescence on growing MTs (172 fluorescence units, Fig. 2.4H), demonstrating the maximum number of GFP-TACC3 molecules that localize to shrinking MTs is not as great as those which can bind to growing MT plus-ends. Thus, our results demonstrate that TACC3 can act as a +TIP in multiple vertebrate embryonic cell types, and also support the notion that TACC3 may either promote MT polymerization or reduce MT catastrophe.

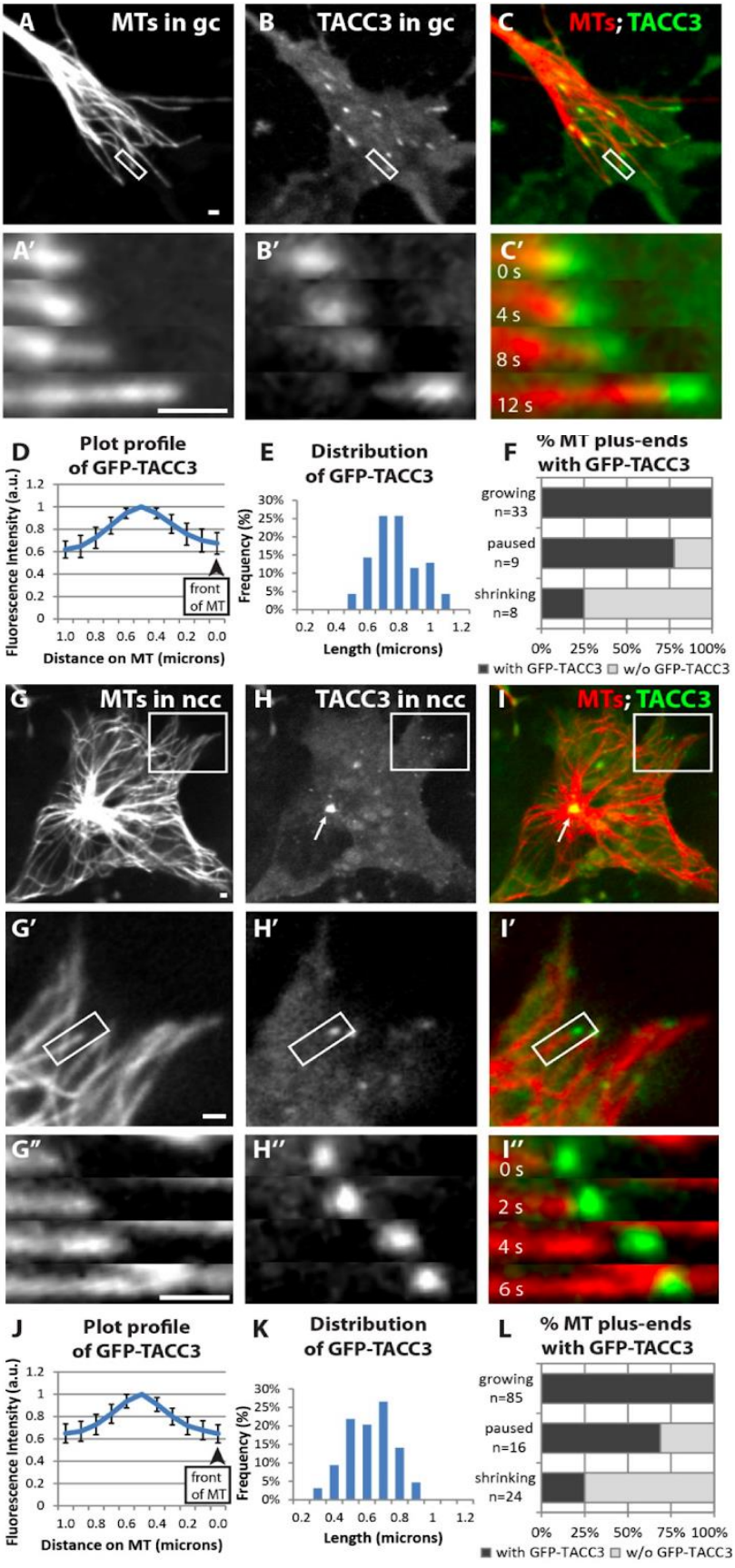

Figure 2.3 TACC3 can act as a +TIP in neuronal growth cones and neural crest cells
(A-C) Expression of mKate2-tubulin (A), GFP-TACC3 (B), and merge (C) in living growth cone (gc). C') Magnified time-lapse montage of the boxed region in (A-C) shows that GFP-TACC3 localizes to growing MT plus-ends. (D) Fluorescence intensity profile of line-scan average from 30 MT-plus-ends in growth cones. (E) Histogram depicting the distribution of lengths of detectable GFP-TACC3 localization on the plus-ends of MTs in growth cones. (F) Bar graph showing the percent of MT plus-ends with GFP-TACC3 localization for different MT dynamics instability states. (G-I) Expression of mKate2-tubulin (G), GFP-TACC3 (H), and merge (I) in living neural crest cell (ncc). See Figure 3 Movie 2. (G'-I') Magnified view of the boxed region in (G-I). See Figure 3 Movie 3. (G''-I'') Magnified time-lapse montage of the boxed region in (G'-I'). (J) Fluorescence intensity profile of line-scan average from 45 MT-plus-ends in neural crest cells. (K) Histogram depicting the distribution of lengths of detectable GFP-TACC3 localization on the plus-ends of MTs. (L) Bar graph showing the percent of MT plus-ends with GFP-TACC3 localization for different MT dynamics instability states. Scale bar is 1 μm.

2.2.4 TACC3 requires its TACC domain for MT plus end tracking

To determine the plus-end tracking mechanism of TACC3, we constructed several structural domain mutants of TACC3 (Fig. 2.5A). Full-length GFP-TACC3 accumulates at all growing MT plus-ends, as designated by mKate2-EB1 comets (Fig. 2.5B Supplemental Movie 7). Deleting the highly-conserved N-terminal domain did not prevent plus-end tracking (Fig. 2.5E-G Supplemental Movie 8). However, it did result in longer GFP-TACC3 plus-end comets compared to controls, as well as longer EB1-GFP comets (Fig. 2.5E-F). This data suggests that the conserved N-terminal domain is involved in restricting TACC3 to the extreme plus-end and also that TACC3 localization may impact EB1 binding to MT plus-ends as well. Conversely, removing either the entire TACC domain (not shown), or even just the second coiled coil domain of the TACC domain, completely abrogated MT plus-end tracking (Fig. 2.5H-J Supplemental Movie 9), demonstrating that the TACC domain, and in particular, the second coiled coil domain, is essential for TACC3 plus-end tracking. We then observed significant interference with plus-end tracking ability when TACC3 was tagged with GFP on the C-terminal end (Fig. 2.5K-M Supplemental Movie 10), further supporting the importance of the TACC domain for plus-end tracking. However, while the TACC domain is necessary for promoting plus-end tracking, it is not sufficient, as the entire TACC domain alone did not localize to MT plus-ends (Fig. 2.5N-P Supplemental Movie 11).

2.2.5 TACC3 localization on MT plus-ends is more distal than EB1 and overlaps with XMAP215

It is well-established that the growing end of a MT is home to many different +TIPs, including EB1, CLASP, and XMAP215 (Akhmanova and Steinmetz, 2008). Different +TIPs have overlapping yet unique localizations on the ends of the MTs, depending on their particular binding affinities.

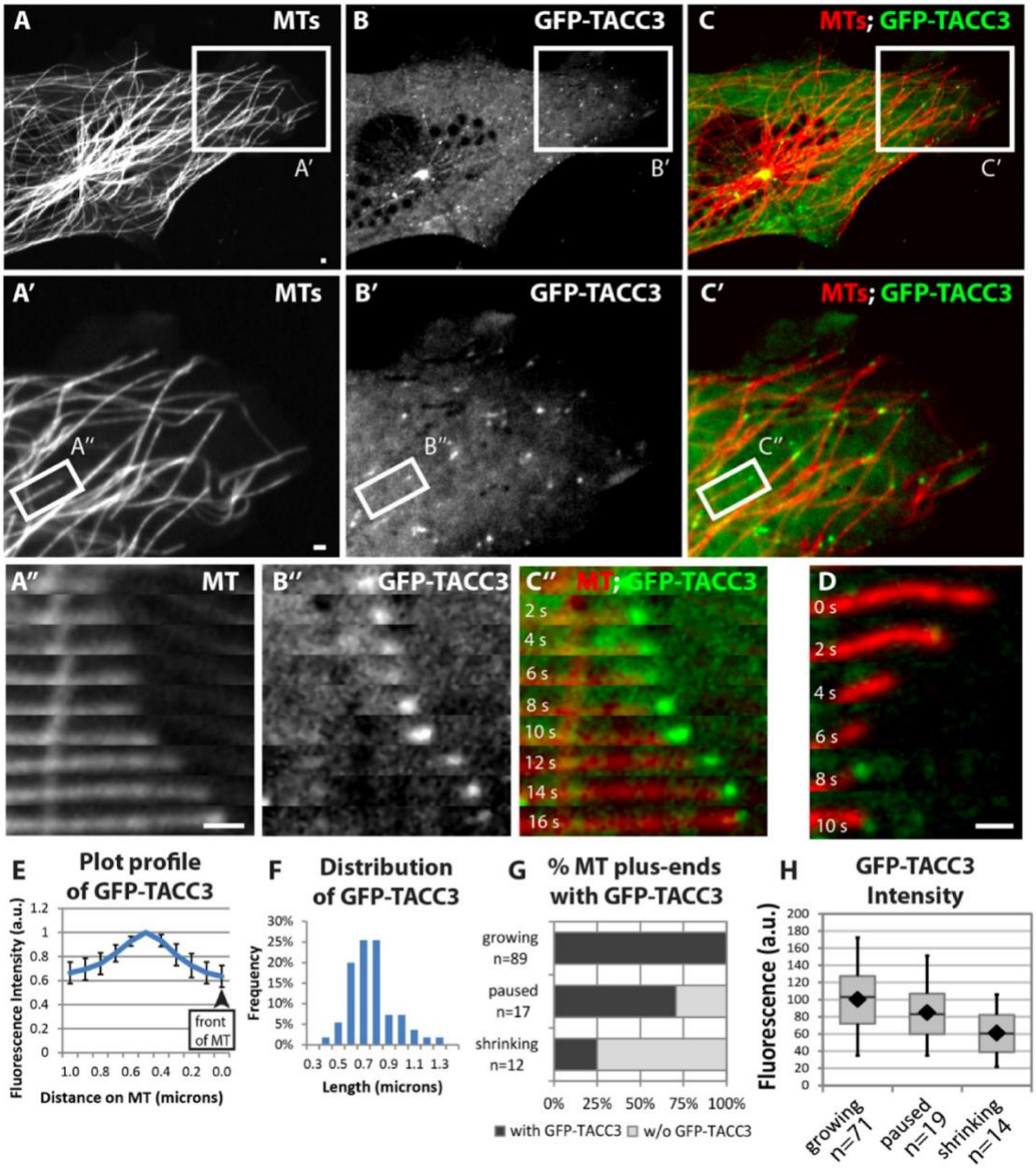

Figure 2.1 TACC3 can act as a +TIP in non-neuronal embryonic cells

(A-C) Expression of mKate2-tubulin (A), GFP-TACC3 (B), and merge (C) in cultured fibroblasts derived from embryonic somitic mesoderm. See Figure 4 Movie 1. (A'-C') Magnified view of the boxed region in (A-C). See Figure 4 Movie 2. (A''-C'') Magnified time-lapse montage of the boxed region in (A'-C'). (D) Time-lapse montage of another MT in the process of undergoing catastrophe, with GFP-TACC3 localizing. (E) Fluorescence intensity profile of line-scan average from 43 MT-plus-ends. (F) Histogram depicting the distribution of lengths of detectable GFP-TACC3 localization on the plus-ends of MTs. (G) Bar graph showing the percent of MT plus-ends with GFP-TACC3 localization for different MT dynamics instability states. (H) Quantification of mean fluorescence intensity of 4x4 pixel square of GFP-TACC3 accumulation on the ends of MTs, when visible. Box-and-whisker plots indicate the mean (diamond), median, extrema and quartiles. Bar is 1 µm

XMAP215 is known as the distal-most +TIP, while EB1 is located directly behind it on MTs (Maurer et al., 2014; Nakamura et al., 2012). Most other +TIPs, including CLASP, partially overlap with EB1 and trail further behind it (Hur et al., 2011). Because the fly ortholog of TACC3 genetically interacts with CLASP (Long et al., 2013), yet TACC3 biochemically interacts with XMAP215 (Kinoshita et al., 2005; O'Brien et al., 2005; Peset et al., 2005), we examined where TACC3 specifically localized on the MT plus-end.

We performed sequential imaging of red and green channels in both time orders, to compare co-localizations between the two proteins. While this type of dual image-comparison analysis allowed for the analysis of co-localization dynamics, we also calculated the frame-to-frame velocity of the growing MT plus-end, in order to account for the 1 second time delay between channels, for each examined MT, and used these measurements to translate one channel in the x-axis to obtain the final images depicted in Figure 6. We also used these time-corrected images for measuring approximate distances between peak intensity values.

We found that TACC3 partially overlaps with, but is distal to, EB1 (Fig. 2.6A-C), with a distance of approximately 0.5 μm between the peak fluorescence intensity profiles of the GFP-TACC3 versus the mKate2-EB1 line-scans (Fig. 2.6D). No matter which channel was imaged first (red or green), TACC3 was always distal to EB1, clearly demonstrating that even without correcting for the time-delay, TACC3 lies distal to EB1. Moreover, when we analyzed the co-localization of tagged TACC3 and tagged XMAP215, we found that they directly overlapped each other (Fig. 2.6E-G), with an almost identical fluorescence intensity plot profile (Fig. 2.6H). As TACC3 and XMAP215 directly overlap, the fluorophore that corresponded to the second channel imaged was always distal to the other (prior to translation correction).

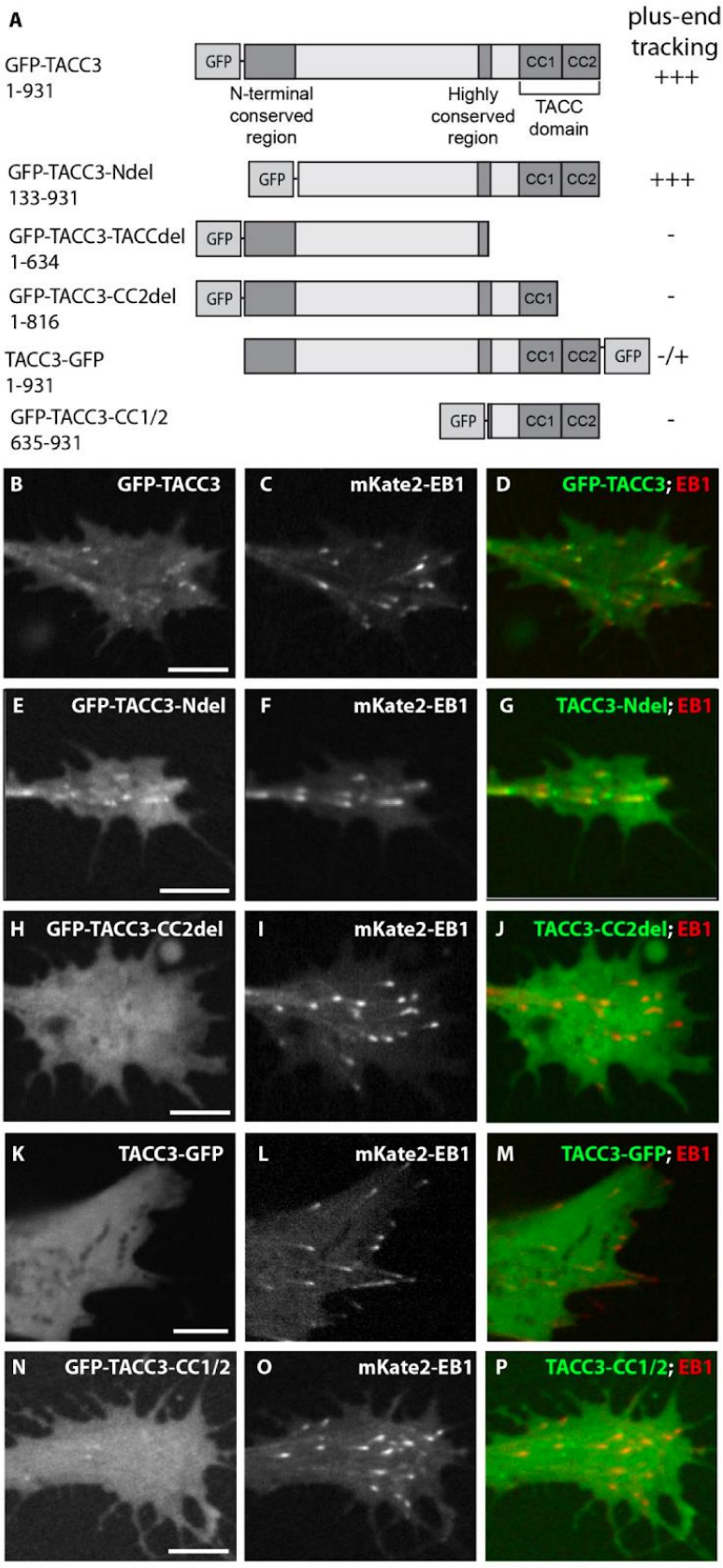

Figure 2.2 The TACC domain is necessary, but not sufficient, for MT plus-end tracking by TACC3

(A) Schematic representation of GFP-tagged TACC3 proteins and deletion constructs, and designation of whether the protein tracks along growing MT plus-ends. The amino acid residue numbers refer to those in full-length *Xenopus laevis* TACC3, from Genbank accession number NP_001081964.1. Conserved domains of TACC3 include an N-terminal conserved region, a C-terminal highly-conserved TACC domain, and a short highly-conserved region, which is located prior to the TACC domain. The TACC domain consists of two coiled-coil (CC) domains, CC1 and CC2. The TACC domain is necessary for localization to the centrosome (Peset et al., 2005, Gergely et al., 2000b) and interacting with XMAP215-family members (Lee et al., 2001; Thakur et al., 2014). (B-M) Expression of GFP-tagged TACC3 constructs (B, E, H, K, N), mKate2-EB1 (to identify MT plus-ends) (C,F,I,L,O), and merged images of both channels (D,G,J,M,P). Plus-end accumulation is apparent in B and E, but not H, K, or N. K-M are images from the edge of a neural crest cell, while all others are growth cones. See Figure 5 Movies 1-5. Bar is 5 μm

Translation based on plus-end velocity led to complete juxtaposition of the two puncta. Together, this data suggests that TACC3 is at the extreme MT plus-end, an ideal position from which to directly regulate MT polymerization by XMAP215.

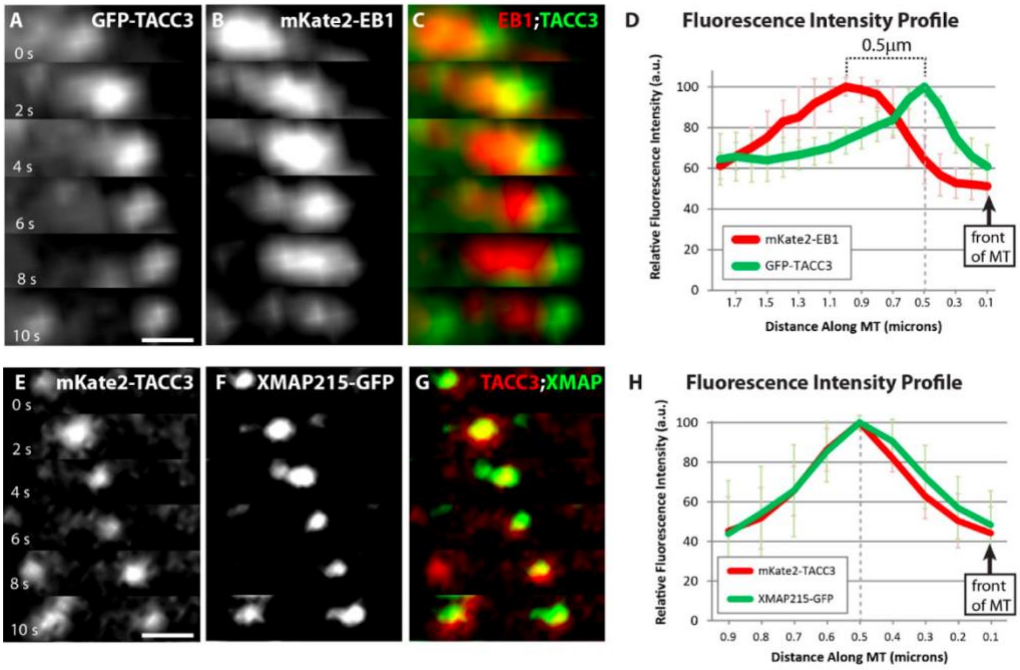

Figure 2.3 TACC3 localization on MT plus-ends is more distal than EB1 and overlaps with XMAP215

(A-C) Representative time-lapse montage of GFP-TACC3 (A) and mKate2-EB1 (B) accumulation on growing MT plus-end. MT is growing to the right. Merged image (C) highlights the spatial arrangement between GFP-TACC3 and mKate2-EB1 localizations. These images were compiled by translating the TACC3 channel in the x-axis, after calculating the frame-to-frame velocity of the growing MT plus-end, in order to account for the 1 second time delay between channels, for each examined MT (using ImageJ Translate function). To further confirm correct translation, uncorrected time-lapse co-localizations were examined with both combinations of imaging red channel first, green channel second; then green channel first, red channel second. (D) Fluorescence intensity profiles of GFP-TACC3 and mKate2-EB1. GFP-TACC3 and mKate2-EB1 signals from 12 individual MTs were quantified by intensity line scans to present the relative fluorescence intensity profiles, with the plus-end of the MT towards the right. The highest intensity peak of GFP-TACC3 is approximately 0.5 µm distal to the peak of mKate2-EB1. (E-G) Representative time-lapse montage of mKate2-TACC3 (E) and XMAP215-GFP (F) accumulation on growing MT plus-end. MT is growing to the right. Merged image (G) shows that mKate2-TACC3 and XMAP215-GFP localizations overlap. (H) Fluorescence intensity profiles of mKate2-TACC3 and XMAP215-GFP. mKate2-TACC3 and XMAP215-GFP signals from 11 individual MTs were quantified by intensity line scans to present the relative fluorescence intensity profiles. Note that peak intensities of mKate2-TACC3 and XMAP215-GFP closely align. Bar is 0.5 µm.

2.2.6 TACC3 and XMAP215 affect each other's protein stability and localization to MT plus-ends

Co-localization of XMAP215 and TACC3 suggests that they may interact at the MT plus-end, consistent with their binding *in vitro* (Kinoshita et al., 2005; O'Brien et al., 2005; Peset et al., 2005). Since TACC3 localizes XMAP215 orthologs to centrosomes (Bellanger and Gonczy, 2003; Cullen and Ohkura, 2001; Le Bot et al., 2003; Lee et al., 2001; O'Brien et al., 2005; Srayko et al., 2003), we wondered if TACC3 was also participating in localizing XMAP215 to MT plus-ends in embryonic cell types. Additionally, since the worm orthologs of TACC3 and XMAP215 are dependent on each other for overall cytoplasmic stability (Bellanger and Gonczy, 2003), we questioned whether this stabilizing activity also occurred with TACC3 and XMAP215 in vertebrate cells.

First, we determined that manipulating overall TACC3 protein levels had a corresponding effect on XMAP215 protein levels in whole embryo lysates. As TACC3 levels were reduced, XMAP215 levels decreased (Fig. 2.7A), while adding back TACC3 mRNA to the TACC3 KD rescued XMAP215 levels (Fig. 2.7A). Consistently, over-expressing TACC3 led to increased levels of XMAP215 (Fig. 2.7B). Furthermore, TACC3 levels appeared to be dependent on XMAP215 as well, as reducing XMAP215 led to a reduction in TACC3 protein (Fig. 2.7C). Notably, over-expressing TACC3 in the XMAP215 KD background partially rescued the reduction in XMAP215 levels (Fig. 2.7C'), consistent with a function for TACC3 in stabilizing XMAP215 protein. Alternatively, as TACC3 is a known translation regulator (Stebbins-Boaz et al., 1999), TACC3 could be increasing XMAP215 levels by increasing its protein synthesis. However, increased XMAP215 levels also had a positive effect on TACC3 levels (Fig. 2.7D).

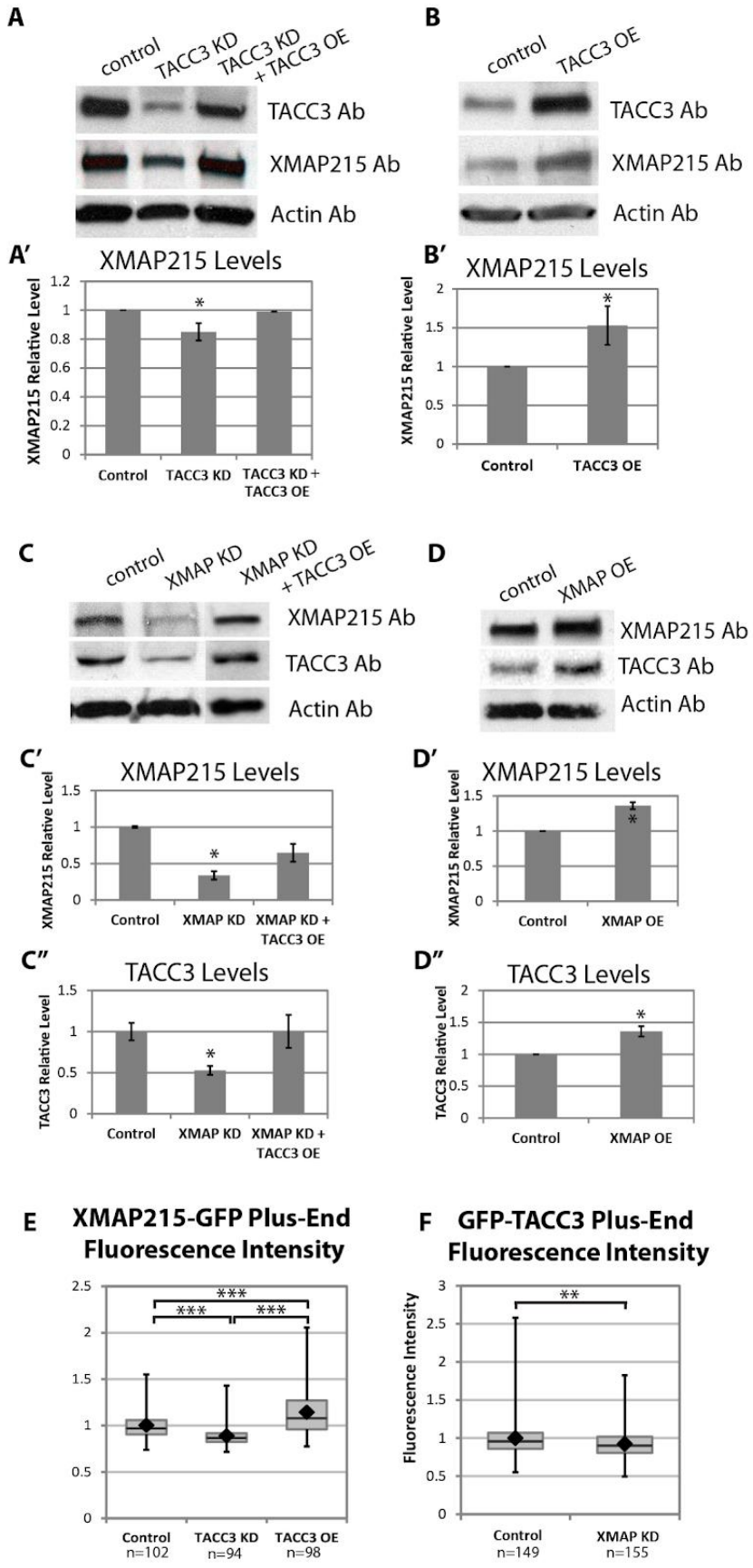

Figure 2.4 TACC3 and XMAP215 levels affect each other's protein stability and localization to MT plus-ends

(A-B) Representative Western blots showing levels of TACC3 and XMAP215 after TACC3 KD **(A)** or over-expression **(B).** The graphs in A' and B' are compilations of 7 and 6 individual Western blot experiments, respectively.**(C-D)** Representative Western blots showing levels of XMAP215 and TACC3 after XMAP215 KD **(C)** or over-expression **(D).** The graphs in **C', C''** are from 6 Western blot experiments, while **D'**, **D''** are from 3 experiments. Bars in graphs of Western densitometry denote standard error. A Kruskal-Wallis test was performed to assess significance of differences in Western blot densitometry. *$p<0.05$**. (E)** Quantification of fluorescence intensity levels of XMAP215-GFP on MT plus-ends in control, TACC3 KD, and TACC3 OE conditions, normalized to cytoplasmic levels. Data represents analysis of approximately 100 individual MTs from numerous growth cones for each condition. **(F)** Quantification of fluorescence intensity levels of GFP-TACC3 on MT plus-ends in control and XMAP215 KD conditions, normalized to cytoplasmic levels. Data represents analysis of 149 and 151 individual MTs from numerous growth cones per condition. Box-and-whisker plots indicate the mean (diamond), median, extrema and quartiles. An unpaired t-test was performed to assess significance between conditions. **$p<0.01$, ***$p<0.001$. ns not significant

We then tested whether TACC3 levels correlated with changes in XMAP215 localization on MT plus-ends. Knocking down TACC3 by 50% led to a small (11%) yet significant reduction in XMAP215-GFP fluorescence intensity on MT plus-ends (Fig. 2.7E). TACC3 OE resulted in a 14% increase of XMAP215-GFP levels on MT plus-ends (Fig. 2.7E). These results suggest that TACC3 may indeed be involved in localizing, or maintaining, XMAP215 on MT plus-ends. Interestingly, reducing XMAP215 levels also leads to mildly reduced GFP-TACC3 localization (by 8%) on MT plus-ends (Fig. 2.7F).

2.3 Discussion

2.3.1 TACC3 is a +TIP that regulates microtubule plus-end dynamics

There has been prior speculation that TACC-family proteins may regulate MT plus-end dynamics (Peset and Vernos, 2008), because the length of centrosomal MTs correlates with the level of TACC3 in multiple systems (Bellanger and Gonczy, 2003; Gergely et al., 2000b; Kinoshita et al., 2005; Le Bot et al., 2003; O'Brien et al., 2005; Srayko et al., 2003). Moreover, studies performed in *Drosophila* and *Dictyostelium* have shown that TACC-domain family members track along growing MT plus-ends (Lee et al., 2001; Samereier et al., 2011). However, in vertebrates, TACC3 localization was thought to be restricted to the centrosome and mitotic spindle, based on TACC3 immunostaining of fixed cells (Groisman et al., 2000; O'Brien et al., 2005). It has been difficult to rationalize the localization of TACC3 at the centrosome with its effects on MT length, because length is primarily controlled by events at the MT plus-end. One previous study examined whether vertebrate TACC3 bound specifically to MT plus-ends (O'Brien et al., 2005), but this study used an indirect method of testing whether TACC3 displayed an increased affinity for experimentally-sheared MTs (which presumably have more plus-ends) using an *in vitro* assay.

However, sheared MT ends would have abnormal MT plus-end structures and are not in the process of growing. As the definition of a +TIP is a protein that tracks along growing MT ends, the most reliable method for defining a +TIP is to examine its potential localization on growing MT plus-ends.

In this study, we expressed GFP-TACC3 and observed its behavior in living vertebrate growth cones, neural crest cells, and mesodermal fibroblasts, and we found that GFP-TACC3 localizes to MT plus-ends in all cell types examined. Thus, this study provides the first evidence that vertebrate TACC3 can directly regulate MT plus-end dynamics by functioning as a +TIP. Previous studies in *Drosophila* and *Dictyostelium* also showed that the highly-conserved C-terminal TACC domain was responsible for plus-end tracking (Lee et al., 2001; Samereier et al., 2011). Our observations with *Xenopus laevis* TACC3 demonstrate that this function of the TACC domain is well-conserved.

2.3.2 Interactions between TACC3 and XMAP215

It is well-established that TACC3 and XMAP215 family members interact *in vitro*, and that TACC3 is required for XMAP215 localization to the centrosome (Bellanger and Gonczy, 2003; Cullen and Ohkura, 2001; Kinoshita et al., 2005; Le Bot et al., 2003; Lee et al., 2001; O'Brien et al., 2005; Peset et al., 2005; Srayko et al., 2003). However, it had been unclear whether TACC3 localizes with XMAP215 at MT plus-ends as well. In our study, we demonstrate that TACC3 and XMAP215 do interact at MT plus-ends, and that this interaction is likely important for regulating MT growth dynamics.

As TACC3 interacts *in vitro* with XMAP215-family members through the TACC domain (Lee et al., 2001; Thakur et al., 2014), and since we determined that the TACC domain is also required for MT plus-end tracking, it is possible that TACC3 is recruited to MT plus-ends through

interaction with XMAP215. However, knocking down TACC3 also reduces XMAP215 plus-end localization, and vice versa. These results suggest that each is required for the other's normal localization to plus-ends. It has previously been suggested that TACC3 might enhance the affinity of XMAP215 for MTs, as a 1:1 TACC3-XMAP215 complex allows more XMAP215 to bind to MTs than XMAP215 alone (Kinoshita et al., 2005; Peset et al., 2005). Thus, TACC3 interaction with XMAP215 may promote XMAP215 binding to plus-ends, driving more efficient MT polymerization. This is supported by our finding that TACC3 OE leads to significantly more

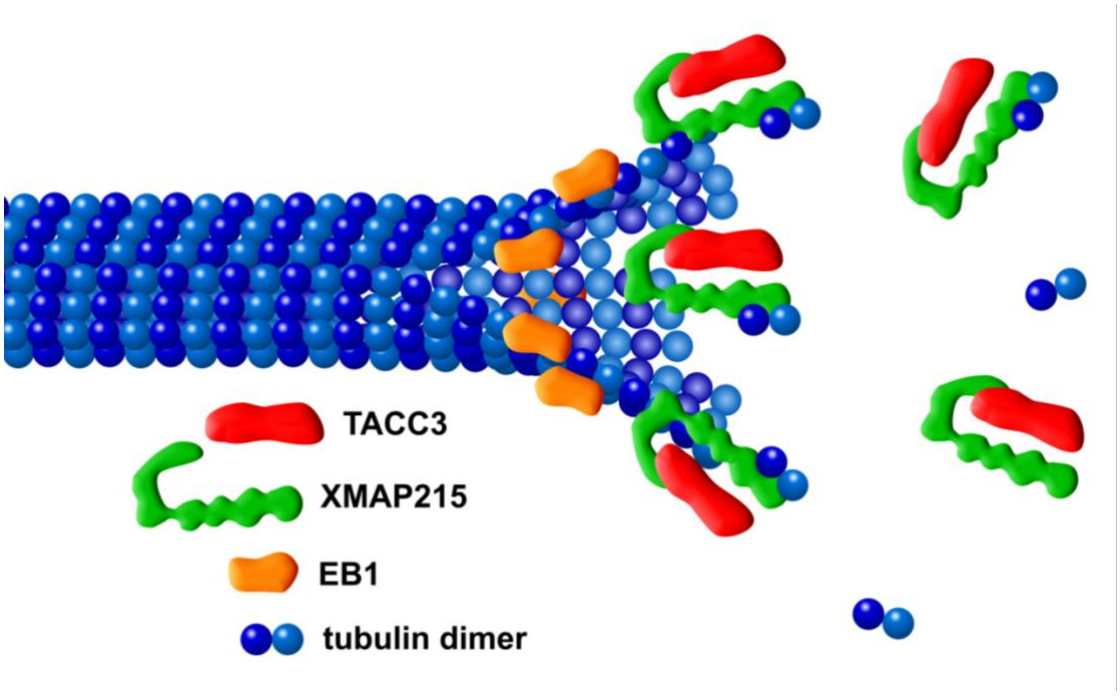

Figure 2.5 Cartoon schematic of proposed model of TACC3 interaction at MT plus-ends

Both TACC3 (red) and XMAP215 (green) bind to the extreme MT plus-end. TACC3 and XMAP215 are known to interact with each other through their C-terminal domains (Lee et al., 2001; Thakur et al., 2014), while XMAP215 can bind to tubulin dimers through its N-terminal TOG domains (Widlund et al., 2011). TACC3 and XMAP215 complex formation in the cytoplasm may serve to stabilize each other (Bellanger and Gonczy, 2003; and Figure 7), and TACC3 interaction with XMAP215 may promote more efficient binding of the complex to MTs in order to drive MT polymerization activity (Kinoshita et al., 2005; Peset et al., 2005). It is currently unknown whether TACC3 can bind to MT plus-ends directly, or only through XMAP215 (as depicted here). EB1 (orange) binding to MT plus-ends is behind TACC3 and XMAP215 (Figure 6). Not drawn to scale.

XMAP215 accumulation on plus-ends, and this extra XMAP215 may account for the faster MT growth velocities that we observe with TACC3 OE (Fig. 2.2D). It is worth noting that two other +TIPs have recently been described that also promote the recruitment of XMAP215 orthologs to MT plus-ends: SLAIN2 in mammalian cells (van der Vaart et al., 2012; van der Vaart et al., 2011) and Sentin in *Drosophila* (Li et al., 2011). Thus, it appears that the regulation of XMAP215 on MT plus-ends is becoming increasingly complicated.

Evidence suggests that the TACC3-XMAP215 complex may generally be more stable than either protein individually, as each of them affects the protein level of the other in *Xenopus* whole embryo lysates. This is consistent with studies in *C. elegans,* showing that normal levels of TACC3 and XMAP215 orthologs are required to maintain the overall cytoplasmic signal of the other (Bellanger and Gonczy, 2003). Together, our data combined with others suggest a model in which XMAP215 and TACC3 form a complex in the cytoplasm which reduces protein turnover and also may increase their binding efficiency to MT plus-ends, thus driving more effective MT polymerization (Fig. 2.8). However, we also note that *Xenopus* TACC3 was first identified as a protein (originally named Maskin) that associates with CPEB to regulates translation in the oocyte (Stebbins-Boaz et al., 1999), and so it is also possible that TACC3 could be regulating XMAP215 protein synthesis rather than, or in addition to, protein stability.

TACC3 and XMAP215 are currently the only two +TIPs known to localize at the extreme MT plus-end to drive MT polymerization. Unlike EB1-GFP, which binds solely to growing MT plus-ends, GFP-TACC3 can also bind to paused and even shrinking MTs (albeit at a lower frequency and intensity compared to growing). Although this is unusual for a +TIP, there is precedence for another +TIP (XMAP215) that tracks shrinking plus-ends *in vivo* (Lowery et al 2013). While it is possible that this back-tracking is due to exogenous expression of the GFP-

TACC3 construct, it also could be that TACC3 recognizes a structural conformation that is present at both growing and shrinking MT plus-ends. Moreover, many +TIPs contain SxIP motifs that facilitate interaction with EB proteins, for recruitment to growing MT plus-ends (Honnappa et al., 2009). We were unable to find an SxIP motif within the TACC domain, however, there is an SxIP-like motif (SPLPIP) at amino acid 311 that may contribute to plus-end recruitment. The exact mechanism by which TACC3 tracks along plus-ends, and whether it requires XMAP215 or EB1, is an important question for the future.

2.3.3 TACC3 regulates axon outgrowth

Axon outgrowth is, in part, regulated by microtubule polymerization (Lowery and Van Vactor, 2009; Tanaka et al., 1995), which is in turn controlled by +TIPs (Akhmanova and Steinmetz, 2008). Yet, only a handful of +TIPs have thus far been functionally implicated within the neuronal growth cone (Hur et al., 2011; Lee et al., 2004; Lowery et al., 2013; Neukirchen and Bradke, 2011; Zhou et al., 2004). Our study shows that TACC3 also functions as a +TIP within the growth cone, and that manipulation of TACC3 levels leads to corresponding changes in axonal outgrowth. Given that these changes correlate with similar alterations in microtubule polymerization rates within growth cones (Figure 2), it is possible that TACC3 regulates axonal outgrowth by regulating microtubule polymerization rates. This is partially supported by the classic findings that disrupting MT dynamics with low levels of MT depolymerizing drugs also results in reduced axon outgrowth (Rochlin et al., 1996; Tanaka et al., 1995). However, the role of TACC3, and +TIPs in general, in promoting axon outgrowth, is likely much more sophisticated than simply controlling the rates of polymerization. It has also been suggested that some +TIPs regulate how MTs interact with F-actin in growth cones (e.g. (Engel et al., 2014)), and future studies may uncover whether TACC3 plays a role in this as well.

In conclusion, we have used live imaging in cultured embryonic cells to demonstrate that vertebrate TACC3 regulates specific aspects of microtubule growth dynamics. We show that TACC3 can function as a +TIP, closely overlapping with XMAP215 at the extreme MT plus-end. We also establish a role for TACC3 in the promotion of axonal outgrowth. As TACC3 localization is controlled by phosphorylation (Barnard et al., 2005; Giet et al., 2002; Kinoshita et al., 2005), an important question for the future is how TACC3 may function to integrate signaling cascades downstream of axon guidance cue signals, in order to control MT dynamics in growth cones, as well as in other cell types.

2.4 Material and Methods

2.4.1 Embryos

Eggs obtained from female *Xenopus laevis* frogs (NASCO) were fertilized *in vitro*, dejellied, and cultured at 13 – 22℃ in 0.1X Marc's modified Ringer's (MMR) using standard methods (Sive et al., 2010). Embryos were staged according to Nieuwkoop and Faber (Nieuwkoop and Faber, 1994). All experiments were approved by the Boston College Institutional Animal Care and Use Committee (IACUC) and were performed according to national regulatory standards.

2.4.2 Culture of *Xenopus* Embryonic Explants

Embryos were cultured in 0.1X MMR at 22°C to stage 22-24, and each neural tube was dissected into approximately twenty similarly-sized explants (Lowery et al., 2013; Tanaka and Kirschner, 1991). The neural tube explants were plated in culture medium on poly-L-lysine- (100 µg /mL) and laminin-coated (20 µg/mL) coverslips, attached to a plastic culture dish with a hole drilled in the center (imaging chambers described in (Gomez et al., 2003)). Outgrowing axons and neural crest cells were imaged at room temperature 18 - 24 hours after plating. For imaging of non-neural

cells, somite tissue flanking the neural tube was dissected and plated on poly-L-lysine- (100 µg /mL) and fibronectin-coated (100 µg/mL) coverslips.

2.4.3 Constructs and RNA

Capped mRNA was transcribed *in vitro* using SP6 or T7 mMessage mMachine Kit (Ambion). RNA was purified with LiCl precipitation and re-suspended in nuclease free water. Constructs used: GFP-TACC3 (TACC3 pET30a was gift from Richter lab (U Mass Medical)), GFP-TACC3-Ndel, GFP-TACC3-CC2del, GFP-TACC3-CC1/2 (see Figure 5A for amino acid residues for each deletion construct, based on Genbank accession number NP_001081964.1), TACC3-GFP, mKate2-TACC3 (all TACC3 constructs sub-cloned into pCS2+ vector), mKate2-tubulin (Shcherbo et al., 2009) in pT7TS, EB1-GFP in pCS107 (gift from Danilchik lab (Oregon Health Sciences University), mKate2-EB1 in pCS2+, XMAP215-GFP (gift from the Hyman lab, (Widlund et al., 2011)) subcloned into pT7TS. The dorsal blastomeres of embryos were injected four times at the two-to-four cell stage (in 0.1X MMR containing 5% Ficoll) with total mRNA amount per embryo: 100 to 300 pg EB1-GFP or mKate2-EB1, 3000 pg XMAP215-GFP, 900 pg mKate2-tubulin, 1000 pg GFP-TACC3, mKate2-TACC3, or TACC3-mEmerald.

2.4.4 Morpholinos

Morpholino antisense oligonucleotides (MO) targeted to the translation start site of *Xenopus laevis* TACC3 (5'-AGTTGTAGGCTCATTCTAAACAGGA-3'), start site of XMAP215 (Lowery et al., 2013), or standard control MO (5'-cctcttacctcagttacaatttata'3') (purchased from Gene Tools, LLC) were injected into two-to-four cell stage embryos (50 to 80 ng/embryo for TACC3 and control MOs, 6-8ng/embryo for XMAP215 MO). Protein knockdown was assessed by Western blot of

embryos at stage 35-36. In rescue experiments, MO was injected along with mRNA in the same injection solution.

2.4.5 Western Blotting and Immunoprecipitation

Embryos were lysed in buffer (50 mM Tris pH 7.5, 5% glycerol, 0.2% IGEPAL, 1.5 mM MgCl2, 125 mM NaCl, 25 mM NaF, 1 mM Na3V04, 1mM DTT, supplemented with Complete Protease Inhibitor cocktail with or without EDTA (Roche)). Blotting was carried out using goat anti-*Xenopus laevis* TACC3 (Santa Cruz Biotechnology, cat # sc-27046, 1:500) and rabbit anti-XMAP215 (gift from the Hyman lab (Max Planck Institute), 1:2500). Mouse anti-beta-actin (Abcam, ab8224, 1:2500) was used as a loading control. For TACC3 detection, 1% IgG-free BSA in PBST was used to block nitrocellulose membrane. For other antibodies, 2% non-fat milk was used. Detection was done by chemiluminescence using Amersham ECL Western Blot reagent (GE Healthcare). The bands were quantified by densitometry using Photoshop (Adobe) and the data and graphs were compiled in Excel (Microsoft).

2.4.6 Immunocytochemistry

Embryonic explant cultures were fixed in 100% cold methanol for 3 minutes, then rinsed in PBST and blocked in 0.1% Triton-X, 1% IgG-free BSA in PBS, prior to antibody incubation. Immunostaining was carried out using goat anti-TACC3 (Santa Cruz Biotechnology, cat # sc-27046, 1:1000) and mouse anti-tubulin DM1alpha (Sigma, 1:1000). Donkey anti-goat Alexa Fluor 488 and donkey anti-mouse Alexa Fluor 568 antibodies (Invitrogen, 1:1000) were used as secondary antibodies.

2.4.7 Confocal Microscopy

Both live and fixed images were collected with a Yokogawa CSU-X1M 5000 spinning disk confocal on a Zeiss Axio Observer inverted motorized microscope with a Zeiss 63X Plan Apo 1.4

NA lens. Images were acquired with a Hamamatsu ORCA R2 CCD camera controlled with Zen software (Zeiss). For time-lapse, images were collected every two seconds for one to three minutes. Laser power for 488 nm was 30%, with exposure time 1000-1500 ms. Laser power of 561 nm was 25%, with exposure time 850-1500 ms. For imaging of immunostaining, laser power for 488 was set to 25%, with 95 ms exposure; for 561, laser was 12% with exposure time 800 ms. For two-color co-localizations in Figure 6, the TACC3 channel was translated in the x-axis, after calculating the frame-to-frame velocity of the growing MT plus-end, in order to account for the 1 second time delay between channels, for each examined MT (using ImageJ Translate function). To further confirm correct translation, time-lapse co-localizations were examined with both combinations of imaging red channel first, green channel second; then green channel first, red channel second.

2.4.8 Axon Outgrowth Imaging

For axon outgrowth analysis, images were collected on a Zeiss Axio Observer inverted motorized microscope with a Zeiss 20X N-Achroplan 0.45 NA phase contrast lens, using a Zeiss AxioCam camera controlled with Zen software (Zeiss). Images were compiled and analyzed for axon outgrowth parameters (numbers of axons per explant and length of axons) using ImageJ.

2.4.9 PlusTipTracker Software Analysis

MT dynamics were analyzed from EB1-GFP or mKate2-EB1 movies using plusTipTracker (Applegate et al., 2011; Lowery et al., 2013; Stout et al., 2014). We have previously validated the imaging conditions and tracking parameters used in this study, for accurate detection of EB1 comets in *Xenopus laevis* growth cones (Stout et al., 2014). The same parameters were used for all movies: maximum gap length, 8 frames; minimum track length, 3 frames; search radius range, 5 to 12 pixels; maximum forward angle, 50°, maximum backward angle, 10°; maximum shrinkage

factor, 0.8; fluctuation radius, 2.5 pixels; time interval 2 sec. Only growth cones with a minimum number of 10 MT tracks in a one-minute time-lapse were included for analysis. The Peltier Tech Box and Whisker Chart Utility for Excel was used to make box-plots. As MT dynamics parameters were compiled from multiple individual experiments, and there can be significant day-to-day fluctuations in control MT dynamics (in part, based on room temperature fluctuations), the final compiled data was normalized relative to the mean of the control data for each experiment.

2.4.10 Image Analysis and Statistics

Phenotypic quantification was typically performed blind of genotype and from multiple experiments to ensure reproducibility. Fluorescently-tagged-TACC3 and XMAP215 MT plus-end accumulations were measured with the Line tool in ImageJ (NIH) along their longest axis, which was defined from their trajectory in the previous and subsequent frames. Line intensities were gathered using Plot Profile, and puncta lengths were determined where fluorescent signal became visually and statistically higher than noise. Cytoplasmic measurements were also obtained and used to normalize for overall expression level of each construct. Graphs were made in Microsoft Excel, and histograms were generated using the Analysis ToolPak. To determine statistical differences for axon and MT parameters, unpaired two-tailed t-tests were used for comparing two conditions, while ANOVA tests were used to compare multiple conditions (GraphPad). For determining statistical differences for Western blot densitometry, since the distributions were not normal, a Kruskal-Wallis test was used (www.XLSTAT.com)

Chapter 3

The microtubule plus-end tracking protein TACC3 promotes persistent axon outgrowth and mediates responses to axon guidance signals during development

The content in this chapter was adapted from:

Erdogan B., Cammarata G.M., Lee E.J., Pratt B.C, Francl A.F., Rutherford E.L., Lowery L.A. The microtubule plus-end tracking protein TACC3 promotes persistent axon outgrowth and mediates responses to axon guidance signals during development.
Neural Development (2017) 12:3

3.1 Introduction

Plus-end tracking proteins (+TIPs) selectively bind to the dynamic plus-ends of microtubules (MTs), which extend into the distal part of the axon and growth cone (Lowery and Van Vactor, 2009). This enables +TIPs to come into close contact with the cell cortex, where guidance cue receptors reside. These receptors transduce asymmetrically-distributed guidance signals down to intracellular effectors, which then regulate MT dynamics in a spatially-restricted manner that likely plays a key role in growth cone turning events (Bearce et al., 2015; Cammarata et al., 2016). Thus, +TIPs deserve attention for their potential function in regulating MT dynamics during axon guidance. One of the first +TIPs to be discovered for its role in axon guidance was CLASP (Lee et al., 2004). Genetic studies in *Drosophila* demonstrated that *CLASP* is a downstream target of Abelson tyrosine kinase (Abl) in the Slit/Robo guidance pathway during central nervous system midline crossing (Lee et al., 2004). Moreover, the +TIP and MT polymerase, *msps* (fly ortholog of XMAP215/ch-TOG) interacts with *CLASP* antagonistically during this guidance decision in an Abl-dependent manner (Lowery et al., 2010). In addition to its role in *Drosophila*, XMAP215 has been implicated in promoting axon outgrowth in vertebrates (Lowery et al., 2013). We have recently shown that the XMAP215-interactor, TACC3, is also a +TIP that regulates MT dynamics in vertebrate growth cones and is essential for normal axonal outgrowth (Nwagbara et al., 2014). However, how TACC3 specifically affects axon outgrowth and whether TACC3 plays a role during axon guidance remain to be explored.

In this study, we examine the role of TACC3 in axon outgrowth and pathfinding *in vivo* within the developing nervous system of *Xenopus laevis* which is a great model for studying cytoskeletal dynamics during axon growth and guidance (Erdogan et al., 2016; Slater et al., 2017). Using time-lapse live imaging, we demonstrate that TACC3 is required for persistent axon

outgrowth in *Xenopus laevis*, and that both the N- and C- terminal conserved domains of TACC3 are necessary for enhanced axon outgrowth. Moreover, TACC3-overexpressing growth cones can mitigate the reductive impacts of the MT-depolymerizing agent, Nocodazole, on MT dynamics parameters. We also show that TACC3 and XMAP215 display a synergistic effect and promote axon outgrowth *ex vivo*. Finally, examination of whole mount *Xenopus* spinal cords shows defects in axon guidance in motor neurons when TACC3 levels are depleted, and manipulation of TACC3 levels impacts the growth cone response to the repellent guidance cue Slit2 in cultured *Xenopus* spinal neurons. Together, these investigations provide new insights into the mechanism by which TACC3 functions either alone or in combination with other +TIPs, such as XMAP215, to regulate MT dynamics during axon outgrowth and guidance.

3.2 Results

3.2.1 TACC3 promotes persistent axon outgrowth by preventing spontaneous axon retractions

We previously showed that normal axonal outgrowth requires TACC3 (Nwagbara et al., 2014).To gain further insight into the mechanism by which TACC3 promotes axon outgrowth, we examined the effect of TACC3 knockdown (KD) and overexpression (OE) on dynamic axon outgrowth parameters. Time-lapse imaging demonstrated that TACC3 KD significantly reduced axon outgrowth velocity by 25% relative to control conditions (TACC3 KD, 0.74 ± 0.03, n=46, versus control, 1.04 ± 0.03 n= 57, ***p<0.0001, Fig. 3.1A). In addition to the reduced outgrowth velocity, TACC3 reduction dramatically increased axon retraction rates by 5-fold in comparison to control axons (TACC3 KD, 5.27 ± 1.22, n=107, versus control, 1.06 ± 0.35, n=99, **p=0.0015, Fig. 3.1B). Conversely, when TACC3 levels were elevated, the frequency of axon retraction rates was reduced

significantly by 45% compared to controls (TACC3 OE, 0.54 ± 0.12, n= 155, versus control, 0.99 ± 0.12, n=180, *p=0.01, Fig. 3.1B). Although TACC3 OE led to increased axonal length (Fig. 3.1F), TACC3 OE actually reduced axon outgrowth velocity by 14% (0.89 ± 0.32, n=103, versus control, 1.04 ± 0.033, n= 57, *p<0.0268, Fig. 3.1A), suggesting that the increased axonal length may result from reduced axon retraction rather than a change in outgrowth velocity.

To further explore the TACC3 KD phenotype, we examined axon outgrowth of cultured neurons in which TACC3 was acutely inhibited by the TACC3 specific inhibitor, KHS-101 (Wurdak et al., 2010). Consistent with the effect seen in TACC3 KD, KHS-101-induced acute inhibition of TACC3 significantly reduced MT growth velocity by 28 % (15.09 ± 0.86 μm/ min (before drug treatment); 10.84 ± 0.75 μm/ min (after drug), **p<0.0019, Fig. 3.1C). Moreover, acute inhibition led to an immediate reduction in axon length by 26% compared to vehicle treated controls (KHS-101, 0.71 ± 0.05, n=12, versus DMSO, 0.96 ± 0.03, n= 9, ***p=0.0007, Fig. 3.1D).

In order to determine which domains of TACC3 are involved in axon outgrowth, we tested various truncation mutants of TACC3. We found that, while full-length TACC3 and ΔN (lacking conserved N-terminal domain) significantly increased axon outgrowth by 30% (1.30 ± 0.03, n=787, ***p<0.0001) and 18% (1.18 ± 0.31, n=613, ***p<0.0001) respectively, expression of ΔTACC (lacking conserved TACC domain, which has shown to be required for centrosome localization, MT polymerase XMAP215 interaction) caused a significant reduction by 12% in axon length (0.87 ± 0.021, n=764, ***p=0.0002) in comparison to wild-type neurons (0.99 ± 0.02, n=997) (Fig 3.1F). On the other hand, the larger N-term deletion (lacking both conserved N-terminus and putative SxIP-like motif that mediates EB1 interaction) showed no significant

difference (1.04 ± 0.028, n=563, p=0.2012). Additionally, none of the deletion constructs that promoted axon outgrowth were as effective as full-length TACC3 OE (Fig. 3.1F).

Together, our findings suggest that TACC3 is required for proper axon outgrowth by opposing axonal retracting forces. Additionally, full-length TACC3 is more efficient in promoting axon outgrowth than its truncation mutants, while expression of a version lacking the TACC domain results in a mild dominant negative effect.

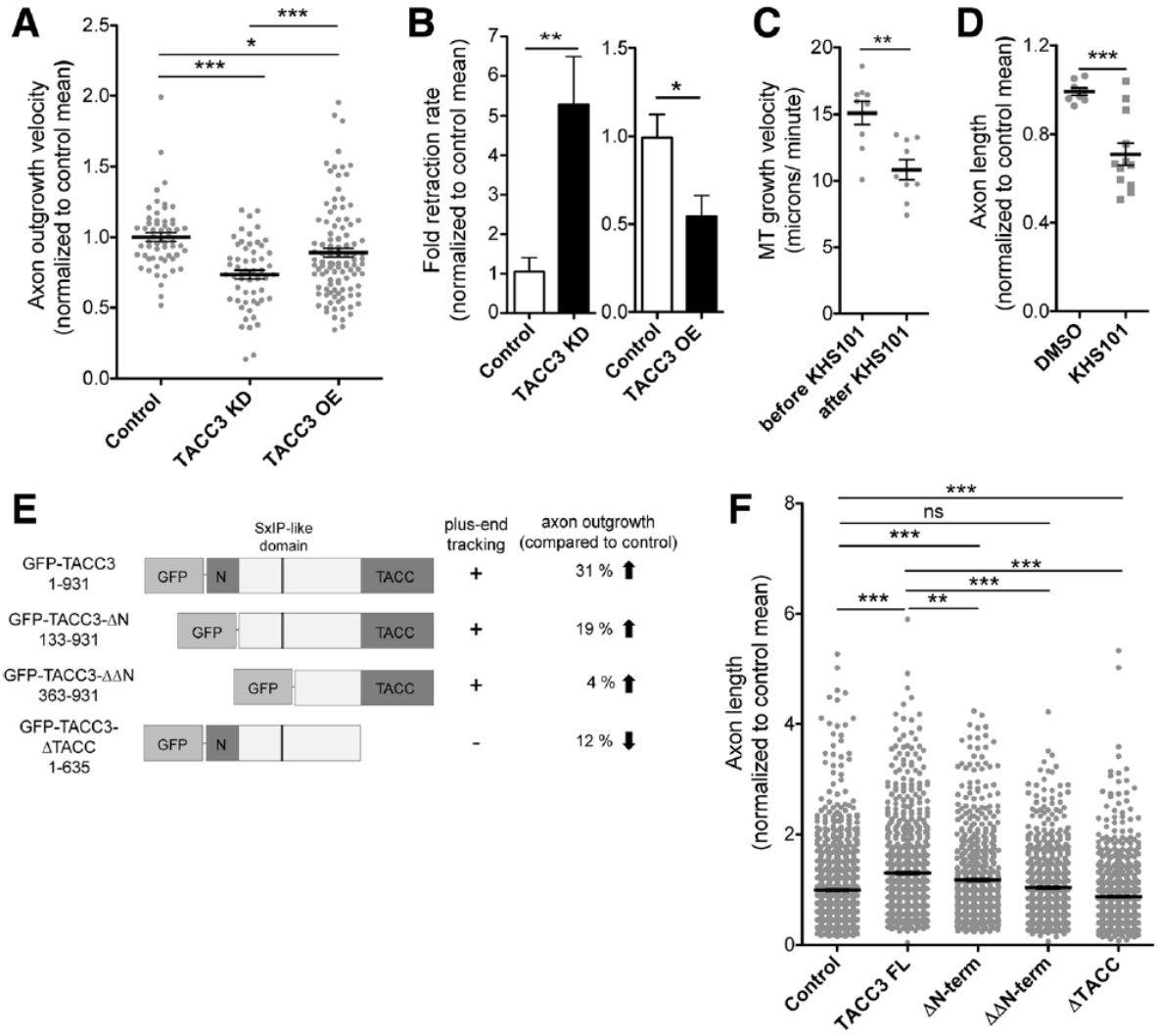

Figure 3.1 TACC3 promotes axon outgrowth velocity and prevents spontaneous axon retractions

(A) Axon outgrowth velocity is significantly decreased in TACC3-depleted axons by 27% ($n = 56$) and in TACC3 OE, to a lesser extent, by 11% ($n = 106$) compared to control (GFP only) conditions ($n = 58$). **(B)** Retraction rate increased 5-fold in TACC3 KD ($n = 107$) and decreased 0.6-fold in TACC3 OE ($n = 155$) in comparison to their corresponding non-injected ($n = 95$) and GFP injected ($n = 180$) controls respectively. (**C-D)** MT growth velocity (DMSO, $n = 9$, KHS-101, $n = 9$) (**C**) and axon outgrowth length (DMSO, $n = 8$, KHS-101, $n = 12$) (**D**) are significantly reduced by 28 and 26% respectively after acute depletion of TACC3 by the inhibitor KHS101. **(E)** Schematic representation of GFP-tagged TACC3 full-length and deletion constructs, along with plus-end tracking ability (denoted by "+") and impact on axon outgrowth length. **(F)** Quantification of axon outgrowth length in cultured neural explants of GFP injected control ($n = 997$), full-length GFP-TACC3 (1-931aa) ($n = 787$), GFP-TACC3-ΔN (133–931) ($n = 613$), GFP-TACC3- ΔΔN (363–931) ($n = 563$) and GFP-ΔTACC domain (1-635aa) ($n = 764$). $*p < 0.05$, $**p < 0.01$, $***p < 0.001$. ns not significant. n = axon/growth cone number

3.2.2 TACC3 antagonizes nocodazole-induced MT depolymerization but does not affect MT lattice stability

Previously, we determined that TACC3 promotes efficient MT polymerization by enhancing MT growth velocity within growth cones (Nwagbara et al., 2014). However, the mechanism by which TACC3 affects MT polymerization remains to be elucidated. Thus, we sought to gain further insight by assessing the impact of low doses of the MT depolymerizing drug, nocodazole, after TACC3 manipulation.

We observed that a low dose of nocodazole led to reduction in several parameters of MT dynamics, and that TACC3 OE could mitigate these effects. While control growth cones exhibited a marked 20% decrease in MT growth speed after treatment with 50 pM nocodazole (before, 1.00 ± 0.04, n=22, after treatment, 0.79 ± 0.03, n=22, ***p=0.0001), TACC3 OE growth cones showed reduction by only 12% (before, 1.08 ± 0.04, n=21, after nocodazole, 0.95 ± 0.03, n=21, *p=0.0316, Fig. 3.2A). Similar trends were observed with MT growth lifetime, in which control growth cones showed a 15% reduction (before, 1.00 ± 0.03 seconds, n=22, after nocodazole , 0.84 ± 0.03 seconds, n=22,***p=0.0008) versus only a 3% reduction with TACC3 OE (before, 0.91 ± 0.03, n=21, after nocodazole , 0.87 ± 0.03, n=21, p=0.4305, Fig. 3.2B), and for MT growth length, there

was a 35% reduction in controls (before, 1.00 ± 0.05, n=22, after nocodazole , 0.65 ± 0.03, n=22, ***p<0.0001) versus 14% in TACC3 OE (before, 1.00 ± 0.04, n=21, after nocodazole, 0.85 ± 0.04, n=21, *p=0.02, Fig. 3.2C). These results suggest that TACC3 can mitigate the nocodazole-induced reduction in MT growth dynamics parameters. This mitigation can be more clearly visualized when the nocodazole-induced change is represented as the ratio of after treatment/ before treatment. Although the relative reduction in MT growth speed when TACC3 is overexpressed is only slightly less compared to controls (0.91 ± 0.06 n=21 versus control 0.82 ± 0.04 n=22, ns p=0.2, Fig. 3.2A'), for other MT growth parameters TACC3 OE significantly dampens the nocodazole induced reduction in lifetime (0.99 ± 0.047 n=21 versus control 0.86 ± 0.03 n=22, *p=0.03, Fig. 3.2B') and length (0.91 ± 0.08 n=21 versus control 0.68 ± 0.04 n=22, *p=0.01, Fig. 3.2C') compared to controls.

In addition to MT polymerization, MT stabilization is considered to be an important parameter for axon outgrowth and growth cone turning events (Challacombe et al., 1997). Hence, we measured the fluorescence intensities of tyrosinated and de-tyrosinated tubulin in the growth cone and assessed dynamic and stable MT lattice profiles, in TACC3-manipulated growth cones. We found that the ratio of tyrosinated tubulin versus de-tyrosinated tubulin did not statistically differ in TACC3 KD (0.87±0.07, n=37, p=0.2394) nor in TACC3 OE (1.01±0.11, n=129, p=0.9673) growth cones, with respect to control growth cones (1.00±0.09, n=143, Fig. 3.2 D-F). This suggests that TACC3 may not specifically regulate MT lattice stability in growth cones.

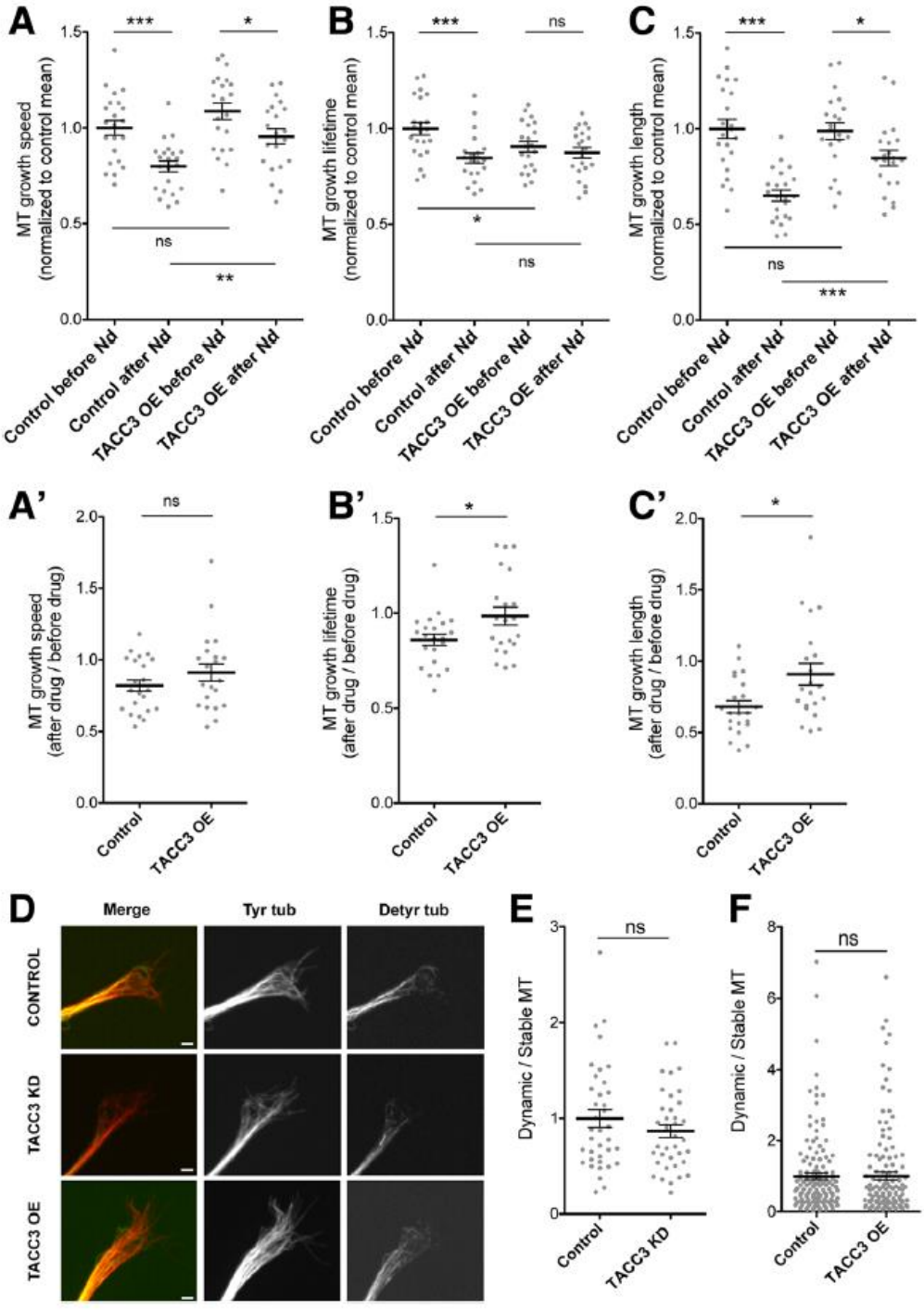

Figure 3.2 TACC3 antagonizes Nocodazole-induced MT depolymerization but does not affect MT stability

(A-C) Quantification of the MT dynamics shows significant reduction in MT growth speed (**A**), MT lifetime (**B**) and MT growth length (**C**) in control ($n = 22$) and TACC3 OE ($n = 21$) growth cones in response to 50 pM Nocodazole before and 5 min after drug treatment. However, the effect of Nocodazole on TACC3 OE growth cones is dampened compared to controls. **(A'-C')**, Although not significant,

reduction in MT growth speed (**A'**) is more prominent in control growth cones compared to TACC3 OE growth cones while the reduction in both lifetime (**B'**) and length (**C'**) in control growth cones are significantly higher than the TACC3 OE growth cones (**D**) Representative growth cone images of control, TACC3 KD and TACC3 OE, immunostained for tyrosinated tubulin (*red*) and de-tyrosinated tubulin (*green*) to label dynamic versus stable MTs, respectively. **(E-F)**, Quantification of the fluorescence intensity of imaging data in G, with TACC3 KD ($n = 38$) (**E**) and TACC3 OE ($n = 129$) (**F**) growth cones showing no significant changes in dynamic/stable MTs compared to corresponding control growth cones ($n = 37$ and $n = 143$, respectively). $*p < 0.05$, $**p < 0.01$, $***p < 0.001$. ns not significant. n = growth cone number. Scale bar, 2 μm.

3.2.3 TACC3 and XMAP215 interact to promote axon outgrowth

We previously found that the TACC3 interactor and MT polymerase, XMAP215, also promotes axon outgrowth (Lowery et al., 2013), and that TACC3 and XMAP215 co-localize at the extreme plus-end of MTs in growth cones in a co-dependent manner (Nwagbara et al., 2014). However, the consequences of their interaction on axon development have not been elucidated. Therefore, we sought to test whether TACC3 and XMAP215 might cooperate synergistically to promote axon outgrowth by partially elevating or reducing TACC3 and XMAP215 levels alone and in combination with each other. While partial TACC3 KD led to 10% reduction in axon outgrowth (204.7 ± 4.8 μm, n=487, p=0.3528) and partial XMAP215 KD led to 13% reduction (185.6 ± 6.4 μm, n=312, *p=0.0116), partial knockdown of both reduced axon length significantly by 34% (140.6 ± 3.5 μm, n= 552, ***p<0.0001) compared to control axons (213.6 ± 9.6 μm, n=219, Fig. 3.3A). Conversely, overexpression of both (double OE) increased axon length by 32.7% (237.7 ± 5.4 μm, n=654, ***p<0.0001) while TACC3 OE alone increased by 11% (198.9 ±3.2, n=1585, ***p<0.0001) and XMAP215 OE increased by 30.9 % (234.5 ± 4.3 μm, n=1227, ***p<0.0001) in comparison to controls (179.1 ±3.2 μm, n=1288, Fig. 3.3B). Interestingly, while double OE significantly increased axon length in comparison to TACC3 OE alone (***p<0.0001), it did not show a difference when compared to XMAP215 alone (p=0.6421) suggesting that there may be an upper threshold that is reached with XMAP215 OE by itself.

We next asked whether overexpression of one +TIP might rescue the reduced axon length in the absence of the other. We observed that overexpressing XMAP215 in the TACC3 KD background brought axon outgrowth length to control levels (TACC3 KD + XMAP215 OE, 149.4 ± 5.2 μm, n=313, $^{**}p$=0.005, versus control, 148.8 ± 3.6 μm, n=558, p=0.9331) by increasing the length 15% in comparison to TACC3 KD (129.7 ± 4.477μm, n=289, $^{**}p$=0.0015, Fig. 3.3C). On the other hand, overexpression of TACC3 in the XMAP215 KD background increased axon outgrowth length by 30% (XMAP215 KD + TACC3 OE, 262.2±7.8 μm, n=397, $^{***}p$<0.0001) in comparison to XMAP215 KD (201.3 ± 7.2 μm, n= 299); however, the rescue was not complete when compared to control axons (Control, 304.9 ± 8.5 μm, n=463, $^{***}p$=0.003, Fig. 3.3D). These findings suggest that TACC3 and XMAP215 cooperate during axon outgrowth, with XMAP215 showing more additive effects on TACC3-mediated axon outgrowth.

3.2.4 TACC3 affects axon guidance *in vivo* and *ex vivo*

The direction that the growth cone acquires during outgrowth is a result of local modulation of MT dynamics in response to guidance signals (Challacombe et al., 1997; Sabry et al., 1991; Tanaka and Kirschner, 1995; Williamson et al., 1996). Thus, we wondered whether TACC3 regulation of MT dynamics could play a role during axon guidance. We first examined motor neuron axon outgrowth from the spinal cord in embryos at an early developmental stage (st 28), and we discovered that reduction of TACC3 caused significantly impaired outgrowth and severely disrupted morphology in all embryos examined (Fig. 3.4A-C). To gain greater insight into whether TACC3 manipulation causes this disorganization under specific guidance signals, we examined growth cone behavior in response to the guidance molecule, Slit2, applied in culture media.

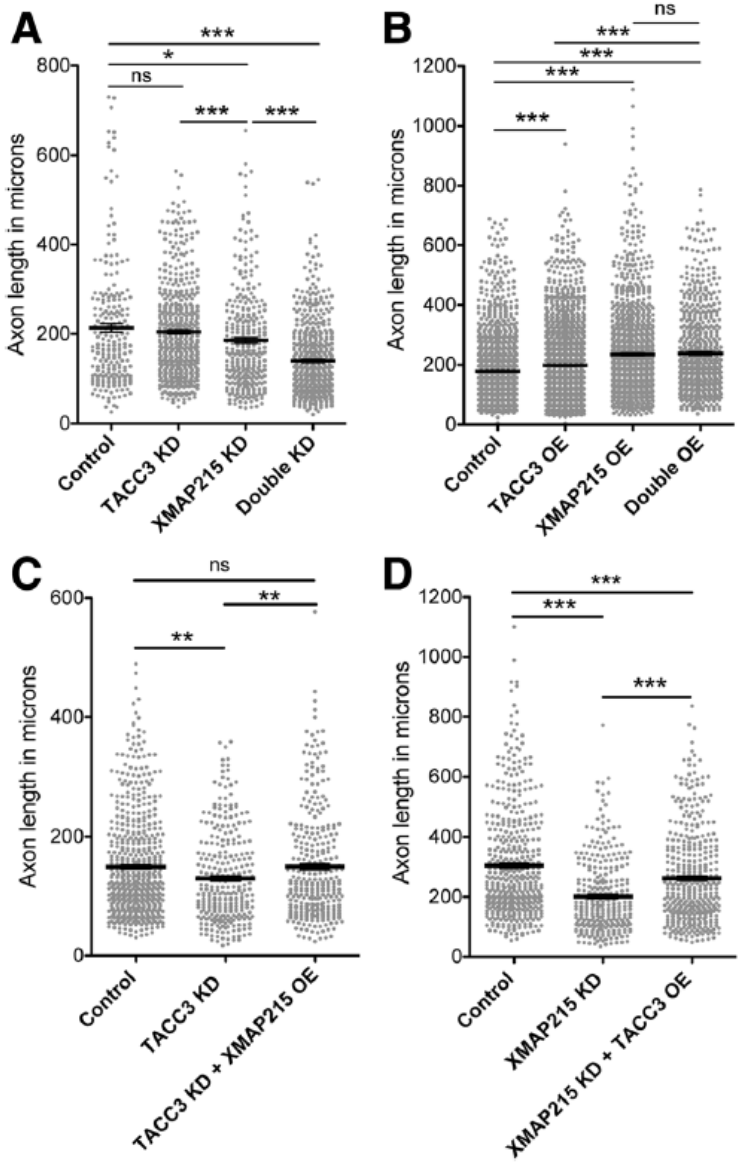

Figure 3.3 TACC3 and XMAP215 interacts to promote axon outgrowth

(A-B) Combinatorial reduction or elevation of TACC3 and XMAP215 levels reveals synergistics in axon outgrowth. Knocking down both TACC3 and XMAP215 ($n = 312$) showed significant reduction in axon length in comparison to control ($n = 219$), TACC3 KD ($n = 487$) and XMAP21 KD alone ($n = 312$) (**A**). Overexpression of both ($n = 654$) showed significant increase in axon length in comparison to control ($n = 1288$) and TACC3 OE ($n = 1585$), while double overexpression had no additive effect in comparison to XMAP215 OE ($n = 1227$) (**B**). **(C-D)** Reduced axon outgrowth in TACC3 KD ($n = 289$) (**C**) or XMAP215 KD ($n = 299$) (**D**) neurons is rescued by the overexpression of XMAP215 ($n = 313$) or TACC3 ($n = 397$), respectively. $*p < 0.05$, $**p < 0.01$, $***p < 0.001$. ns not significant. n = axon number

Slit2 is a repellent guidance cue and we began to work with it since Slit has been previously studied with other +TIPs such as CLASP (Lee et al., 2004) and the response of growth cones of different neuron types isolated from Xenopus embryos at different stages has been documented before (Myers et al., 2012; Piper et al., 2006; Stein and Tessier-Lavigne, 2001). We monitored the changes in growth cone behavior for 10 min prior and for 30 min after addition of Slit2. Growth cones that show persistent growth were picked to be analyzed for their behavior after Slit2 addition. Growth cones that had reduced lamellipodial area was considered as collapsed. We found that

TACC3 OE growth cones had significantly fewer growth cone collapse and axon retraction events (TACC3 OE, 21.28 ± 7.24 n=76 versus control, 54.72 ± 4.26 n=44, *p=0.0164) in response to Slit2, when compared to wild type growth cones (Fig. 3.4D-E). This suggests that overexpressing TACC3 can counteract Slit2-induced growth cone collapse.

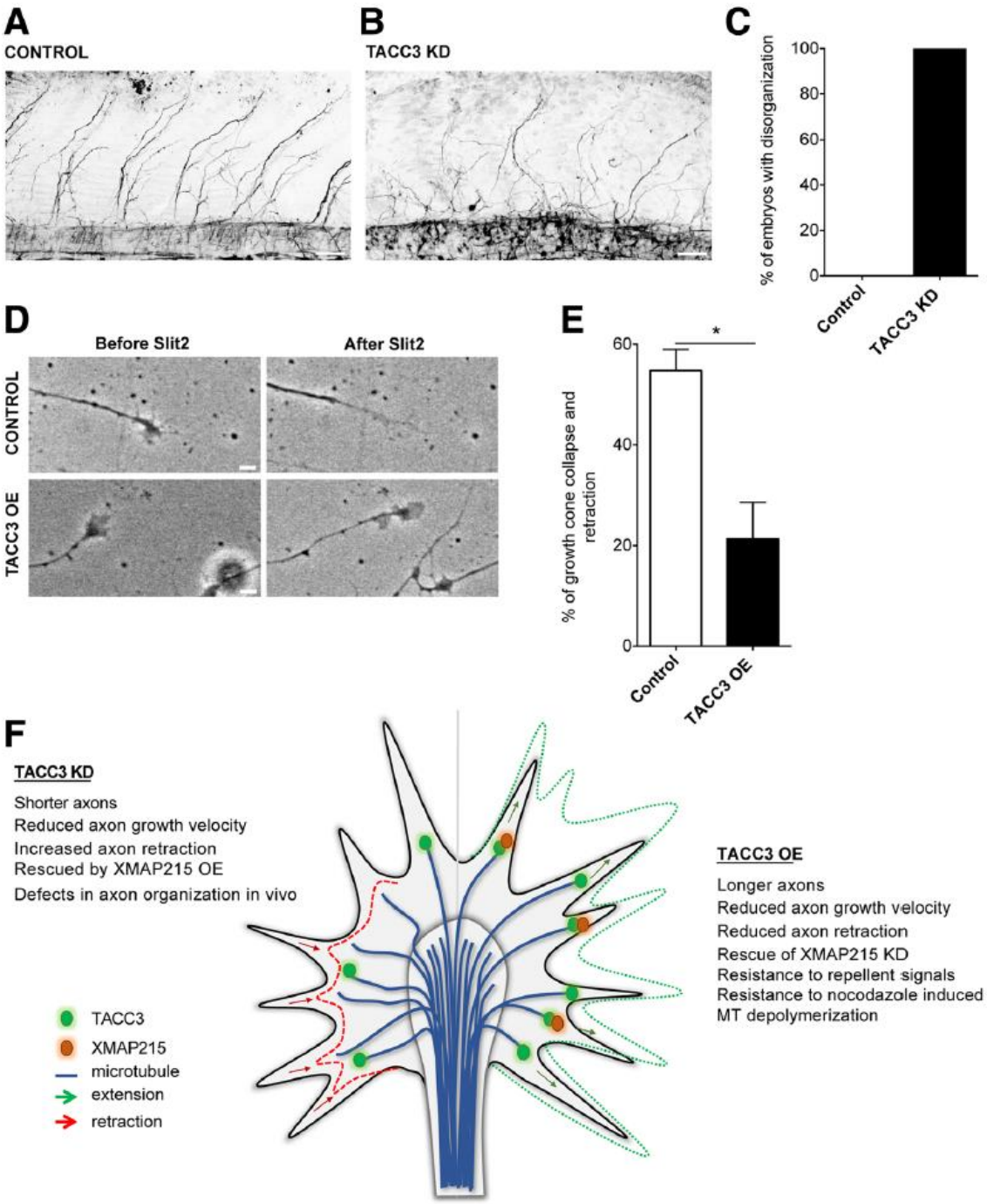

Figure 3.4 TACC3 affects axon guidance *in vivo* and *ex vivo*

(A-B) Confocal images of laterally-viewed whole-mount Xenopus spinal cord fluorescently labeled for acetylated tubulin, showing peripheral axon outgrowth in control (A) and TACC3 KD (B) embryos at 2 dpf. c, Quantitation of the embryos with motor neuron guidance defects ($n = 5$ embryos). (D) Representative neural tube growth cone images of control and TACC3 OE, before and after addition of 400 ng/ml Slit2. (E) Quantification of the percentage of the growth cone collapse events in control ($n = 48$) and TACC3 OE ($n = 82$) growth cones show significant reduction in growth cone collapse in TACC3 overexpressing growth cones. f, Cartoon model for the role of TACC3 at MT plus ends during axon outgrowth and guidance. Microtubule (*blue*) plus-ends decorated by TACC3 (*green*) promotes axon outgrowth, reduces axon retraction, dampens nocodazole induced reduction in MT dynamics parameters, rescues XMAP215 KD induced axon length reduction and opposes repellent guidance signals effect. $*p < 0.05$, $**p < 0.01$, $***p < 0.001$. ns not significant. n = growth cone number. Scale bar, 50 μm and 5 μm.

3.3 Discussion

Dynamic spatial and temporal regulation of MTs within the growth cone is considered to be of key importance during axon outgrowth, guidance decisions and regeneration events (Buck and Zheng, 2002; Challacombe et al., 1997; Chen et al., 2015; Sabry et al., 1991; Tanaka and Kirschner, 1995; Williamson et al., 1996). Accordingly, MT plus-end tracking proteins (+TIPs) likely play a critical role during axon guidance, as +TIPs dominate the dynamic portion of MTs that reaches the growth cone periphery, where guidance cue receptors reside (Bearce et al., 2015). However, few +TIPs have been examined within the context of the embryonic growth cone. We previously characterized a MT plus-end tracking function for TACC3 and showed that it can promote MT polymerization and is required for proper axonal development (Nwagbara et al., 2014). Here, we sought to uncover new insights into the mechanism underlying axonal regulation by TACC3.

First, we found that the shorter axons that result from reduced levels of TACC3 were due to slower axon outgrowth velocity along with significantly increased retraction rate. Moreover, TACC3 overexpression leads to longer axons, not because of fast axon outgrowth velocity (the outgrowth rate was actually slower than in controls), but because of reduced axon retraction rate. This suggests that TACC3-mediated MT dynamics may be required for opposing the normally-

occurring retractive forces within axons. Another possible explanation is that the reduced axon outgrowth velocity and reduced axonal retraction rates after TACC3 OE could be due to stronger anchorage to the underlying substrate and adhesion turnover. While there are +TIPs that have been implicated to mediate MT – FA interactions (Stehbens and Wittmann, 2012), TACC3 has not yet been explored in focal adhesion (or point contacts, in the case of growth cone) regulation. However, since TACC3 has been identified as an interactor of CLASP (Long et al., 2013), and given that CLASP is known to function during focal adhesion turnover (Stehbens et al., 2014), future studies should examine whether TACC3 also plays a role at focal adhesions/point contacts.

+TIPs modulate MT dynamic instability in various ways; for example, XMAP215 promotes MT growth by catalyzing addition of tubulin dimers (Brouhard et al., 2008), while CLASP and APC rescue MT from catastrophe by increasing MT stability (Mimori-Kiyosue et al., 2005; Wen et al., 2004; Zumbrunn et al., 2001). Here, we showed that TACC3 OE can dampen nocodazole-induced reduction in MT growth speed, length and lifetime. However, this was not achieved by increased MT lattice stability, as immunofluorescence analysis of dynamic versus stable MTs revealed that TACC3 has no apparent impact on MT stability within the growth cone. It is unclear how TACC3 is able to mitigate the reduction in MT growth speed, length and lifetime as a result of nocodazole application. One possibility could be that TACC3 overexpression, which enhances XMAP215 localization at MT plus ends (Nwagbara et al., 2014), may simply promote more efficient and processive MT polymerization by XMAP215 to counteract the nocodazole-induced effects.

Individual +TIPs comprise a network of proteins at MT plus-ends which can co-localize and function together to modulate MT dynamics. We have previously shown such cooperation

between TACC3 and XMAP215 in growth cones, as we demonstrated that TACC3 and XMAP215 co-localize at MT plus-ends in co-dependent manner (Nwagbara et al., 2014).

Here, we found that TACC3 and XMAP215 interact to promote axon outgrowth (Fig 3.3). Partially knocking down both TACC3 and XMAP215 resulted in further reduction in axon outgrowth length, which suggests a synergistic interaction between the two proteins. However, overexpression of both +TIPs did not show further increase in axon length in comparison to XMAP215 OE alone. This might be due to an upper threshold that is reached with overexpression of XMAP215 alone. Conversely, rescue studies show that XMAP215 can fully restore TACC3 KD-mediated reduced axon length to control levels, whereas TACC3 OE fails to show the same impact over XMAP215 KD. As XMAP215 is a processive MT polymerase, reduction in XMAP215 levels may exert more dramatic effect than the reduction in the levels of TACC3, which may play more of an accessory role. Considering that every TACC3 molecule is thought to interact with two molecules of XMAP215 (Mortuza et al., 2014), reduced levels of XMAP215 could be a limiting factor. Even though TACC3 OE functions to increase available XMAP215 at MT plus-ends, the reduction in overall XMAP215 levels may result in poor axon outgrowth. While knock down approaches provide supporting evidence regarding the combinatorial role of TACC3 and XMAP215 during axon outgrowth, future studies should utilize mutations that disrupt their interaction (Mortuza et al., 2014) in order to understand the dependence of these two proteins on one another during axon outgrowth.

In addition to their role in axon outgrowth, several +TIPs have been implicated in participating in growth cone steering decisions in response to extracellular cues. The first of which is *orbit/MAST*, the fly ortholog of mammalian CLASP, that has been identified to cooperate with Abelson kinase (Abl) downstream of Slit/Robo guidance pathway (Lee et al., 2004). In a parallel

genetic and proteomic screen in fruit flies, *minispindles* (*msps*), a fly ortholog of Xenopus XMAP215, was identified to function antagonistically against CLASP and Abl during embryonic central nervous system development (Lowery et al., 2010), while another genetic interaction study in flies identified *d-tacc* as an antagonist of CLASP (Long et al., 2013), reminiscent of the interaction between CLASP and TACC partner, *msps*. Combining these previous works with our findings on the role of TACC3 in axon outgrowth led us to ask whether TACC3 functions during axon guidance. As demonstrated in Fig 3.4A, our initial observations revealed that reduction in TACC3 levels impairs the normal organization of axons exiting the spinal cord in embryos at st 28. Stimulation of cultured *Xenopus* retinal neurons at stage 32 or beyond with bath-applied Slit2 has been shown to cause growth cone collapse (Piper et al., 2006). Additionally, spinal neurons derived from st 28 *Xenopus* embryos have been previously shown to be repelled by Slit2 (Stein and Tessier-Lavigne, 2001). Here, we found that Slit2-induced neural tube growth cone collapse events can be reduced by 60% in TACC3 overexpressing growth cones in comparison to control, suggesting an opposing role for TACC3 in Slit2-induced growth cone collapse. Based on its role in MT polymerization (Nwagbara et al., 2014), its co-dependent localization at MT plus ends with XMAP215 (Nwagbara et al., 2014) , and their interaction during axon outgrowth (Fig 3.3), we propose that TACC3 OE will excessively occupy MT ends subsequently driving increased recruitment of XMAP215, prompting enhanced MT polymerization in all directions. This global increase in MT polymerization would disturb local MT modulation, which is the underlying mechanism for growth cone steering events and it would result in an aberrant, non-obedient growth cone advance (Fig. 3.4F).

It remains to be determined whether these effects are specific to Slit2 or if TACC3 could exert similar opposing effects in response to other repellent signals, and/or if TACC3 mediates

attractive signals as well. Finally, other TACC members, namely, TACC1 and TACC2, have recently been characterized as +TIPs that can promote MT polymerization in *Xenopus* embryonic cells (Lucaj et al., 2015; Rutherford et al., 2016). Although their expression and MT regulatory function show cell type specificity, it would be intriguing to study whether other members of the TACC family also play a role in axon outgrowth and guidance decisions.

3.4 Materials and Methods

3.4.1 Xenopus embryonic explants

Egg collection and culturing of Xenopus embryonic explants (from embryos of either sex) were performed as described (Lowery et al., 2012; Nwagbara et al., 2014). All experiments were approved by the Boston College Institutional Animal Care and Use Committee and were performed according to national regulatory standards.

3.4.2 Constructs and RNA

Capped mRNA constructs were transcribed and purified as previously described (Lowery et al., 2013; Nwagbara et al., 2014) Constructs used were GFP-TACC3 (TACC3 pET30a was gift from the Richter lab, University of Massachusetts Medical School, Worcester, MA), GFP-TACC3-ΔN, GFP-TACC3-ΔΔN, GFP-TACC3-ΔTACC (see Figure 1E for amino acid residues for full length and each deletion construct, based on GenBank accession number NP-001081964.1) all TACC3 constructs were subcloned into pSC2+ vector. GFP-MACF 43 (a gift from Hoogenraad Lab) in pCS2+, XMAP215-GFP (a gift from the Hyman lab, Max Planck Institute of Molecular Cell Biology and Genetics, Dresden, Germany; (Widlund et al., 2011)) subcloned into pT7TS. Embryos either at 2 cell or 4 cell received injections 4 times total in 0.1X MMR containing 5% Ficoll with the following total mRNA amount per embryo; 100pg of GFP-MACF43 as a control for TACC3 or XMAP215 overexpression, 2000 pg of GFP-TACC3 full-length and deletion constructs deletion

constructs are expressed in wildtype embryos), 3000 pg of XMAP215. For double overexpression 1000 pg of TACC3 and XMAP215 were injected in total.

3.4.3 Morpholinos

Morpholinos (MOs) were previously described (Lowery et al., 2013; Nwagbara et al., 2014). In knockdown (KD) experiments, TACC3 and control MOs were injected at 80 ng/embryo. For TACC3 and XMAP215 double KD analysis, 20 ng/embryo for TACC3 and control MOs and 2 ng/embryo for XMAP215 MO were injected. In rescue experiments, MO (amounts used as in KD which is 80 ng/ embryo) was injected with mRNA (same amount as in OE which is 2000 pg / embryo for GFP-TACC3 and 3000pg/embryo for GFP-XMAP215) in the same injection solution. The efficacy of MOs has been previously assessed by Western blot of 35-36 stage embryos, as described (Lowery et al., 2013; Nwagbara et al., 2014).

3.4.4 Whole-mount immunohistochemistry

Two-day-old embryos were fixed as described (Lowery et al., 2013). Primary antibody (diluted in blocking buffer made up by 1% DMSO, 1% Triton, 1% BSA, in PBS) to acetylated tubulin (1:1000, monoclonal, clone 6-11B-1, Sigma, St. Louis, MO, USA) and goat anti-mouse Alexa-Fluor 568 conjugate secondary antibody (1:1000, polyclonal, A-1100, Life Technologies) were used. For imaging, the spinal cord was exposed by peeling off skin, and somites were kept intact. Embryos were transferred in a drop of benzoate:benzyl alcohol (BB:BA) to the imaging chamber (made by placing Gene Frame, sticky on both sides, onto a microscope slide). After the tissue was cleared, it was covered with a 1.5x coverslip. Image acquisition and quantitation of fixed and labeled explants were described previously (Lowery et al., 2013). TACC3 KD induced change is scored based on the percentage of embryos with disorganized axons in each condition.

3.4.5 Immunocytochemistry

Embryonic explant cultures were fixed and labelled (Challacombe et al., 1997) with primary antibodies (1:1000 diluted in blocking buffer made up by 1% non-fat dry milk in calcium and magnesium free PBS) to tyrosinated tubulin (rat monoclonal, ab6160, Abcam) and de-tyrosinated tubulin (rabbit polyclonal, AB3201, Millipore), and with the secondary antibodies goat anti-rat Alexa Fluor 568 (1:1000, ab175476, Abcam) and goat anti-rabbit Alexa Fluor 488 (1:1000, A-11008, Life Technologies), respectively.

3.4.6 Growth cone response assay

Recombinant mouse Slit2 protein (R&D Systems) (400 ng/ml) was administered to cultured neural tube explants derived from stage 28 Xenopus embryos in 400 µl culture media supplemented with 1% Penicillin/ Streptomycin and 0.1% BSA. A perfusion chamber was set up to exchange media with Slit2-containing culture media. Time-lapse images of growth cones were acquired for 10 min with 30 sec intervals before and immediately after Slit2 addition for 30 min with 30 sec intervals, using a Zeiss Axio Observer inverted motorized microscope with a Zeiss 20x/0.8 Plan Apo phase objective. Frame to frame axon growth was tracked manually and retraction or growth cone collapse events were recorded over a movie. Ratio of the number of retracting frames over total frames for each axon was scored. Images given in the figures show the image of growth cone right before adding Slit2 and the image growth cone at collapse.

3.4.7 Nocodazole application

Nocodazole to final concentration of 50pM was administered in 400 µl culture media (Nwagbara et al., 2014). Concentration of Nocodazole was determined after series of titrations and 50pM was found to be the optimum to keep the MTs intact in order to perform MT dynamics analyses. Time-lapse images of growth cones were acquired for 1 min with 2 sec intervals before and 5 min after

Nocodazole administration, using Yokogawa CSU-X1M 5000 spinning disk confocal on a Zeiss inverted motorized microscope with a Zeiss 63x Plan Apo 1.4 NA and a Hamamatsu ORCA R2 CCD camera. MT dynamics were assessed, as described (Nwagbara et al., 2014).

3.4.8 PlusTipTracker software analysis

MT dynamics were analyzed from GFP-MACF43 movies using plusTipTracker (Applegate et al., 2011; Lowery et al., 2012). Imaging conditions and tracking parameters were previously validated and same parameters were used: maximum gap length is 8 frames; minimum track length is 3 frames; search radius range 5-12 pixels; maximum forward angle, 50˚, maximum backward angle, 10˚; maximum shrinkage factor, 0.8; fluctuation radius, 2.5 pixels; time interval, 2s. MT growth lifetime is the measure of persistent outgrowth till MT undergoes catastrophe. MT growth length is the total growth over a movie and MT growth velocity is the average of each MT growth event. MT dynamics parameters were compiled from multiple individual experiments and to avoid day-to-day fluctuations the final complied data were normalized to the mean of the control data for each experiment.

3.4.9 Image acquisition and analysis

For axon outgrowth imaging, phase contrast images of axons were collected on a Zeiss Axio Observer inverted motorized microscope with a Zeiss 20x/0.5 Plan Apo phase objective and analyzed using ImageJ (Nwagbara et al., 2014). Time-lapse images for axon outgrowth velocity was collected for 4 hours with 20 min intervals and images were analyzed using plusTipTracker QFSM plugin and velocity was measured as the average of instantaneous velocity per axon as described (Lowery et al., 2013). Axon retraction events were analyzed from the same data set used to assess axon growth velocity. Frame to frame axon growth was tracked manually and retraction

events were recorded over a movie. Ratio of the number of retracting frames over total frames for each axon was scored.

Axon outgrowth and MT dynamics data were normalized to controls, to account for day-to-day fluctuations in room temperature. Image acquisition and quantitation of fluorescence intensity of fixed and labeled explants were described previously (Nwagbara et al., 2014). Experiments were performed multiple times to ensure reproducibility. Graphs were made in GraphPad Prism. Statistical differences were determined using unpaired two tailed t-tests when comparing two conditions and one-way analysis of variance with Tukey's post-hoc analysis when multiple conditions were compared.

Chapter 4

Abelson induced phosphorylation of TACC3 modulates its interaction with microtubules and affect its impact on axon outgrowth and guidance

The content in this chapter was adapted from the following unpublished manuscript:

Erdogan B., St-Clair R., Zaccaro T., Cammarata G.M., Ballif B., Lowery L.A. Abelson induced phosphorylation of TACC3 modulates its interaction with microtubules and affect its impact on axon outgrowth and guidance (in preparation)

4.1 Introduction

Regulation of cytoskeletal dynamics within the growth cone is essential for growth cone motility and navigation as the axon travels to its target. Guidance molecules that the growth cone encounters during its trip can act as repellent or attractant depending on the time, location and the signal composition of the environment that the growth cone passes. Integration and interpretation of these signals relies on signaling cascades that are initiated downstream of guidance cue receptors which will ultimately converge upon cytoskeletal elements for their rearrangements and initiation of growth cone motility.

Guidance signals are not homogeneously presented to the growth cone *in vivo*. While the growth cone might be exposed to repellent signals on one side, it can be exposed to attractant signals on the other side, which necessitates the asymmetric reorganization of the underlying cytoskeleton. In order to manage this asymmetric regulation, signals received by guidance cue receptors must be processed locally and immediately downstream of the site that the signal is received without necessarily leading to a global response. For example, repulsive guidance cues can cause a global growth cone collapse when they are bath applied, whereas their local application causes collapse on the side that the protein is received, which results in growth cone steering away from the source of the signal.

The immediate interaction between guidance cue receptors and downstream effectors required for asymmetrical remodeling make microtubule plus-end tracking proteins (+TIPs) a great target for their close proximity within the growth cone periphery. Retaining their interaction with microtubules at the plus-ends is important for regulating microtubule growth dynamics and signal exchange between the growth cone periphery and the central domain.

The interaction between +TIPs and microtubules can be modulated by guidance signals and the intracellular signaling events initiated downstream. Phosphorylation of +TIPs is one such event that has been shown to modulate +TIP affinity for microtubules. For example, affinity of CLASP for microtubules has been shown to be regulated differentially in the growth cone depending on its phosphorylation status by GSK3 kinase. Increased microtubule lattice binding activity of CLASP, as a result of GSK3 inhibition, results in axon growth inhibition through inhibition of MT advance into the growth cone periphery. On the other hand, plus-end binding of CLASP, as a result of GSK3 activity, promotes axon outgrowth via stabilization of microtubules (Hur et al., 2011).

In addition to GSK3, CLASP is also identified as a target for Abelson (Abl) tyrosine kinase. Expression of Slit along the neural cord midline restricts axon fascicles to either side of the midline. Ectopic midline crossing of axon fascicles, which is observed in Abl loss-of-function mutants, is also phenocopied by *orbit/MAST* (fly ortholog of human CLASP) mutants in *Drosophila* embryos, suggesting a genetic interaction between the two genes. This also positions CLASP as a potential target downstream of the Slit2 pathway (Lee et al., 2004). Further examination of the interaction between CLASP and Abl in *Xenopus* spinal neurons identified CLASP as a target for Abl phosphorylation and showed that phosphorylation can affect CLASP localization in neuronal growth cones (Lee et al., 2004).

Similar to CLASP, several +TIPs have been implicated to be involved in microtubule dynamics regulation during directional movement of cells and growth cones (Bearce et al., 2015). However, only a few of them have been studied and implicated as a target for guidance cue-initiated intracellular signals (Bearce et al., 2015). We have previously characterized a microtubule plus-end tracking function for TACC3 in neuronal growth cones and showed that TACC3

overexpression enhances microtubule growth dynamics and promotes axon outgrowth (Nwagbara et al., 2014). Additionally, we have proposed a function for TACC3 during axon guidance. Reducing levels of TACC3 resulted in disorganized axon elongation of neural tube neurons in *Xenopus laevis* embryos and its overexpression mitigated growth cone collapse induced by bath applied Slit2 in cultured neural tube explants (Erdogan et al., 2017). To further investigate the mechanism of how TACC3 overexpression exerts this opposing role against Slit2 activity, we became interested in looking at potential phosphorylation events that might target TACC3.

In a genetic and proteomic screen performed in flies, CLASP was identified as an interactor of microtubule polymerase XMAP215 as well as TACC3. The same study also identified XMAP215 as a genetic interactor of Abelson kinase. XMAP215, which is a well-studied physical interactor of TACC3, led us to question whether TACC3 might be an interactor of Abelson kinase (Lowery et al., 2010).Thus, we become interested in testing whether TACC3 could be a target for Abl phosphorylation downstream of Slit2 and whether its phosphorylation status would alter TACC3's interaction with microtubules and hence TACC3's impact on axon outgrowth and guidance.

4.2 Results

4.2.1 Abelson kinase induces phosphorylation of TACC3

To investigate whether Abelson kinase (Abl) induces phosphorylation of TACC3, we co-expressed GFP-TACC3 and Abl in HEK293 cells. Tyrosine phosphorylation of TACC3, following GFP immunoprecipitation of GFP-TACC3, was observed with 4G10, an antibody that specifically labels phosphorylated tyrosine residues (Fig.4.1A, lane 4). Phosphorylation of TACC3 was only observed when it is co-expressed with Abl (Fig.4.1A, lane 3 vs lane 4). Additionally, this phosphorylation specifically happens with Abl, since Fyn, which is another

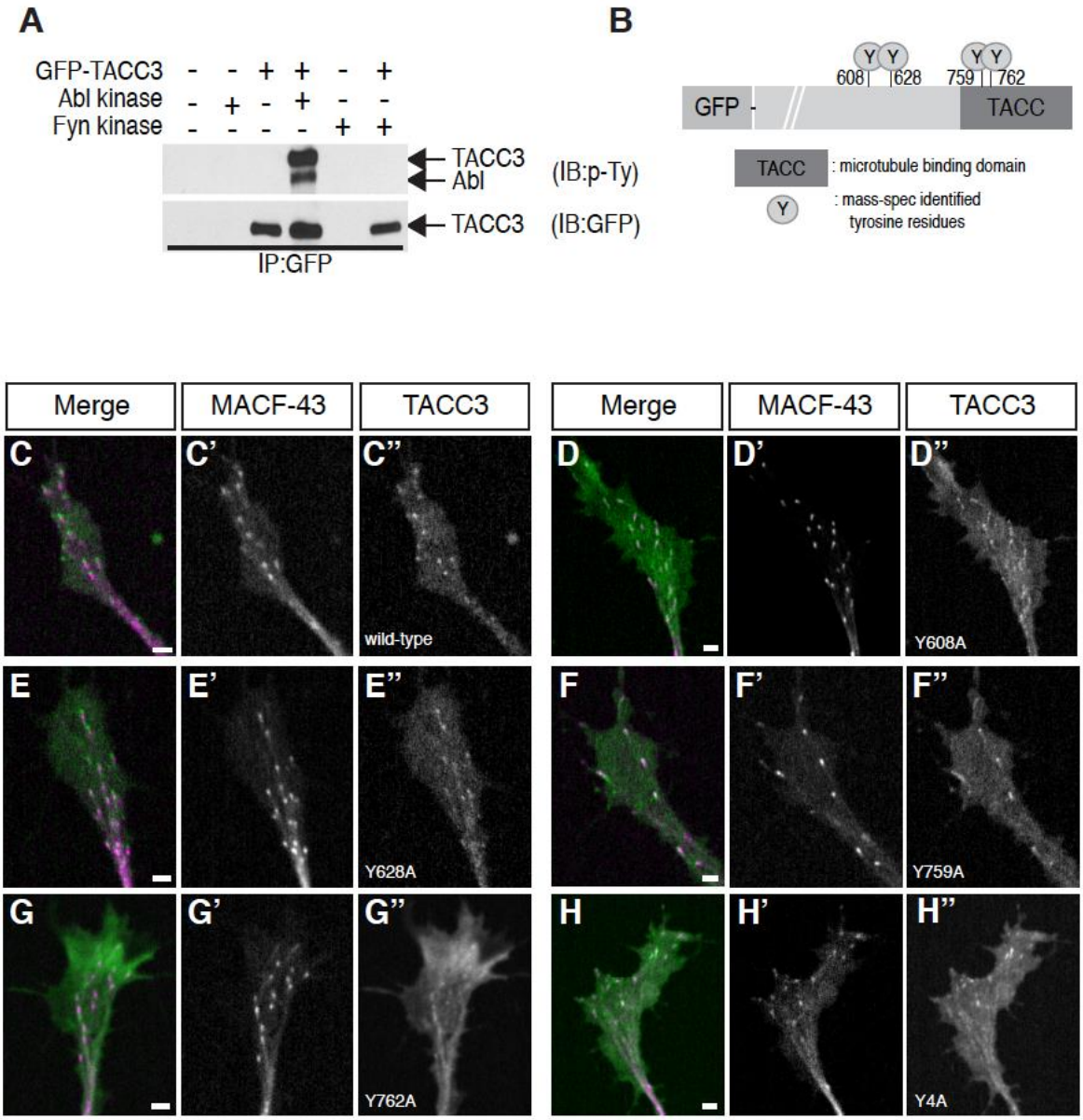

Figure 4.1 Abelson kinase induces phosphorylation of TACC3

(A) Western blot performed with phospho-tyrosine specific antibody showing Abelson-induced tyrosine phosphorylation of full-length TACC3 (lane 4). Phosphorylation signal is not present when TACC3 is expressed alone (lane 2) or with another tyrosine kinase Fyn (lane 6). (B) Cartoon showing mass-spec-identified tyrosine residues of TACC3 targeted by Abl phosphorylation. (C-G) Confocal images of growth cones expressing MACF-43 (magenta) and TACC3 (green) with phospho-null mutations at identified residues showing localization of TACC3 phospho-null mutants to microtubules. (H) Western blot performed with phospho-tyrosine specific antibody showing no change in Abelson induced tyrosine phosphorylation levels between wild-type TACC3 (lane 4) and phospho-null mutant TACC3 (lane 5) with all four mass-spec identified tyrosine residues mutated to alanine (Y4A).

tyrosine kinase, does not induce TACC3 tyrosine phosphorylation (Fig.4.1A, lane 6). Although it is not determined whether this induced tyrosine phosphorylation is a result of direct interaction between Abl and TACC3 or not, these data show that Abl is involved in inducing TACC3 tyrosine phosphorylation.

In order to study the role of TACC3 phosphorylation, we next wanted to identify the tyrosine residues that are targeted by Abl. Mass - spec analysis of full-length TACC3 identified 4 tyrosine residues: two (Y759, Y762) in the conserved TACC domain, the domain that is responsible for microtubule plus-end binding, and two (Y608, Y628) outside of the TACC domain (Fig. 4.1B).

To assess the importance of these tyrosine residues, we generated single and combinatorial phospho-null mutants by substituting tyrosine with alanine or phenylalanine. However, neither single nor combinatorial phospho-null mutations caused a reduction in tyrosine phosphorylation levels, determined by Western blot analysis (Fig.4.2 A-D). Moreover, all of the single and combinatorial mutants were still able to track microtubule plus-ends (Fig. 4.1 C-H Supplemental Movie 12-17). This initial examination suggests that other tyrosine residues might also be getting phosphorylated and contributing to the overall phospho-tyrosine signal detected by Western blot.

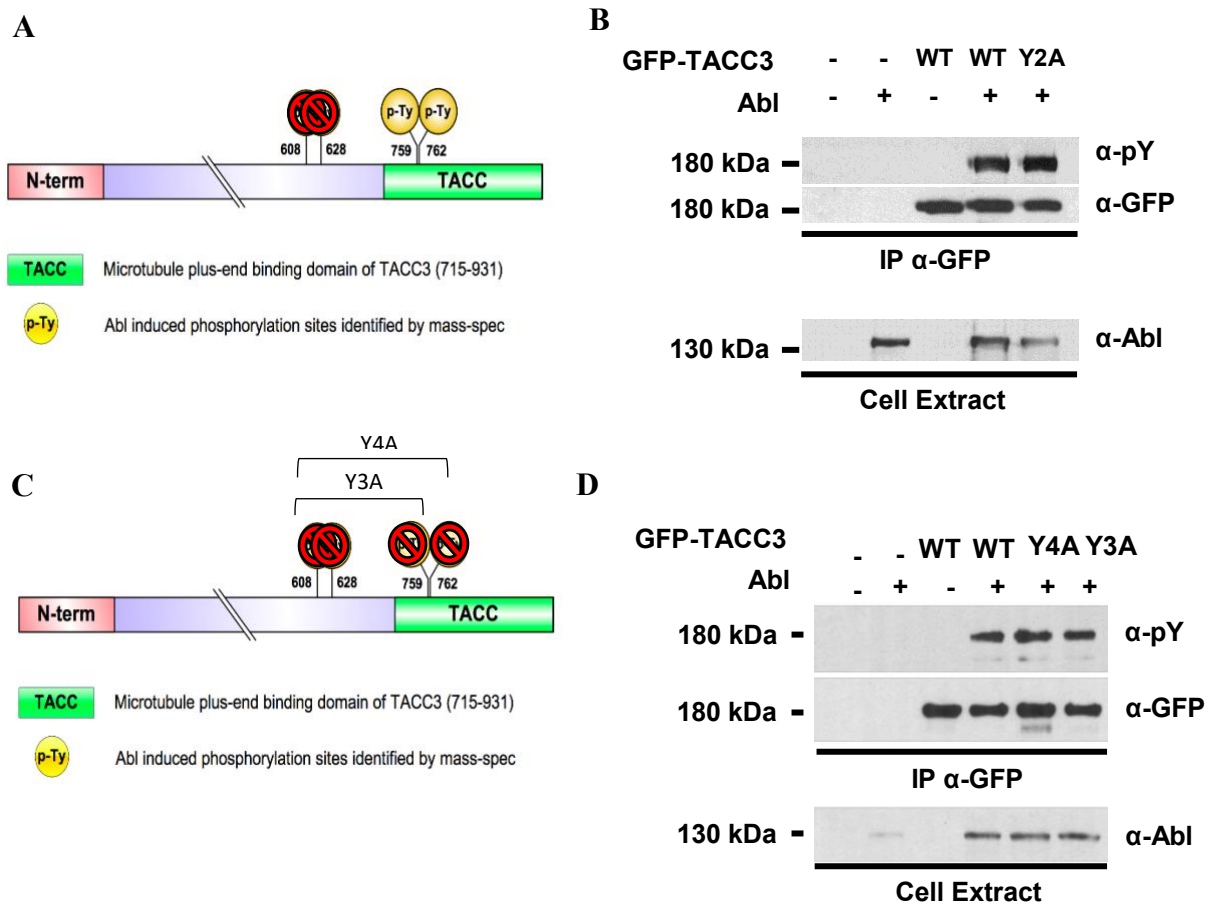

Figure 4.2 Phospho-null mutations at Mass-spec identified Abelson targeting tyrosine residues do not show reduction in phosphor-tyrosine signal levels detected by western blot.

(A-C) Schematic representation of TACC3 full-length protein showing potential tyrosine residues (Y608, Y628, Y759, Y762) targeted for Abelson induced phosphorylation. Combinatorial phospho-null mutants were created for sites Y608 and Y628 (Y2A) (A) or for sites Y608A, Y628A andY759A (Y3A) or for all Y4A (C), by substituting tyrosine residues with alanine (indicated by red circle with cross). (B-D) Western blot performed with phospho-tyrosine specific antibody (p-Ty) showing Abelson induced tyrosine phosphorylation of immunoprecipitated full-length wild-type and phospho-null mutant GFP-TACC3 in the presence of Abelson kinase (top blot). α-GFP shows the expression level of GFP-TACC3 (middle blot) and α-Abl shows the expression of Abelson kinase (bottom blot). Phosphorylation signal is still present to similar extent as compared to wild type (lane 4) when mass-spec identified tyrosine residues are substituted with alanine Y2A, lane 5 (B) Y4A, lane 5; Y3A, lane 6 (D).

4.2.2 Tyrosine phospho-null mutations in the TACC domain impairs the localization of TACC3 at microtubule plus-ends in growth cones and mesenchymal cells

Since none of the phospho-null mutants of mass-spec identified tyrosine residues showed a reduction in phosphorylation signal and they were still able to localize to microtubules, we decided to examine other tyrosine residues. The full-length TACC3 possesses a total of 11 tyrosine residues throughout the entire protein. Six of these tyrosine residues (Y725, Y759, Y762, Y832, Y846, Y857) are in the TACC domain (aa715-aa931), one (Y130) is in the N-terminal domain (aa1-aa133), and four (Y320, Y428, Y608, Y628) are in the middle domain (aa134-aa634) (Fig. 4.3).

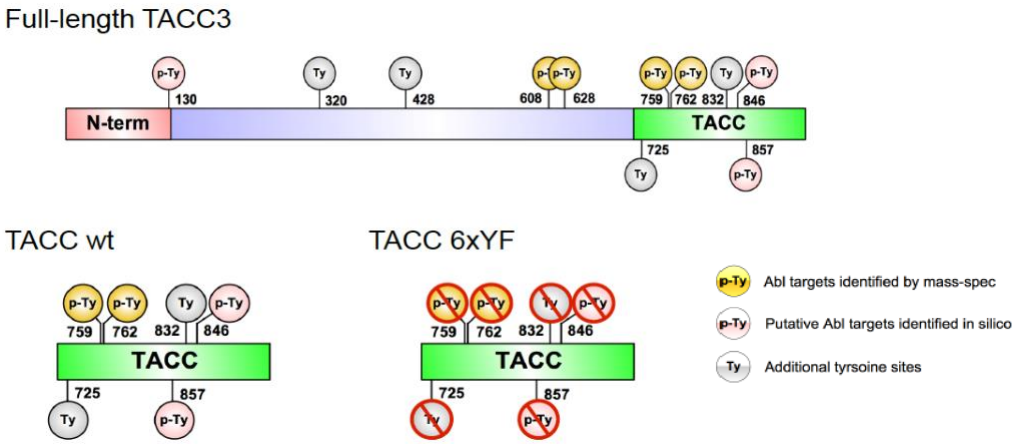

Figure 4.3 Cartoon depicting the tyrosine residues (Y) found in full length TACC3 and in the truncated TACC domain, which are mutated into phenylalanine to block phosphorylation.

The TACC domain of the TACC3 protein shows high sequence similarity among vertebrates as well as among other TACC family members (Peset and Vernos, 2008). Moreover, the TACC domain is the portion of the TACC3 protein that is responsible for its microtubule plus-end tracking behavior (Nwagbara et al., 2014) and also for interacting with microtubule polymerase XMAP215 (Mortuza et al., 2014). Therefore, we decided to investigate the importance

of tyrosine residues within the TACC domain to see whether they might be contributing to the Abl-induced phosphorylation we observed earlier. To investigate this, we mutated all of the tyrosine residues to phenylalanine within the TACC domain and tested these mutants for their phosphorylation status. Interestingly, despite lacking a phosphorylatable tyrosine with the TACC sequence, GFP-TACC phospho null (p-null) mutants showed similar phospho-tyrosine signals compared to the wild-type TACC domain, as verified with Western blot (Fig.4.4 B). Since there are no tyrosines left in the TACC domain. the only other source that might contribute to that signal could be GFP. Therefore, we performed a Western blot for the GFP tag alone with a phospho-tyrosine specific antibody, and we found that GFP was indeed getting phosphorylated in the presence of Abelson (Fig.4.4 D). Thus, GFP itself was probably contributing to the overall signal that we obtained with the GFP-tagged TACC constructs previously.

While we do not know the exact mechanism of how TACC3 gets phosphorylated by Abelson, we found that both full length TACC3 (data not shown) and TACC domain-only constructs showed changes in their microtubule localization behavior when they had tyrosine phospho-null (p-null) mutations (Fig. 4.5 A-B, Supplemental Movie 18-19). In both neuronal growth cones and mesenchymal cells isolated from *Xenopus* embryos, TACC p-null mutants showed less localization along microtubules, determined by line-scan averages of fluorescent intensities obtained from microtubule plus-ends (Fig. 4.5 C-D, G). TACC p-null mutant remained cytoplasmic in 80% of the growth cones and showed microtubule localization in 20% of the growth cones examined while wild-type TACC localized at microtubule plus-ends in 92.5% of growth cones examined (Fig. 4.5 F). We also confirmed the expression by Western blot and showed that the GFP-TACC mutant expression was comparable to GFP-TACC (Fig. 4.5E). These data suggest

that retaining phosphorylatable tyrosines within the TACC domain is important for TACC localization along microtubules.

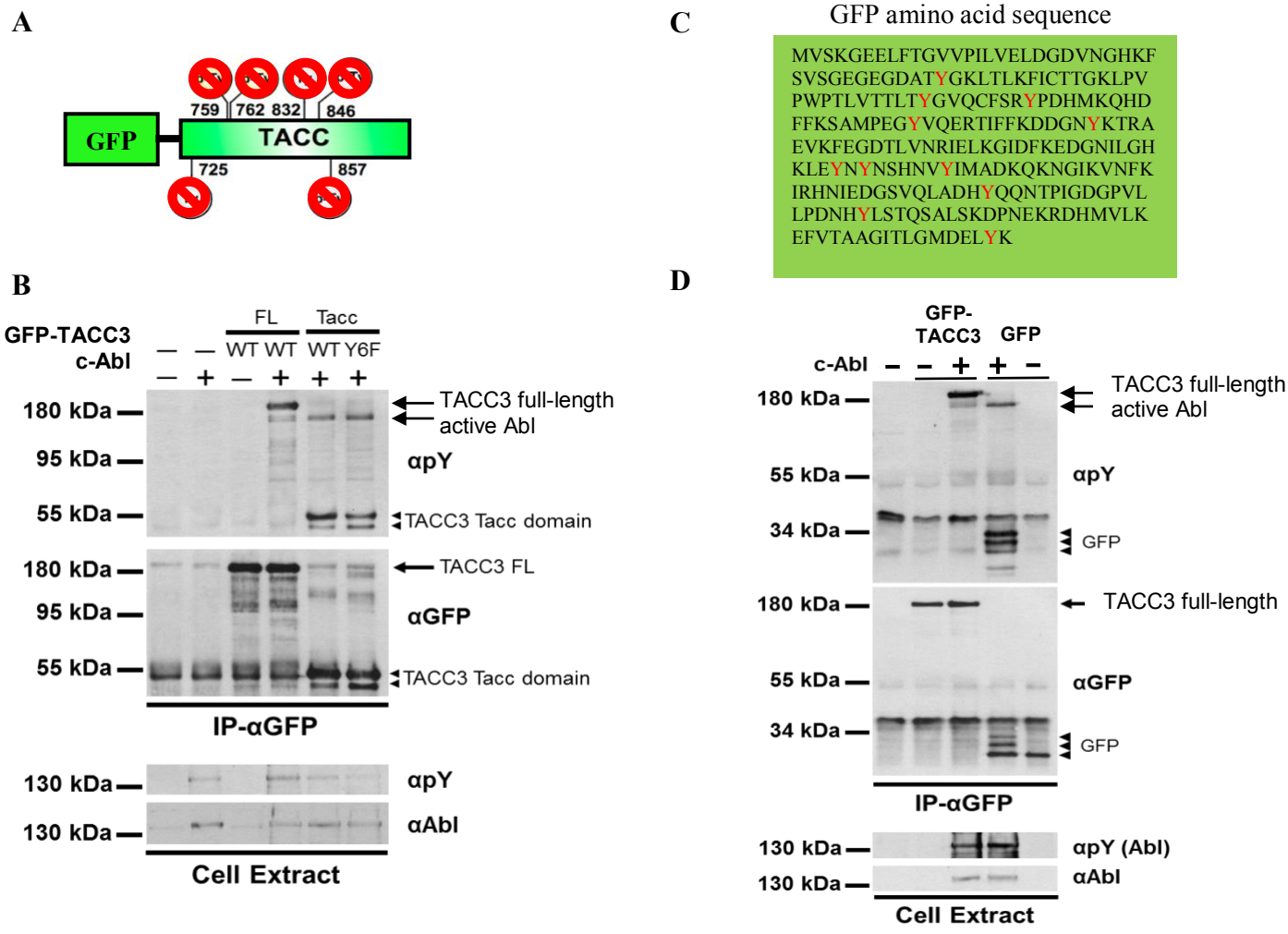

Figure 4.4 GFP gets phosphorylated in the presence of Abelson kinase and contributes to p-Ty signal obtained with TACC domain tyrosine phospho-null mutant

(A) Schematic representation of GFP-TACC domain showing potential tyrosine residues (Y725, Y759, Y762, Y832, Y846 and Y857) targeted for Abelson induced phosphorylation. Red circle with cross indicates that these residues are substituted with non-phosphorylatable phenylalanine. (B) Western blot performed with phospho-tyrosine specific antibody (αpY, top blot) showing tyrosine phosphorylation levels of immunoprecipitated wild-type full-length GFP-TACC3 with (lane 4, arrow) and without (lane 3, arrow) Abelson kinase and GFP-TACC domain wild-type (lane 5, arrow head) and phospho-null mutant (Y6F, lane6, arrow head) with Abelson kinase. Phosphorylation signal is still present in GFP-TACC phospho null mutant (lane6) to a similar extent as compared to wild type TACC domain (lane 5). 2nd blot from top targeted with α-GFP shows the expression level of GFP-TACC3 and GFP-TACC domain. 3rd blot from top targeted with α-pY shows the phosphorylation levels of Abelson kinase and bottom blot targeted with α-Abl shows the expression of Abelson kinase. IP-αGFP; indicate immunoprecipitation is performed

with anti GFP antibody. (C) Amino acid sequence of GFP, tyrosine residues (Y) are indicated in red. (D) Western blot performed with phospho-tyrosine specific antibody (αpY, top blot) showing tyrosine phosphorylation levels of immunoprecipitated wild-type full-length GFP-TACC3 with (lane 3) and without (lane 2) Abelson kinase and GFP with (lane 4) and without (lane 5) Abelson kinase. Bands on lane 4 pointed with arrowheads demonstrating phosphorylated GFP in the presence of Abelson. 2nd blot from top targeted with α-GFP shows the expression of GFP-TACC3 (arrow) and GFP (arrow head). 3rd blot from top targeted with α-pY shows the phosphorylation levels of Abelson kinase and bottom blot targeted with α-Abl shows the expression of Abelson kinase. IP-αGFP; indicates immunoprecipitation is performed with anti GFP antibody.

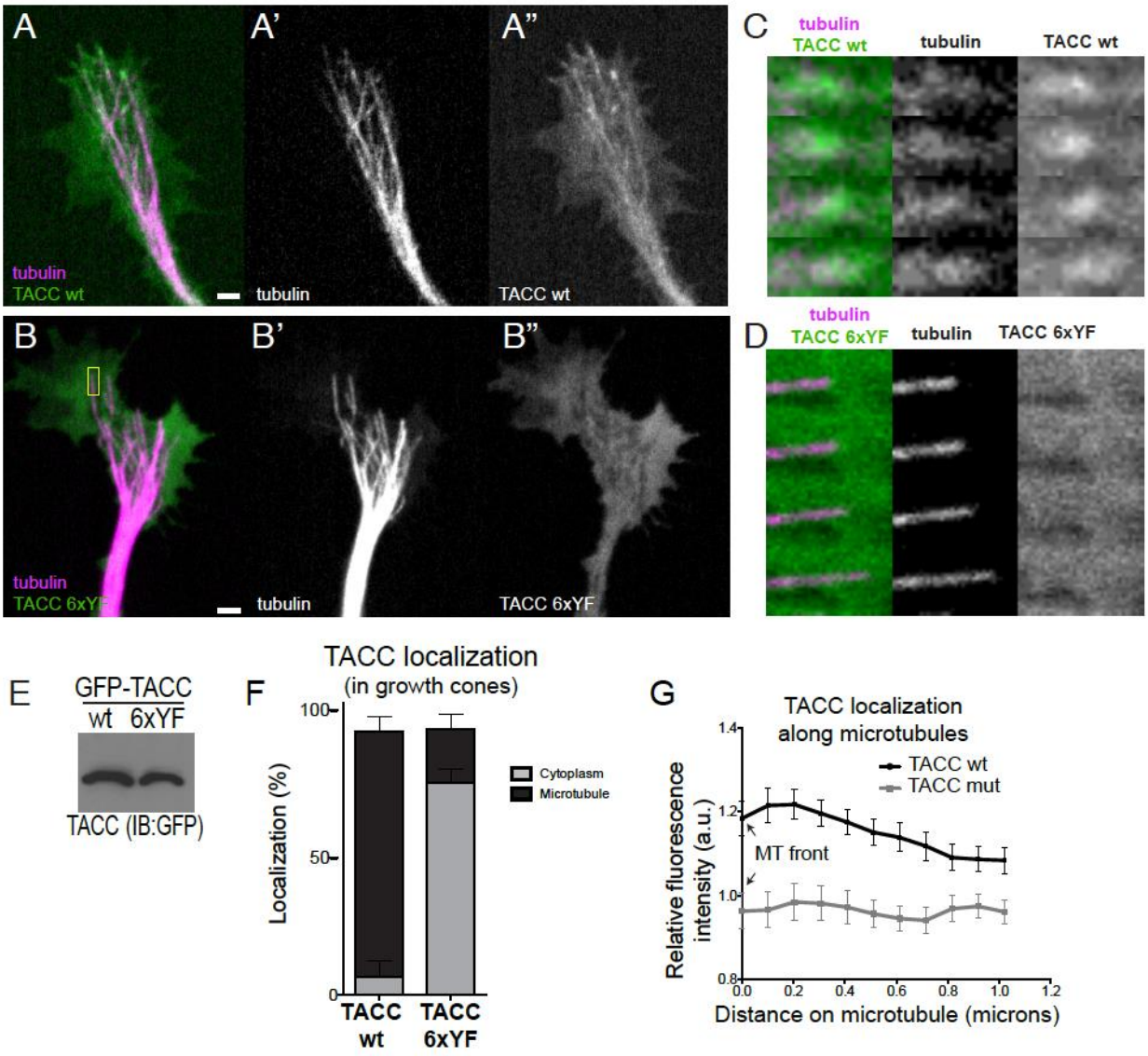

Figure 4.5 Tyrosine phospho-null mutations impairs the localization of TACC domain at microtubule plus-ends in growth cones and mesenchymal cells

(A-B) Confocal images of neuronal growth cones, obtained from time-lapse recordings expressing tubulin (magenta) (A', B') and TACC (green) wild-type (A") or tyrosine phospho-null mutant (B"). (C-D)

Magnified montages of time-lapse sequences of the boxed regions in B-C respectively. TACC wild-type (green) localizes to microtubule (magenta) plus-ends (C) while TACC tyrosine phospho-null mutant (green) is absent from microtubule (magenta) plus-ends and remains mostly cytoplasmic (D). (E) Western blot performed with GFP antibody showing the expression of GFP-TACC wild-type and GFP-TACC p-null mutant. (F) Plot showing the quantification of microtubule plus-end versus cytoplasmic localization of TACC constructs within the growth cones as percentage of total growth cones examined. On average, TACC wild-type shows microtubule plus-end binding in 92.5% of the growth cones examined while TACC tyrosine p-null mutant showed plus-end localization in 20% of the growth cones and remained mostly cytoplasmic in 80% of the growth cones examined. (G) Fluorescent intensity profile (y-axis) along microtubules (x-axis) determined by line-scan analysis showing green fluorescent intensity (TACC wt or TACC p-null mutant) relative to background. Line is drawn starting from the beginning of the microtubule plus-end. Scale bar, 2μm.

4.2.3 Tyrosine phospho-null mutations in the TACC domain affect microtubule dynamics regulation

We next wanted to investigate the impact of the reduced interaction between the phospho-null TACC mutant and microtubules, as pertaining to microtubule dynamics parameters such as microtubule growth speed, lifetime and length. Interestingly, despite lacking an interaction with microtubules, over-expression of the TACC p-null mutant significantly increased microtubule growth speed by 10% and microtubule growth length by 17% compared to control growth cones (Fig. 4.6A-C), while over-expression of wild-type TACC domain increased microtubule growth speed by 4% and growth length by 17%. Microtubule growth lifetime, on the other hand, was not affected by the mutant TACC while wild-type TACC increased it by 11%. None of the microtubule dynamics parameters, however, differed significantly between the wild-type and mutant TACC conditions. GFP-MACF43 comet morphology and linearity of microtubule growth track seemed to be similar in control, TACC wild-type and TACC phospho-null mutants (Fig. 4.6 D-F, Supplemental Movie 20-22). Given that the TACC mutant cannot bind well to microtubules, these observations raise the possibility that the TACC mutant might be contributing to changes in microtubule dynamics via a mechanism that is independent of a requirement for an interaction with microtubules.

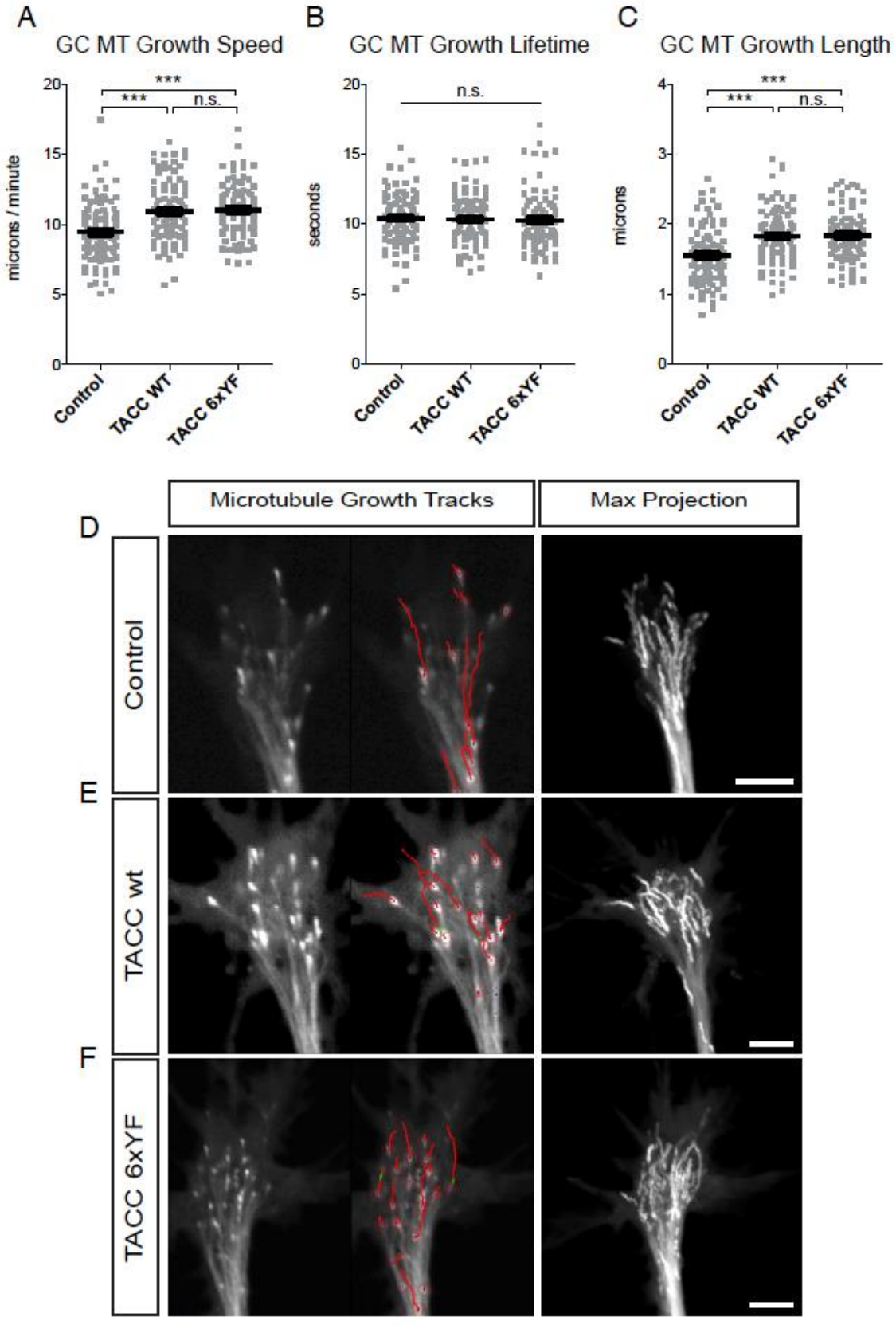
A
GC MT Growth Speed
microns / minute
20
15
10
5
0
***
***
n.s.
Control
TACC WT
TACC 6xYF
B
GC MT Growth Lifetime
seconds
20
15
10
5
0
n.s.
Control
TACC WT
TACC 6xYF
C
GC MT Growth Length
microns
4
3
2
1
0
***
***
n.s.
Control
TACC WT
TACC 6xYF
Microtubule Growth Tracks
Max Projection
D
Control
E
TACC wt
F
TACC 6xYF

Figure 4.6 TACC phospho- null mutant increases microtubule growth speed and length compared to control while do not show difference compared to TACC wild-type

(A-C) Quantification of MT growth parameters in cultured neuronal growth cones (GC) isolated from embryonic spinal cord expressing TACC wt and TACC phospho-null mutant. Automated plusTipTracker based tracking of GFP-MACF-43 comets (D-F) calculate MT growth speed (A), lifetime (B) and length (C) from time-lapse videos taken for 1 min with 2 sec intervals. Mean values of parameters obtained from three independent experiments: GC MT growth speed, control (MACF-43 only), 9.0 microns/min; TACC wt, 10 microns/min; TACC p-null, 10.5 microns/min. GC MT growth lifetime, control, 10.2 s; TACC wt, 10.7 s; TACC p-null, 10.2 s. GC MT growth length, control, 1.4 microns, TACC wt 1.7 microns, TACC p-null 1.7 microns. TACC phospho-null mutant increased microtubule growth speed and length by 10% (**p) and 17%(***p) respectively compared to control growth cones while doesn't differ significantly from TACC wt. TACC wt expressing growth cones on the other hand increases speed by 4% (n.s.) and length by 17% (***p). Microtubule growth lifetime on the other hand is not affected by TACC p-null while TACC wt increases it by 10% (***p). Control data represents 53; TACC wt represents 57 and TACC p-null mutant represents 46 growth cones combined from three independent experiments. The asterisk (*) indicates statistical significance with $\alpha < 0.05$ * $P < 0.05$, ** $P < 0.01$, **** $P < 0.0001$, ns: not significant, from an ANOVA analysis comparing multiple conditions with Tukey's post hoc analysis. Scale bar, 5μm.

Since microtubule growth dynamics are critical for axon elongation, we next wanted to examine whether the increased microtubule growth speed and length seen with overexpression of the TACC domains might be translated into increased axon elongation.

4.2.4 TACC tyrosine phospho-null mutant-expressing axons grow less persistently, thereby resulting in shorter axons compared to TACC wild-type-expressing axons

We have previously shown that TACC3 is important for promoting axon outgrowth (Nwagbara et al., 2014). To test whether phosphorylation is important in regulating axon outgrowth parameters, we measured the length of axons in cultured *Xenopus laevis* neural tube explants of TACC wt and TACC p-null mutant. While expression of TACC wt led to formation of longer axons, expression of the TACC p-null mutant (0.8563 ± 0.04222 N=155) showed a 16.8% reduction in axon length compared to control (1.000 ± 0.03446 N=277) and 34% reduction compared to TACC wt (1.147 ± 0.05667 N=199) (Fig. 4.7A).

To further assess the difference in axon length between the TACC wt and p-null mutant, we measured the axon growth velocity. We found that the average normalized axon forward

movement velocity was 8% faster in TACC p-null mutant conditions (1.089 ± 0.02725 N=172, *p) compared to control (1.000 ± 0.02020 N=198) and 3.5% slower, compared to TACC wt (1.127 ± 0.02517 N=217, not significant). Average growth velocity in TACC wt-expressing axons on the other hand was 10% faster compared to control axons (Fig. 4.7B). Our data suggests that TACC p-null mutant-expressing axons grow with similar rates, as compared to TACC wt, while they grow faster compared to controls, suggesting that the reduced axon length could be due to another parameter of axon growth than simply growth velocity.

To further investigate this, we also tracked the growth behavior of axons and recorded the number of frames that they moved forward, paused and/or retracted over the course of 4h long time lapse imaging with 5 min intervals (Fig 4.7C, Supplemental Movie 23-24). We found that TACC p-null mutant-expressing axons (69.61 ± 1.686 N=168) spent 18% less time moving forward compared to controls (82.30 ± 1.538 N=183, ***p) and 12% less compared to TACC wt (78.20 ± 1.373 N=218, ***p) (Fig 4.7D, green dots). Additionally, TACC p-null mutant axons (20.20 ± 1.150 N=168) spent 42% more time pausing compared to controls (11.67 ± 1.002 N=183, ***p) and 27% more compared to TACC wt 14.67 ± 0.9787 N=218, ***p) (Fig 4.7D, orange dots). They also tended to retract more frequently: 39% compared to controls (6.125 ± 0.8957 N=183) and 30% compared to TACC wt (7.098 ± 0.6700 N=218) (Fig 4.7D, red dots, Supplemental Movie 25). TACC wt expressing axons also demonstrated less forward movement compared to control (by 5%) but it was not statistically significant. TACC wt also showed slightly more pausing (by 21%) and retraction (by 13%) but, again, the difference was not significant with those parameters either (Fig. 4.7D).

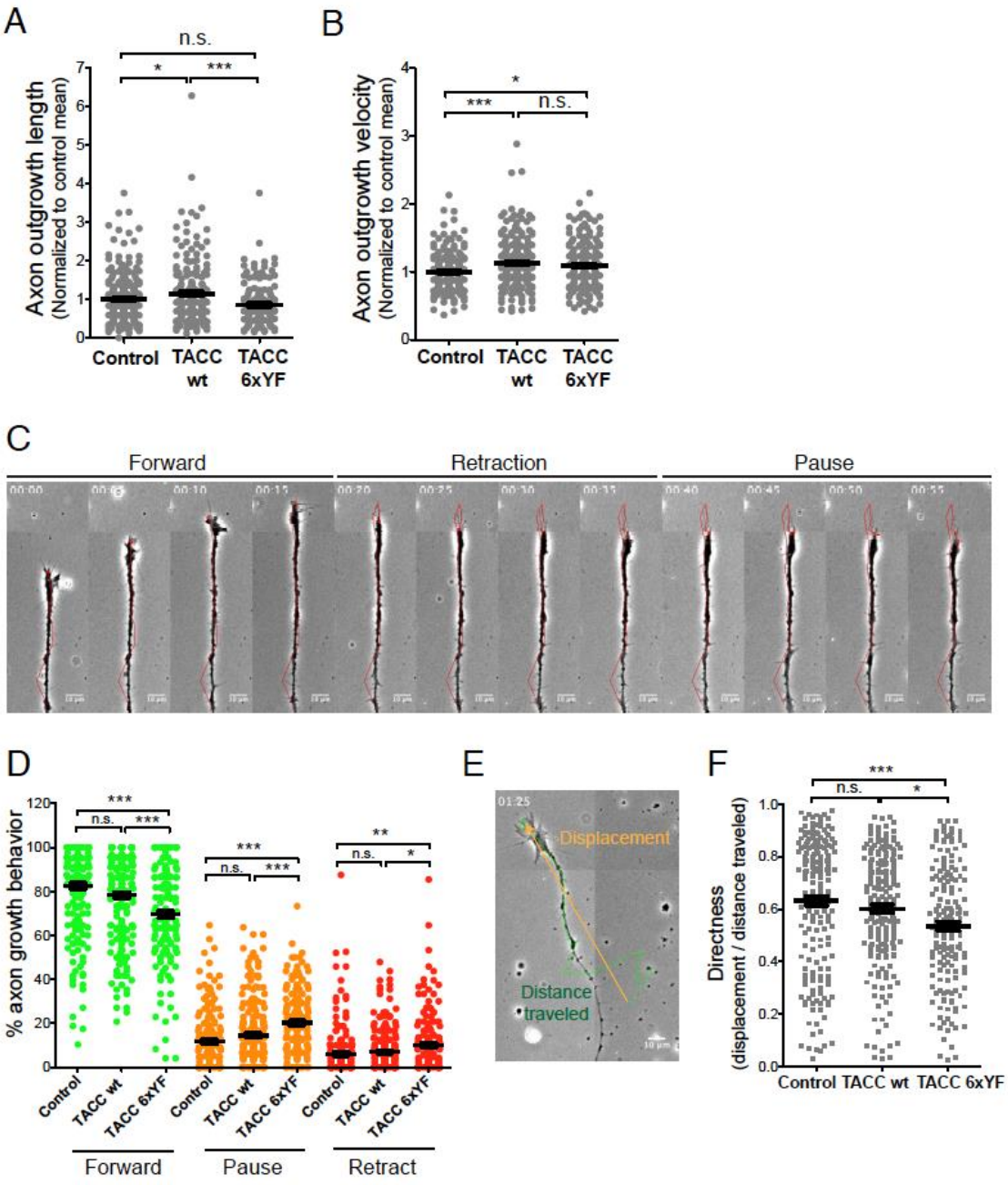

Figure 4.7 TACC tyrosine p-null mutant expressing axons grow less persistently thereby grow shorter axons compared to TACC wt axons

(A) Quantification of axon length in cultured neural tube explants shows TACC p-null mutant expressing neurons grow axons shorter by 16.8% compared to control and 34% compared to TACC wt, while TACC wt expressing explants grow axons longer by 12.8% compared to control. (B) Measurement of axon forward movement velocity showing TACC wt increases axon forward movement velocity by 10% compared to control while TACC p-null mutant increases by 8%. (C) Representative phase contrast image montage of an axon depicting phases of forward movement, retraction and pause. (D) Plot showing the percentage of forward movement (green), pause (orange) and retraction (red) of axon growth. TACC p-null mutant expressing axons spend 18% less time moving forward compared to control and 12% compared to TACC

wt (green dots). TACC p-null mutant axons (20.20 ± 1.150 N=168) spent 42% more time pausing compared to control and 27% compared to TACC wt (orange dots). They also tend to retract more frequently; 39% compared to control and 30% compared to TACC wt. (E) Representative image of an axon growth track depicting displacement and distance traveled between t=0 and t=1h 25min (F) Plot showing the directness of axon growth. TACC p-null mutant axons grow 12% less directly compared to TACC wt) and 17% compared to control axons. TACC wt axons also grow 5% less directly compared to control but it was not significant. The asterisk (*) indicates statistical significance with $\alpha < 0.05$ * $P < 0.05$, ** $P < 0.01$, **** $P < 0.0001$, ns: not significant, from an ANOVA analysis comparing multiple conditions with Tukey's post hoc analysis. Values given are mean of normalized data pooled from independent experiments.

In addition to pause and frequency rates, we also examined the directness of axon outgrowth. The still images of neural tube explants that were used to measure axon length shows the displacement of an axon. However, axons do not necessarily follow a linear trajectory as they grow. In fact, they often spend time wandering, which is part of their exploratory behavior. Therefore, the directness of growth can be determined by dividing the displacement distance by the total distance traveled (Fig. 4.7E). We found that TACC p-null mutant axons (0.5353 ± 0.01649 N=179) grow 12% less directly compared to TACC wt (0.6012 ± 0.01575 N=195) and 17% less compared to control (0.6313 ± 0.01813 N=192) axons. TACC wt axons also grow 5% less directly compared to controls but it was not significant (Fig. 4.7F).

These data suggest that while axon growth speed is not affected by TACC tyrosine phospho-null mutations, growth persistency, which is determined by pause and retraction frequency, and growth directionality, seemed to be impaired in TACC p-null mutant expressing axons. Thus, this could explain the shorter axon length that we observed in TACC p-null mutant-expressing neural tube explants.

4.2.5 TACC tyrosine phospho-null mutants increase the number of filopodia that contain microtubules

Dynamic regulation of microtubules is key to growth cone protrusion and, thus, axon outgrowth. It is intriguing that while the TACC p-null mutant is able to increase microtubule

growth speed and length, it fails to promote axon growth. Moreover, axons of neurons expressing TACC p-null mutant tend to stop and retract more frequently compared to those expressing wild-type TACC. Additionally, we observe that their growth is less directed compared to TACC wt and controls. An inverse correlation between growth cone advance rate and growth cone size has been reported previously (Ren and Suter, 2016). Enlarged growth cones are often associated with slowly protruding and less dynamic growth cones. Therefore, we became interested in examining the growth cone size, along with other morphological features, to see whether increased pause and retraction rates in TACC p-null mutant-expressing growth cones might exhibit changes in growth cone morphology. We initially examined the growth cone area (Fig, 4.8a), filopodia length (Fig, 4.8b), and filopodia number (Fig, 4.8c) in cultured neural tube explants that are fixed and stained for microtubules (tubulin) and actin (phalloidin) followed by high resolution Structured Illumination Microscopy (SIM) imaging

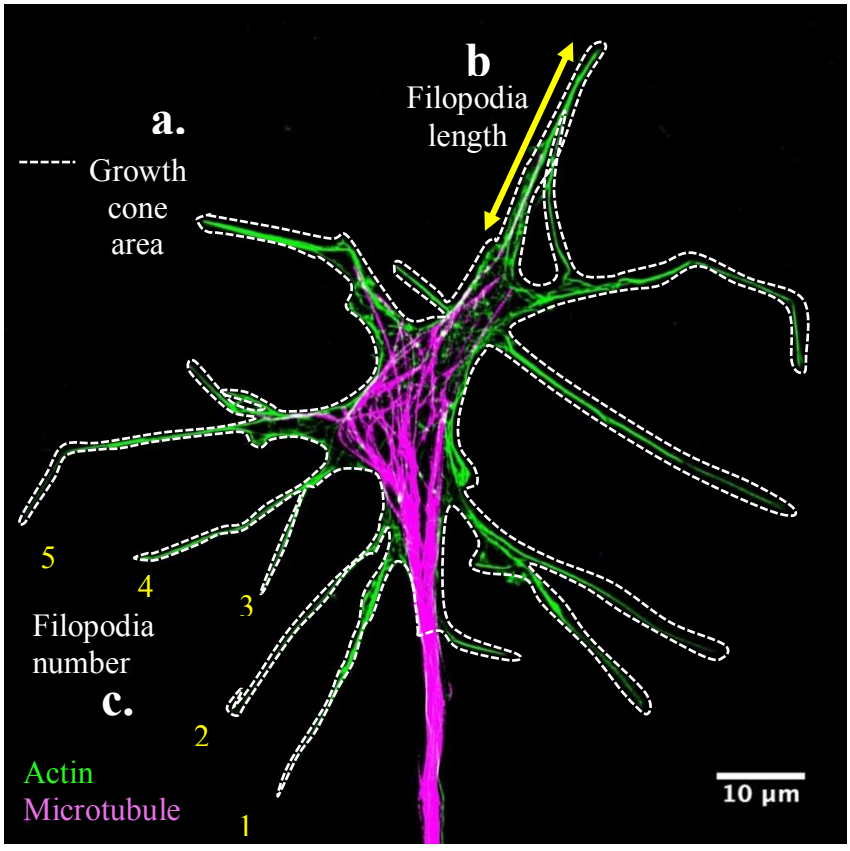

Figure 4.8 Representative SIM image of a fixed growth cone.

The growth cone stained with tubulin for labeling microtubules (magenta) and phalloidin for labeling actin (green) showing the morphological features; growth cone area (a), filopodia length (b) and filopodia number (c) examined.

We found no significant difference in any of the morphological features examined (Fig. 4.9 A-C). The average growth cone area of TACC mutant (406.5 ± 37.17 μm, N=88) expressing growth cones was 13% smaller than control (432.6 ± 39.62 μm, N=77) and 6% larger than TACC wt (382.5 ± 30.17 μm, N=94) (Fig. 4.9A). The average filopodia number did not differ across conditions either. TACC p-null mutant growth cones had an average of 6.9 ± 0.4130 N=93 filopodia which was 10% less than control growth cones (7.6 ± 0.4510 N=89) while TACC wt had 9% fewer filopodia than control (7.0 ± 0.3812 N=101) (Fig. 4.9B). The average filopodia length in TACC p-null mutant growth cones was 17.03 ± 0.8448μm, N=113, while it was 16.07 ± 0.7707 μm, N=119 in control growth cones, and 15.96 ± 0.5079 μm, N=126 in TACC wt expressing growth cones (Fig. 4.9C). While average filopodia number was similar among conditions, the number of filopodia that contained microtubules was found to be significantly higher in the TACC p-null mutant expressing growth cones. Almost 30% of the filopodia had microtubules in the TACC p-null mutant growth cones (29.13 ± 2.932 percent of total filopodia examined, N=82), which is 63% more than control growth cones (10.92 ± 2.011 percent of total filopodia examined, N=90), that had only 11% of their filopodia invaded by microtubules. TACC wt-expressing growth cones also had a greater number of filopodia with microtubules (25.82 ± 2.446 N=92) compared to controls. While not significant, TACC p-null growth cones had 11% more filopodia with microtubules compared to TACC wt (Fig. 4.9F). Although we observed increased pausing with TACC mutant-expressing axons, our data on growth cone morphology do not suggest any correlation between growth cone morphology and axon growth. However, the increased number of filopodia with microtubules could relate to the increased rates of microtubule growth tracks that we identified earlier.

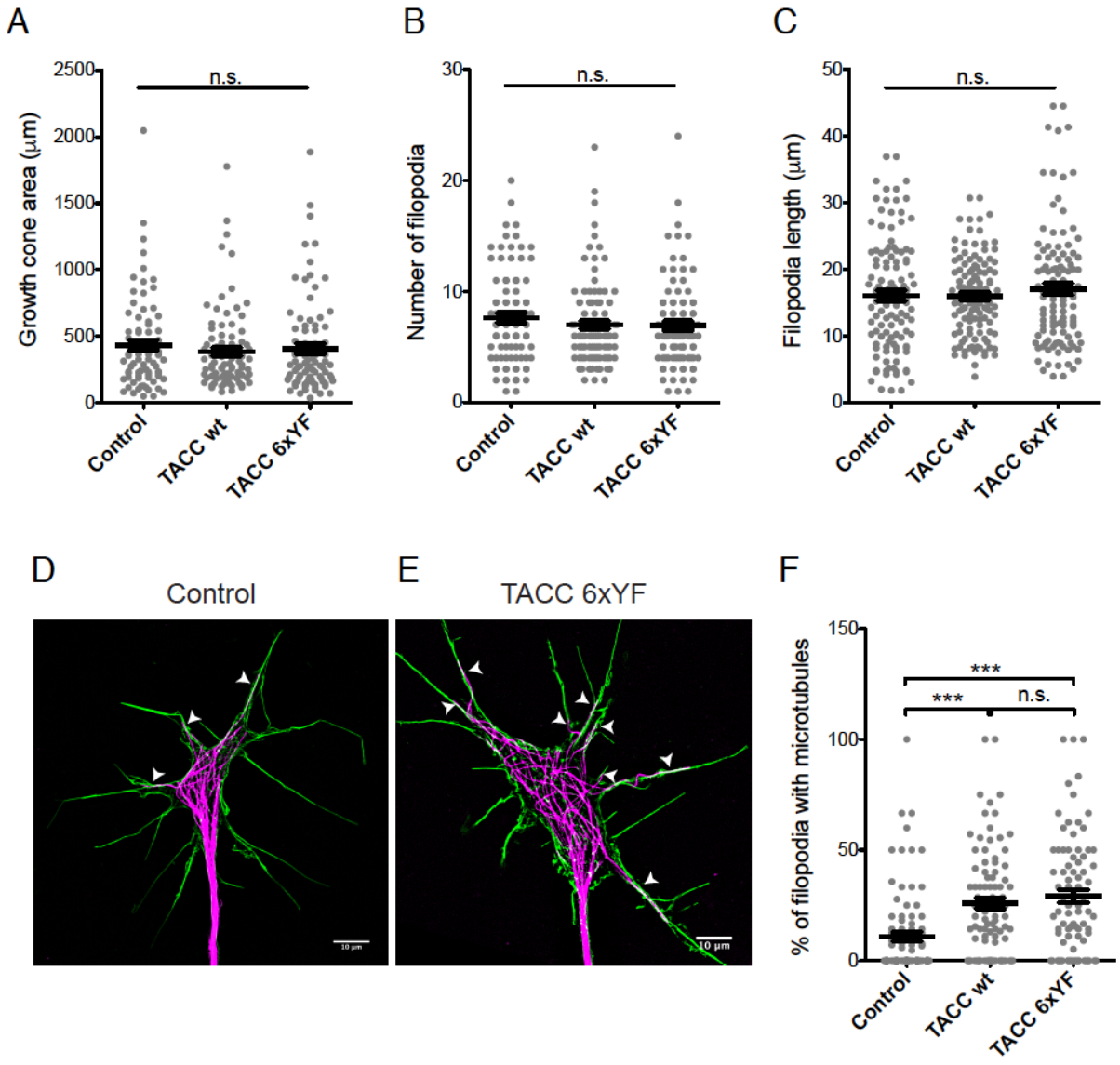

Figure 4.9 TACC tyrosine phospho-null mutants increase number of filopodia with microtubules

(A-C) The average growth cone area of TACC mutant (406.5 ± 37.17 µm, N=88) expressing growth cones was 13% smaller than control (432.6 ± 39.62 µm, N=77) and 6% larger than TACC wt (382.5 ± 30.17 µm, N=94) (A). TACC p-null mutant growth cones had an average of 6.9 ± 0.4130 N=93 filopodia which was 10% less than control growth cones (7.6 ± 0.4510 N=89) while TACC wt had 9% fewer filopodia than control (7.0 ± 0.3812 N=101) (B). The average filopodia length in TACC p-null mutant growth cones was 17.03 ± 0.8448µm, N=113, while it was 16.07 ± 0.7707 µm, N=119 in control growth cones, and 15.96 ± 0.5079 µm, N=126 in TACC wt expressing growth cones (C). Almost 30% of the filopodia had microtubules in the TACC p-null mutant growth cones (29.13 ± 2.932 percent of total filopodia examined, N=82, E), which is 63% more than control growth cones (10.92 ± 2.011 percent of total filopodia examined, N=90, D), that had only 11% of their filopodia invaded by microtubules. TACC wt-expressing growth cones also had a greater number of filopodia with microtubules (25.82 ± 2.446 N=92) compared to controls. While not significant, TACC p-null growth cones had 11% more filopodia with microtubules compared to TACC wt (F).

4.2.6 TACC tyrosine phospho-null mutant expressing-axons are more responsive to repellent guidance signals

We have previously tested TACC3 downstream of Slit2 and found that growth cones overexpressing TACC3 were more resilient to bath-applied Slit2-induced growth cone collapse compared to control growth cones (Erdogan et al., 2017).While bath application of guidance proteins is useful to test how manipulation of protein levels would alter the growth cone's reaction (read out as morphological changes) to an applied guidance molecule, it does not convey information regarding the ability of the growth cone to make guidance choices such as steering. In order to test that, we utilized an approach where the repellent guidance protein Ephrin-A5 is coated on a glass coverslip in zigzag patterns and neural tube explants are cultured on top of these cue-coated coverslips. After 12-18 h of culturing, explants are fixed and stained for tubulin and actin to examine axon responsiveness to Ephrin-A5. The responsiveness is scored based on how many of the axons that grow out from the given explant preferred to stay on the Ephrin-A5 free (growth permissive) surface versus how many of them cross that barrier and grow on the Ephrin-A5 (non-permissive) surface.

We found that control neural tube explants (Fig. 4.10A), composed of a heterogeneous population of neurons, do not show a preference towards a particular surface and grow axons on both permissive (Ephrin-A5 free) and non-permissive (Ephrin-A5) surfaces equally (Fig. 4.10D; Control - off, 50.01 ± 2.930 N=55; Control- on, 49.99 ± 2.930, respectively). However, TACC wt over-expressing neural tube explants (Fig. 4.10B) show a preference for the permissive surfaces, as they grow 25% more axons on permissive surfaces (Fig. 4.10D; 57.18 ± 2.683 N=62, TACC wt - off) compared to the Ephrin-A5 coated surface (TACC wt - on, 42.82 ± 2.683 N=62). TACC p-null mutant (Fig. 4.10C), on the other hand, how an even stronger preference for the permissive

surface, as they grow 41.3% more axons on the permissive surface (Fig. 4.10D; TACC mut - off,63.02 ± 3.036 N=42) compared to the Ephrin-A5 coated non-permissive surface (TACC mut - on, 36.98 ± 3.036 N=42). Together, these data suggest that expression of the TACC domain with the non-phosphorylatable tyrosine residues are less able to grow on the Ephrin surface and are thus more responsive to the Ephrin-A5 repellent guidance cue activity.

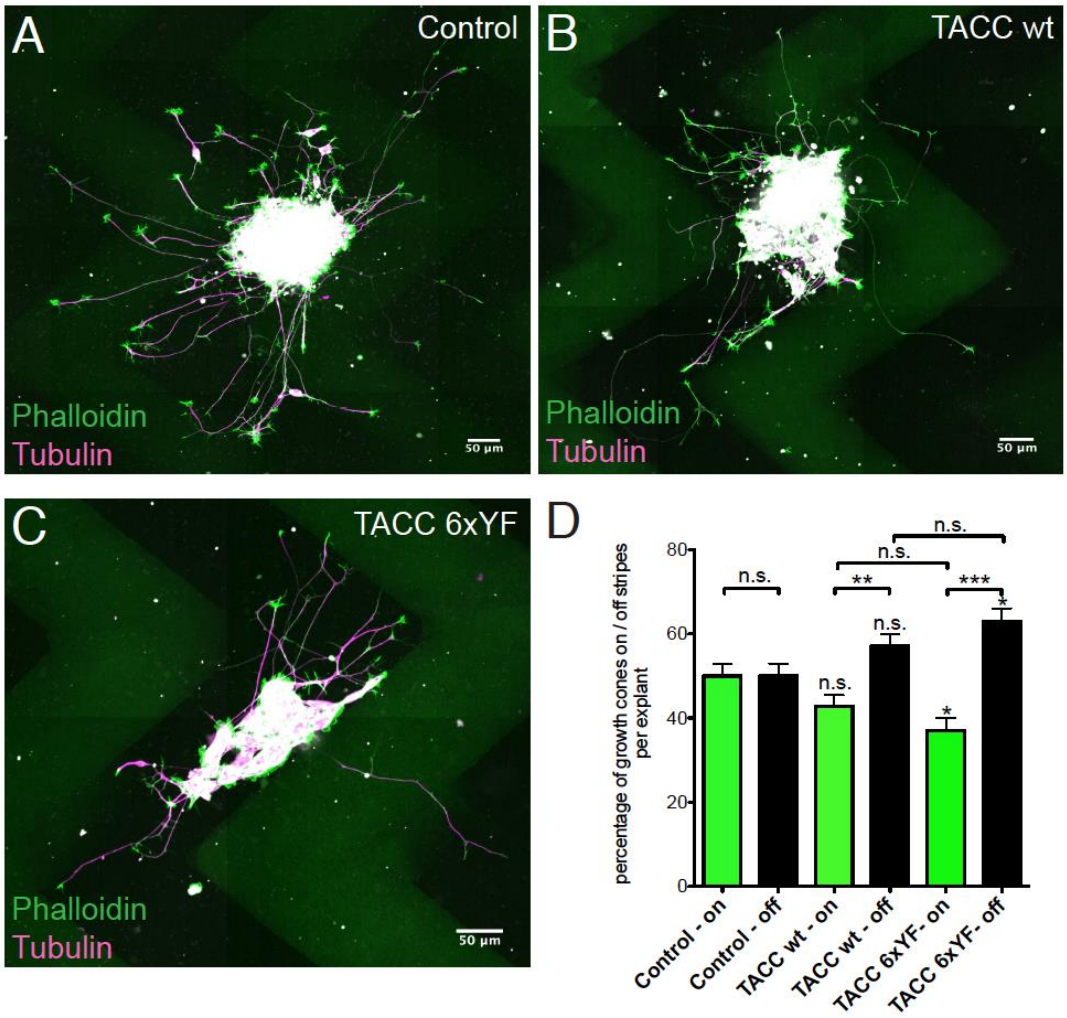

Figure 4.10 TACC tyrosine phospho-null mutants are more resistant to repellent guidance signals

(A-C) Immunofluorescence images of control (A). TACC wt (B) and TACC p-null mut (C) labelled with phalloidin (green) to label growth cones and tubulin (red) to label axons showing axon responsiveness to Ephrin-A5 coated zigzag surfaces (green). (D) Quantification of the number of axons on permissive (Ephrin-A5 free) versus non-permissive (Ephrin-A5) surfaces. Control neural tube explants does not show a preference between permissive versus non-permissive surfaces and grow axons on both surfaces equally (Control - off, 50.01 ± 2.930 N=55; Control- on, 49.99 ± 2.930, respectively). TACC wt expressing neural tube explants grow 25% more axons on permissive surfaces (57.18 ± 2.683 N=62, TACC wt - off) compared to Ephrin-A5 coated surface (TACC wt - on, 42.82 ± 2.683 N=62). TACC p-null mutants grow 41.3% more axons on permissive surface (TACC mut - off,63.02 ± 3.036 N=42) compared to Ephrin-A5 coated non-permissive surface (TACC mut - on, 36.98 ± 3.036 N=42).

4.3 Discussion

4.3.1 Abelson kinase induces phosphorylation of TACC3

In this study, we sought to examine the impact of TACC3 tyrosine phosphorylation on its interaction with microtubules and regulation of axon outgrowth and guidance. We showed that co-expressing TACC3 with Abelson kinase in HEK293 cells induces TACC3 tyrosine phosphorylation, as evident by the phospho-tyrosine signal we obtained by Western blot. Our Western blot analysis also shows that phosphorylation of TACC3 happens only in the presence of Abelson, as we do not observe any phospho-tyrosine signal when TACC3 is expressed alone or with Fyn, which is another tyrosine kinase (Fig. 4.1).

Interestingly, creating single or combinatorial phospho-null mutations at tyrosine residues that we identified as potential targets for Abelson did not show any changes in phospho-tyrosine signal levels (Fig. 4.2) observed with Western blot. In an attempt to identify the source of tyrosine phosphorylation, we tested other tyrosine residues and focused specifically on the ones in the TACC domain (Fig. 4.3), positioned at the C-terminal of TACC3 and which is responsible for microtubule plus-end tracking and interaction with its well-studied partner, microtubule polymerase XMAP215. The TACC domain possesses 6 tyrosine residues with two of them (Y759 and Y762, aa location given based on full length protein) identified as Abelson targets from the mass-spec analysis and three of them (Y832, Y846 and Y857) predicted as putative targets for Abl via *in silico* analysis. Intriguingly, mutating all these tyrosines into non-phosphorylatable phenylalanine did not cause any reduction in the phospho-tyrosine signal level as evident by the Western blot (Fig. 4.4A-B). In spite of the lack of any tyrosines in the TACC domain, it was intriguing to use that there was still a phospho-tyrosine signal in the Western blot. The only possible source of phosphorylatable tyrosine was GFP that is tagged to the TACC domain.

Tyrosine phosphorylation of GFP has not been reported previously, to our knowledge, nor does *in silico* phosphorylation prediction identify any sites by which kinases might target GFP. However, expression of GFP with Abelson clearly showed a strong phospho-tyrosine signal (Fig. 4.4 C-D) suggesting that GFP might be contributing to the phospho-tyrosine signal that we have been observing in GFP-TACC.

4.3.2 Tyrosine residues within the TACC domain are important for TACC localization to microtubules

The impact of phosphorylation on the interaction between +TIPs and microtubules has been studied for several +TIPs, such as CLASP (Hur et al., 2011; Kumar et al., 2012; Kumar et al., 2009; Watanabe et al., 2009), APC (Zhou et al., 2004), ACF7 (Wu et al., 2011), EB1 (Zhang et al., 2016). Here, we demonstrated that tyrosine residues within the TACC domain of TACC3 are important for maintaining the interaction between TACC3 and microtubules. The TACC domain with all tyrosine residues mutated into phenylalanine remains mostly cytoplasmic, while TACC wild-type localizes to microtubules. It should be noted that the wild-type TACC domain, in contrast to full-length TACC3 (which shows primarily plus-end binding), shows strong lattice binding in addition to plus-end localization. Consistent with our previous observations (Nwagbara et al., 2014), this suggest that N-terminus of TACC3 is important for restricting TACC3 localization to the microtubule plus-ends.

+TIPs track microtubule plus-ends either autonomously, through recognition of the growing microtubule structure, or non-autonomously, through an interaction with another plus-end tracking protein such as end-binding (EB) proteins. Although the mechanism of how TACC3 tracks plus-ends is not fully resolved, EB-dependent plus-end tracking can be ruled out as TACC3 does not contain a SxIP motif (serine- any amino acid- isoleucine-proline) that is required for EB

binding. It is believed that TACC3 tracks microtubule plus-ends through its interaction with XMAP215, which is mediated by the TACC domain (Kinoshita et al., 2005; Mortuza et al., 2014; Peset et al., 2005). Therefore, it is possible that the impaired interaction between microtubules and TACC p-null mutant could be arising due to a change in TACC3's ability to interact with XMAP215.

The TACC domain consists of two coiled-coil domains which means that the sequence follows heptad repeats. Presence of these coiled-coil domains are responsible for TACC3's oligomerization, which is important for TACC3's function and its interaction with XMAP215 (Mortuza et al., 2014; Thakur et al., 2014). Using Multicoil, a coiled-coil prediction program, we looked at whether tyrosine-to-phenylalanine mutations might have altered coiled-coil formation or dimerization of TACC domain. Based on this prediction, it seemed as though the TACC phospho-null mutant is still able to dimerize and form a coiled-coil (Fig. 4.11), suggesting that the interaction between XMAP215 and TACC phospho-null mutant might be retained.

Although *in silico* analysis suggests that switching from phosphorylatable tyrosine to non-phosphorylatable phenylalanine does not impact TACC3's coiled-coil structure, reduced interaction between phospho-null TACC mutants and microtubules might be explained by a change in electrostatic interactions between the two. While this could be a possibility, negative charges introduced via phosphorylation often cause dissociation of proteins off the microtubule (Hur et al., 2011; Iimori et al., 2012) which is already loaded with negative charges due to negatively charged residues at the C-terminus of tubulin. While our findings suggest that the tyrosine residues of TACC domain are important for mediating TACC3's interaction with microtubules, the exact mechanism of how they are involved in this interaction remain to be determined.

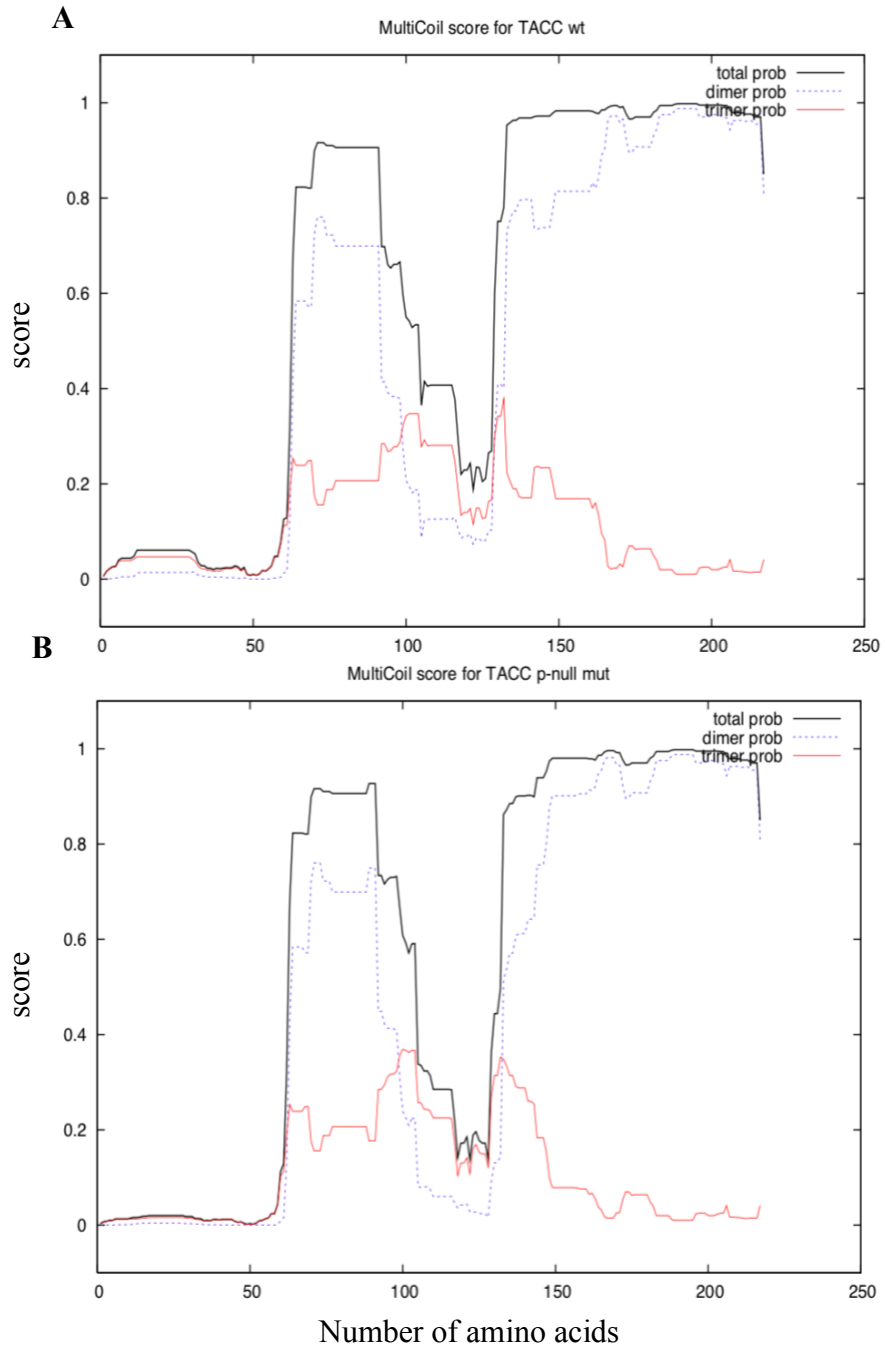

Figure 4.11 *In silico* prediction of oligomerization of TACC domain wild-type and TACC p-null mutant

(A-B) TACC wt and p-null mutant aminoacid sequence were subjected to coiled-coil and oligomerization prediction using MultiCoil software. Oligomerization probability (score is given on the y-axis) of TACC wild-type is shown at the top panel (A) and TACC p-null mutant is shown at the bottom panel (B). Red line; probability of timerization, dashed line; probability of dimerization, black line; total probability

4.3.3 TACC p-null mutant impairs microtubule localization yet enhances microtubule growth parameters

In spite of an absence of an interaction between TACC domain phospho-null mutants and microtubules, TACC p-null mutants are intriguingly still able to influence microtubule dynamics behavior by increasing microtubule growth velocity by 10% and growth length by 17% compared to controls (Fig. 4.6 A-C), although the effects do not differ significantly from TACC wild-type, suggesting that TACC might be able to regulate microtubule dynamics independent of its plus-end tracking activity.

The software (*plusTipTracker*) that we use to assess microtubule dynamics extracts information regarding microtubule growth parameters by tracking the exogenously expressed fluorescently tagged MACF-43 that only binds growing microtubule ends. Therefore, only forward microtubule movement would be tracked. However, microtubules advance forward due to microtubule polymerization *as well as* due to reduced retrograde flow. Since TACC p-null mutant does not interact with microtubules as well as TACC wild-type does, we initially thought that increased microtubule growth speed and length could be due to reduced retrograde flow. Microtubules in the growth cone periphery can track along F-actin bundles by transiently coupling to them. As a result of this coupling, microtubules also experience retrograde flow as actin filaments are pulled backwards through myosin-II activity in the transition zone. This actin coupling-mediated retrograde flow will restrain microtubule advance in the growth cone, hence, it will slow down the forward movement speed of the fluorescent marker at the MT plus-end. Therefore, more frequent transient de-coupling of microtubules from actin retrograde flow will increase microtubule advance rate.

In light of this study, we hypothesize that the TACC phospho-null mutant might be interfering with MT/ F-actin coupling, thereby promoting frequent MT/F-actin decoupling and, hence, reduced MT rearward movement. The distribution of the MT tracks within the growth cone can be a predictor of the level of coupling between microtubules and F-actin. MACF-43 comets that mark the growing microtubule ends often follow a trajectory which can also coincide with the location of F-actin bundles. The linearity and persistence of these trajectories can indicate whether microtubules are tracking along F-actin bundles or not. However, by examining maximum projection of MACF-43 comets from control, TACC wild-type and phospho-null mutants, we note that the tracks do not seem to differ from each other (Fig. 4.6 D-F), suggesting that microtubules in TACC p-null mutant-expressing growth cones might still be able to track along F-actin bundles.

Nevertheless, in order to explain increased MT growth speed and length induced by TACC p-null mutants, this hypothesis should be further tested by performing quantitative speckle microscopy to see whether microtubule movement correlates with actin retrograde flow rates.

4.3.4 TACC p-null mutant axons are shorter due to increased pausing and retraction

Microtubule advance within the growth cone is important for consolidating and driving growth cone forward movement (Lowery and Van Vactor, 2009). Intriguingly, despite increasing microtubule growth speed and length, our data shows that TACC p-null mutant-expressing axons of cultured neural tube explants grow shorter in spite of slightly higher axon forward velocity rates compared to control. When we further examined other axon outgrowth parameters, we found that TACC phospho-null mutants tend to pause and retract more frequently compared to TACC wild-type and controls (Fig. 4.7 D). Additionally, mutant axons tend to grow with less directionality (Fig. 4.7F).

In an attempt to seek further explanation to axon outgrowth behavior, we examined growth cone morphology, since growth cone morphology can often predict the growth behavior of axon (Ren and Suter, 2016). For example, increased growth cone size is often associated with frequently pausing or slow growing axons. Although we did not see a significant difference in growth cone size, filopodia length, or number among conditions (Fig. 4.9 A-C), there was a significant increase in the number of filopodia with microtubules in the TACC p-null mutant-expressing growth cones (Fig. 4.10F).

We know that microtubule can play an instructive role in growth cone directional motility. Having more filopodia with microtubules might generate more alternative routes for the growth cone to extend, which could result in more pausing for decision making and could also cause the growth cone to wander more, which would result in less directed movement. Additionally, contrary to what we speculated earlier, there might be an increased microtubule/ F-actin coupling which would enable microtubules to track along F-actin into the filopodia. In fact, increased coupling could also explain increased retraction rates. As noted earlier, actin filaments in the growth cone are subjected to rearward translocation also known as retrograde flow, due to myosin II activity. The retrograde flow of actin filaments can be attenuated when the F-actin cytoskeleton engages with receptors at point contact sites. This interaction acts as a molecular clutch that will restrain actin retrograde flow, while continuing actin polymerization will generate the force to allow membrane protrusion, thereby growth cone advance. The growth cone retracts when actin retrograde flow fails to be attenuated, which is also an indication of poor surface adhesion. It is known that dynamic microtubules play an important role in facilitating focal adhesion dynamics by transporting molecules that are involved in of focal adhesion turnover (Stehbens and Wittmann, 2012). Several MT plus-end binding proteins have been studied for their association with adhesion

sites (Stehbens et al., 2014; Zhang et al., 2016). Therefore, by facilitating microtubule protrusion into the filopodia, the TACC p-null mutant domain might be playing an indirect a role in adhesion dynamics.

A potential role in point contact regulation can also explain avoidance of EphrinA5-coated repellent substrates. Filopodia with microtubules could be more sensitive to cues, due to the microtubule-mediated signal trafficking, thereby affecting the interaction with the underlying substrate. Moreover, as speculated earlier, having more filopodia with MTs could generate more alternative routes; thus, when the growth cone encounters a non-permissive substrate, it could pick one of these alternative routes and steer away from the repellent source.

In conclusion, we have demonstrated that tyrosine residues within the TACC domain, which is the domain important for mediating microtubule plus-end tracking behavior, are important for localizing the protein to microtubules, regulating axon outgrowth parameters and making guidance decisions. Given the increased number of microtubules in the filopodia when the TACC domain is over-expressed, we hypothesize that the tyrosine residues in the TACC domain might be involved in regulating a potential TACC-mediated interaction between microtubules and F-actin. Such an interaction has not been proposed for TACC3 before, however, there are studies that might offer a potential interaction between TACC3 and the actin cytoskeleton. A proteomic screen previously identified an interaction between TACC3 and actin regulator proteins Ena/VASP (Hubner et al., 2010). Additionally, the close interactor of TACC3, XMAP215, has recently been shown to interact with actin and mediate microtubule/F-actin coupling in growth cones (Slater et al., 2019), which makes TACC3 a candidate to be involved in actin cytoskeleton interaction either direct or indirectly.

Although we initially hypothesized that the increased microtubule growth speed and length which we observed with TACC p-null mutants could be due to reduced MT rearward movement induced by frequent MT/F-actin decoupling, this hypothesis may not fully align with the increased number of filopodia with microtubules. Therefore, while reduced MT rearward movement may still be happening, increased microtubule growth speed and length could also be due to increased microtubule polymerization, which we previously disregarded due to TACC p-null mutant's cytoplasmic localization. However, it is possible that the TACC p-null mutant could increase MT growth by opposing a negative regulator of microtubule polymerization, thereby increasing microtubule growth parameters in an indirect fashion. In fact, such a function for TACC3 has been previously identified. Kinoshita et al. suggests that presence of TACC3 is important for targeting TACC3- XMAP215 to the centrosome to overcome microtubule depolymerizing activity of MCAK at that location.

Finally, in addition to tyrosine phosphorylation, serine/threonine phosphorylation sites would be worthwhile to explore, given that there are several S/T kinases that operate under guidance cues, such as GSK3, which is a well-studied S/T kinase that is already shown to phosphorylate various +TIPs and modulate MT dynamics. Future work can further explore whether TACC3 is targeted by S/T kinases and whether S/T phosphorylation would affect TACC3's function in a similar way, which could shed light on differential and asymmetric regulation of microtubule dynamics under different guidance signals.

4.4 Materials and Methods

4.4.1 Embryos

Eggs collected from *Xenopus laevis* were fertilized *in vitro* and kept between at 13-22˚C in 0.1X Marc's Modified Ringer's (MMR). All experiments were approved by the Boston College

Institutional Animal Care and Use Committee and were performed according to national regulatory standards.

4.4.2 Culture of embryonic explants

Neural tubes of embryos staged according to Nieuwkoop and Faber were dissected at stages between 20-21 as described previously (Lowery et al., 2012). Neural tube explants were cultured on MatTek glass bottom dishes coated with poly-L-lysine (100 µg/ml) and laminin (20 µg/ml). Culture media prepared by mixing L-15 Leibovitz medium and Ringer's solution supplemented with antibiotics NT3 and BDNF to promote neurite outgrowth.

4.4.3 Constructs and RNA

Capped mRNAs were transcribed and purified as previously described (Lowery et al., 2013; Nwagbara et al., 2014). TACC3 pET30a was a gift from the Richter lab, University of Massachusetts Medical School, Worcester, MA and sub-cloned into GFP pCS2+. Tyrosine phospho-null mutations were introduced into wild-type GFP-TACC3 by using overlapping extension PCR method with appropriate primers designed to substitute tyrosine residues with phenylalanine to generate GFP-TACC3 6xYF. Wild-type and phospho-null mutants of TACC domain were cloned from their full-length counterparts. MACF 43 (a gift from Hoogenraad Lab) was sub-cloned into mKate2 pCS2+. Embryos either at the 2-cell or 4-cell stage were injected with the following total mRNA amount per embryo; 100 pg of GFP-MACF43 as a control for GFP-TACC3 and to analyze microtubule dynamics parameters. GFP-TACC3 full-length wild-type or phospho-null mutant injected at 1000 pg. GFP-TACC wild-type or phospho-null mutant were injected at 400pg.

4.4.4 Immunocytochemistry

Embryonic explant cultures were fixed with 0.2% Glutaraldehyde as described (Challacombe et al., 1997) and labelled with primary antibody (1:1000 diluted in blocking buffer made up by 1% non-fat dry milk in calcium and magnesium free PBS) to tyrosinated tubulin [YL1/2] (rat monoclonal, ab6160, Abcam) for 45 min at room temperature which is followed by PBS washes repeated three times and 10 min of blocking. Goat anti-rat AlexaFluor568 (1:500, ab175476, Abcam Technologies) was used as a secondary to tubulin and Phalloidin 488 (1:500, Molecular Probes) was used to label actin. Both reagents are diluted in blocking solution and applied for 45 min at room temperature followed by PBS washes several times. 90% glycerol stock was used as a mounting media for imaging.

4.4.5 Stripe Assay

The stripe assay is performed as described in Knoll et al 2007 (Knöll et al., 2007). 10 ug/ml of Ephrin-A5/Fc (chimera human, Sigma, E0628) and 10ug/ml of Fc are mixed with 2.5 ug/ ml of Anti-human IgG (Fc specific) FITC (Sigma, F9512) and Anti-human IgG (Fc specific) respectively in PBS. Solutions are incubated at room temperature for 30 min to allow for oligomerization. To coat coverslips with Ephrin-A5, a coverslip is attached to a zig-zag patterned silicon matrix and Ephrin-A5 solution is injected with a micropipet through the channel in the silicon. Injected matrices are incubated at 37˚C for 30 min and then rinsed with PBS several times using the same injection method. After rinsing, coverslips are detached from the matrix and placed in a culture dish and 100ul of second stripe solution (Fc only) is applied directly on the coverslip and incubated at 37˚C for 30 min. After incubation is over coverslips are rinsed with PBS and 20 ug / ml of 100ul laminin in PBS is applied on coverslips and incubated for 1h. After laminin incubation coverslips are rinsed with PBS several times. 400ul of culture media is applied on

coverslips and neural tube explants are placed on protein coated area and cultured for 24 h prior to imaging.

4.4.6 Image acquisition and analysis

To assess axon outgrowth parameters, phase contrast images of axons were collected on a Zeiss Axio Observer inverted motorized microscope with a Zeiss 20×/0.5 Plan Apo phase objective. For axon outgrowth length, snap-shots of neural tube explants were taken 12-18h post culturing. Time-lapse images were collected for 4 h with 5 min intervals and axon growth was manually tracked frame by frame using Fiji Manual Tracking plugin. Axon growth velocity information is provided by the Manual Tracking plugin but only the forward movement velocity was included in the analysis. Axon outgrowth forward movement, pause and retraction frequencies (as a percentage of total frames tracked) are scored manually tracking axons frame by frame.

High-resolution images of cultured spinal cord explants were obtained with a CSU-X1M 5000 spinning-disk confocal (Yokogawa) on a Zeiss Axio Observer inverted motorized microscope with a Zeiss Plan-Apochromat 63×/1.40 numerical aperture lens. Images were acquired with an ORCA R2 charge-coupled device camera (Hamamatsu) controlled with Zen software. For microtubule dynamics and TACC localization experiments, images are time lapse images are acquired for 1 min with 2 s intervals.

Structured illumination super-resolution images were collected on a Zeiss Axio Observer.Z1 for super-resolution microscope with Elyra S.1 system, utilizing an Objective Plan-Apochromat 63×/1.40 oil (DIC). Images were acquired with a PCO-Tech Inc.pco.edge 4.2 sCMOS camera. The images were obtained in a chamber at approximately 28°C and utilizing the immersion oil Immersol 518F 30°. Channel alignment and structured illumination processing were applied to the super-resolution images using the Zeiss Black program. Experiments were performed multiple

times to ensure reproducibility. Graphs were made in GraphPad Prism. Statistical differences were determined using unpaired two tailed t-tests when comparing two conditions and one-way analysis of variance (ANOVA) with Tukey's *post-hoc* analysis when multiple conditions were compared.

Chapter 5

Discussion

5.1 TACC3 is a microtubule plus-end tracking protein and regulates microtubule dynamics in the growth cone

The dynamically unstable nature of microtubules poses great importance in regulation of microtubule growth and shrinkage during cellular events which rely on instantaneous control of their growth dynamics. Plus-ends of microtubules, in that regard, where growth and shrinkage events are more pronounced, are critical for controlling the growth dynamics of microtubules. In conjunction with this, proteins that localize at plus-ends bear great potential to regulate microtubule growth dynamics.

In the second chapter, we identified a role for TACC3 as a microtubule plus-end tracking protein in interphase vertebrate cells for the first time. Although a plus-end tracking behavior has previously been proposed, based on studies performed in *Drosophila* and *Dictyostelium*, a deeper characterization of its role in regulating the dynamicity of microtubules was lacking in vertebrate cells. Moreover, while the majority of previous studies focused on identifying a role for TACC3 in the control of mitotic spindles during cell division, other cellular processes that demand high microtubule activity remained largely unexplored. In this work, not only did we characterize a microtubule plus-end function for TACC3, but also, we studied its role in regulation of growth cone microtubule dynamics, which requires rapid changes in growth and shrinkage in order to modulate the growth cone's response to environmental signals to control growth cone motility.

One of the significant finding of this work was that, unlike other +TIPs, TACC3 localizes to the outermost tip of the microtubule plus-ends, which overlaps with XMAP215 localization and precedes EB1 localization. The mechanism of how TACC3 tracks plus-ends is still not fully known, however, as it lacks EB binding motifs SxIP and CAP-Gly, this suggests that TACC3 plus-end tracking is independent of EB proteins. Additionally, unlike EB proteins, which only track

growing microtubule ends, we found that TACC3 tracks microtubule ends at all states; including growth, shrinkage and pause, with increased preference for growing microtubules, which further suggests that TACC3 localization is independent of EB. Given that TACC3 localization overlaps with XMAP215, it is possible that TACC3 is recruited to microtubule plus-ends through its interaction with XMAP215. This co-localization at the microtubule plus-ends seemed to happen in a co-dependent manner; meaning that levels of TACC3 affected the level of XMAP215 at microtubule plus ends, and vice versa. Since we still do not know how TACC3 tracks plus-ends, the increased XMAP215 levels at the plus-ends could be due to increased protein stability or affinity of XMAP215 for microtubules mediated by the interaction between XMAP215 and TACC3, rather than direct recruitment of XMAP215 to the plus-ends by TACC3.

In addition to characterizing its localization, we showed that reducing TACC3 levels by 50% resulted in an 11% reduction in microtubule growth speed, while its ectopic expression resulted in significantly faster growing microtubules in the growth cones. Taken together, our findings suggest that the association of TACC3 and XMAP215 at microtubule plus-ends in a co-dependent manner could correlate with changes we observe in microtubule dynamics.

In addition to microtubule growth dynamics, we have also observed a correlation between TACC3 levels and axon growth length in cultured spinal neurons. Although axon growth is more complicated to be explained than simply by increased microtubule growth, TACC3 as a regulator of microtubule growth offers a great venue to further explore its role in axon growth, which is explored in Chapter 3.

5.2 TACC3 is a potential regulator of axon outgrowth and guidance

Characterization of TACC3 as a microtubule plus-end tracking protein and discovering that it promotes microtubule growth and axon elongation in developing *Xenopus* neurons led us to then further investigate the mechanisms behind these functions. In Chapter 3, we began with examining the mechanism of axon growth length controlled by the levels of TACC3. Surprisingly, axon growth velocity was reduced in both TACC3 knockdown (KD) and TACC3 over-expressing axons; however, axon retraction rates were significantly lower in TACC3 over-expressing axons while it was increased with TACC3 KD. Together, these data suggested that TACC3 induces axon growth by promoting more persistent growth rather than increasing the growth speed. Axon retraction events involve regulation of actin cytoskeleton dynamics and surface adhesion turnovers. The reduced retraction rates we observed with TACC3 overexpression further raised the possibility that TACC3 might participate in regulating actin dynamics in the growth cone. Since TACC3 has been identified as an interactor of CLASP, which is a well-studied actin-interacting +TIP and shown to participate in focal adhesion turnover during cell migration, the function of TACC3 should be explored in these areas, as well.

In Chapter 3, we also sought to further understand the increased microtubule growth rates that we observed with TACC3 overexpression. Microtubule stability is one way to control microtubule growth. While increased microtubule stability perturbs the dynamic nature of microtubules and halts the growth, moderate stabilization can ensure persistent microtubule growth. Combining TACC3 protein level manipulations with low levels of the microtubule depolymerizing agent nocodazole, we aimed to test the resistance of microtubules to the growth ceasing impacts of nocodazole. We found that TACC3 overexpressing growth cones are more resistant to reductions in microtubule growth parameters induced by nocodazole application.

Nocodazole exerts its microtubule growth-reducing effect by sequestering tubulin dimers and reducing free tubulin levels necessary for microtubule polymerization. We propose that the increased XMAP215 levels at plus-ends that occur with TACC3 overexpression (that we identified previously) could compete with nocodazole for free tubulin, thereby continuing microtubule polymerization more efficiently compared to control growth cones.

We also tested the impact of the cooperation between TACC3 and XMAP215 on axon growth parameters and found that TACC3 and XMAP215 interact to promote axon outgrowth. Partial knockdown of both proteins resulted in further reduction in axon outgrowth, suggesting a synergistic interaction between the two proteins. Overexpression of both proteins, however, did not show any further enhancement compared to XMAP215 overexpression alone, suggesting that an upper threshold might have been achieved with XMAP215 overexpression. As a microtubule polymerase, XMAP215 can play a more critical role while TACC3 might be supporting XMAP215. We found a superior role for XMAP215 in our rescue experiment where we observed that XMAP215 overexpression was able to rescue reduced axon growth length caused by TACC3 KD. However, TACC3 overexpression was not sufficient to rescue XMAP215 KD to the control levels, further suggesting that XMAP215 levels play a more critical role while TACC3 plays a more accessory role.

In this chapter, in addition to seeking further explanation for TACC3's role in microtubule dynamics regulation and axon outgrowth, we examined a role for TACC3 in axon guidance. Slit2 is a repellent guidance protein that acts along the neural tube midline during embryonic development to ensure that axons that cross the neural tube midline can extend on the contralateral side without crossing back. Slit2 has been tested with *Xenopus laevis* spinal neurons before and has been shown to induce growth cone collapse (Stein and Tessier-Lavigne, 2001). In our

experiments, we found that TACC3 overexpression can reduce the number of collapse events compared to control growth cones. While in some cases, growth cone collapse involves filopodia and lamellipodia retraction with microtubules remaining intact prior to the collapse event, in other more severe cases, microtubules can undergo catastrophe as well, resulting in axon retraction prior to the growth cone collapse. One possibility is that TACC3 counteracts Slit2-induced collapse due to increased microtubule stability that TACC3 provides as a result of its interaction with XMAP215. As discussed previously, XMAP215 levels increased with TACC3 could provide more sustained and efficient microtubule growth rates while the actin cytoskeleton undergoes depolymerization. Microtubules are known to traffic actin associated proteins involved in actin polymerization, such as RAC1, CDC42 Arp2/3 (Tojima et al., 2011). Moreover, actin polymerization from microtubule plus-ends has been studied in plants and yeast and more recently defined in *in vitro* reconstitution systems (Henty-Ridilla et al., 2016). Presence of more resistant microtubules, therefore, might provide support by both transporting actin associated proteins and also by promoting localized actin polymerization from microtubule plus-ends, all of which require dynamic microtubules capable of growing and extending into the growth cone periphery. Therefore, by ensuring microtubule stability and growth, TACC3 can provide resistance for microtubules and perhaps recovery from the devastating effect of repellent cue activity on the actin cytoskeleton.

As a microtubule plus-end tracking protein, TACC3's association with microtubules, therefore, is important to exert these functions. Thus, Chapter 4 is devoted to exploring the impact of phosphorylation, induced by guidance signals, on TACC3's ability to interact with microtubules.

5.3 TACC domain phosphorylation as an important regulator of TACC3's function

Phosphorylation is one of the well-studied post-translational modifications that +TIPs experience. As discussed earlier, phosphorylation of +TIPs can happen in a spatially-controlled manner in cells to modulate microtubule dynamics locally and asymmetrically during cell migration or in the growth cone in response to growth factors to ensure directed axon growth. The impact of phosphorylation can be experienced by a change in a protein's capacity to interact with its partners, which could be due to a change in its electrostatic status or a change in conformation that blocks the interacting sites. Phosphorylation increases the overall negative charge of the protein, which can interfere with the interaction between the protein and the negatively charged microtubule. In our case, mutating tyrosine residues in the TACC domain into non-phosphorylatable phenylalanines resulted in loss of interaction between the TACC domain and the microtubules, leaving the mutant TACC protein mostly cytoplasmic. Although we don't know the exact mechanism of how TACC3 tracks microtubule plus-ends, it has been suggested that it happens through its interaction with XMAP215 and minimal domains necessary for this interaction has been studied by Mortuza et al. (Mortuza et al., 2014). These minimal XMAP215-interacting domains of TACC3 reside in the TACC domain and spans a 220 aa region that falls in between aa 711 and aa 931, which includes the tyrosine residues Y725, Y759, Y762, Y832 and Y846 that we tested. Therefore, we speculate that the failure in plus-end tracking could be due to a failure in the interaction between the TACC domain and XMAP215, which is currently being investigated by co-immunoprecipitation assays.

Additionally, we looked at whether the structure of the TACC domain, which forms a coiled-coil and often dimerizes, might have been disturbed by the mutations that we introduced. *In silico* analysis performed with coiled-coil and dimerization prediction sites (MultiCoil) revealed

that the TACC domain with tyrosine mutations seemed to be able to form dimers and, in fact, the sites that we have mutated mostly remain outside of the heptad repeats that promote the coiled-coil formation. Although we don't know the mechanism of how tyrosine mutations leads to disruption of the interaction with microtubules, we found that these mutations have some consequences on TACC3's role in microtubule dynamics and axon outgrowth. Our data suggested that, despite not being able to interact with microtubules, TACC phospho-null mutants increase microtubule growth rates to a similar extent as compared to the wild-type TACC domain. More interestingly, even though the microtubule growth rates were increased, axon outgrowth length was reduced when the TACC phospho-null mutant was over-expressed. Our data suggests that shorter axons could be due to increased pause and retraction events that TACC phospho-null-expressing axons experience, in addition to increased wandering that results in less directed movement. These observations, along with our finding of increased numbers of filopodia invaded by microtubules, led us to propose a role for the tyrosine mutations in the regulation of microtubule-actin crosstalk. At first, it was plausible to think that the increased microtubule growth rates could be due to a reduction in microtubule rearward movement. Microtubules experience rearward movement when they are coupled to actin that undergoes retrograde flow. Therefore, we thought that overexpression of the TACC phospho-null mutant somehow might be reducing the coupling between the two polymers, thereby freeing microtubules from the actin retrograde moving forces. However, this idea was later challenged with the observation that TACC phospho-null mutant expressing growth cones were found to possess more filopodia with microtubules, suggesting that, on the contrary, there might be an increase in coupling between the two polymers. This hypothesis could also explain the increased pause and retraction rates we found with TACC phospho null mutants.

Although tracking along F-actin bundles can guide growing microtubules into the growth cone periphery, extensive retrograde flow employed on F-actin can also halt microtubule advance unless F-actin bundles are coupled to the extracellular matrix via integrin receptors and point contact (focal adhesion) adaptor proteins, which altogether attenuate actin retrograde flow. The retrograde flow mechanism therefore offers two potential roles for the TACC phospho-null mutant. One is that the TACC phospho-null mutant might be increasing the coupling between microtubule and F-actin bundles, therefore exposing microtubules to more retrograde flow that results in more frequent pause and retraction. The second role could be an indirect one, where the TACC phospho-null mutant could play a role in point contact turnover by either reducing the number of contacts or affecting their turnover rates, which at the end may impair the F-actin clutching to the extracellular matrix and attenuate retrograde flow. A role in point contact formation may also help to explain the increased avoidance of Ephrin repellent-coated substrates we observed with TACC phospho-null mutant axons. Surface attachment is better when the growth cone travels through a permissive surface. The TACC phospho-null mutant-expressing condition has significantly more axons on Ephrin-free (permissive) surfaces, whereas in control conditions, there was no preference towards one surface and axons tend to grow on both Ephrin (non-permissive) and Ephrin-free (permissive) surfaces equally. TACC phospho-null mutant expressing growth cones may not be as good at point contact formation overall as control growth cones, which could be advantageous when encountering a non-permissive surface. Poor adhesion could result in increased avoidance of the ephrin repellent cue.

Considering that its partner, XMAP215, has recently been shown to interact with actin and involved in aligning microtubules along F-actin bundles (Slater et al., 2019), it is plausible to suggest a role for TACC3 in microtubule/F-actin crosstalk as well. Moreover, in addition to

XMAP215, TACC3 has also been identified to genetically interact with another microtubule-actin crosslinker, CLASP. In fact, a more direct interaction has been demonstrated through a proteomic screen, where TACC3 is identified to interact with Ena/VASP (Hubner et al., 2010), which is an actin barbed end anti-capping protein that blocks the action of capping protein in order to allow actin polymerization.

Overall, we have attempted to identify a role for Abl kinase-induced phosphorylation of TACC3 in regulating microtubule dynamics, axon growth and guidance. Although, we have demonstrated that Abelson kinase induces phosphorylation of TACC3 and identified tyrosine residues targeted by Abelson, mutations at those identified residues did not seem to impede TACC3's interaction with microtubules. However, examination of other tyrosine residues in the TACC domain, which might be targeted by other tyrosine kinases, suggested an important role for these residues in regulating TACC3's interaction with microtubules and its impact on axon outgrowth and guidance.

5.4 Future Directions

We have characterized a microtubule plus-end tracking function for TACC3 for the first time in vertebrate neuronal growth cones and identified roles for TACC3 in axon outgrowth and guidance during *Xenopus laevis* embryonic development. However, there are still questions that remain, and the following section will discuss some of these questions briefly.

5.4.1 Could TACC3 regulate microtubule dynamics locally under different signaling pathways?

A major focus of this thesis was to identify a role for TACC3 during axon guidance under guidance signals. We showed that TACC3 overexpression mitigated bath applied Slit2 repellent guidance protein-induced growth cone collapse. However, the mechanism of how TACC3 exerts

this function remains to be elucidated. Examining TACC3 phosphorylation and its impact on TACC3's function was an initial attempt to answer this question. However, to gain better insight, localized changes should be examined since, in reality, growth cones will encounter and respond to multiple signals at different levels at the same time. Therefore, stimulating growth cones with different guidance signals asymmetrically and determining whether the localization of TACC3 in the growth cone and the behavior of microtubules would be affected in response to those signals would be interesting to pursue. This local and asymmetric modulation will be useful to test with both attractant and repellent guidance proteins to see if TACC3 would have any preference for mediating certain signals and how microtubules would accompany these changes.

Moreover, in addition to tyrosine kinase signaling pathways, serine/threonine kinases that are known to operate downstream of guidance signals are worthwhile to explore. GSK3 kinase is one candidate that is known to be an important factor to establish neuronal polarity and asymmetrical axonal extension (Kim et al., 2011). Moreover, it has been studied under guidance signals, such as Slit2 , sema3A, netrin and NGF (Kim et al., 2011) and shown to target several +TIPs, including CLASP, which has been identified to interact with TACC3 genetically (Lowery et al., 2010). The phosphorylation prediction site (NetPhos 3.1 server) also identifies putative GSK3β consensus sites in full-length TACC3, although with low scores remaining under the threshold except for S638, which is located outside of the TACC domain and has a score above the 0.5 threshold.

Identifying a role for TACC3 under different signaling cascades is not only important for understanding its interaction with microtubules, but also with other +TIPs. Although wild-type TACC3 localization is distinct compared to other +TIPs (TACC3 localization precedes EB1 and co-localizes with XMAP215), some forms of phosphorylated TACC3 could localize differently

and may compete with other +TIPs for microtubule binding. Additionally, phosphorylation could induce a conformational change and promote novel interaction events. For example, although TACC phospho-null mutants do not interact with microtubules, we observed an increase in microtubule growth dynamics compared to control growth cones. It is possible that phospho-null mutations may induce an interaction between the TACC mutant and another protein that would impede microtubule growth. Therefore, it is possible that the TACC phospho-null mutant might be promoting microtubule growth by sequestering anti-growth factors.

Overall, interaction of TACC3 with microtubules and other +TIPs should be identified under different guidance and kinase signaling pathways for a more detailed understanding.

5.4.2 Could TACC3 regulate microtubule-actin crosstalk and point contact turnover?

This thesis started off with a focus on identifying TACC3's impact on microtubule dynamics regulation during axon growth and guidance. However, findings from Chapter 4 raised the question of whether TACC3 could be involved in regulating the actin cytoskeleton in addition to microtubules. This question has emerged with the finding of increased number of filopodia within microtubules that we observed in TACC phospho-null mutant-expressing growth cones. Since TACC phospho-null mutants do not interact with microtubules, it could play an indirect role in this microtubule / F-actin crosstalk, perhaps by sequestering another factor that would impede the interaction between microtubule and actin bundles. It is also possible that this indirect role could be exerted through a potential role in point contact formation. This idea becomes prominent with the finding of increased pause and retraction rates that we observed after expressing the TACC phospho-null mutant, as pause and retraction rates are dependent on the contact made between the growth cone and the extracellular matrix. Through a mechanism yet to be defined, increased coupling between microtubules and F-actin, perhaps mediated by TACC phospho-null

mutants, along with reduced point contact formation or turnover, the molecular clutch might not engage, therefore actin retrograde flow and microtubule rearward movement would increase resulting in increased retraction. The fluorescent speckle microscopy technique can be applied to test the actin and microtubule flow rates in the growth cone in order to assess whether microtubule movement is coupled to F-actin flow and whether it can explain the change in microtubule growth rates. Additionally, point contact markers can be examined in immunostained growth cones to assess whether TACC phospho-null mutants impact the number and the size of these contacts, which could help us to understand the axon growth dynamics further.

5.4.3 Could TACC3's interacting partners be a target downstream of guidance signals?

In addition to these questions that mostly focus on TACC3, it will be intriguing to study other members of the TACC family, TACC1 and TACC2. Like TACC3, TACC1 and TACC2 also localize to the distal most ends of the microtubule and interact with XMAP215 and promote microtubule growth. Although we didn't see any synergistic effect among the TACC members on microtubule growth (Lucaj et al., 2015; Rutherford et al., 2016), it will be intriguing to test whether they were all subjected to phosphorylation downstream of guidance signals and, if so, would the extent differ among the members. Another intriguing question would be whether their phosphorylation would alter their localization and cause them to fill the spot emptied by another.

Another interesting question to test would be whether XMAP215 gets phosphorylated in response to guidance signals. Since XMAP215 and its interaction with microtubules is better characterized, and sites that mediate this interaction are known, it will be intriguing to study whether XMAP215 is subjected to any phosphorylation events under any guidance signals and whether this phosphorylation affects its polymerase activity or its interaction with microtubules or with other +TIPs, particularly with TACC3.

While all these questions are very exciting to test, one last critical point to consider is to perform all these proposed experiments by adding back the mutant in the background where the endogenous protein levels are reduced. In the experiments we performed so far, the phospho-null mutants were ectopically expressed. However, the true impact of the mutants can be better assessed if we first deplete the endogenous wild-type protein and then add back the mutant to see if the mutant can rescue or worsen the phenotype. While we attempted to perform these experiments, we have encountered some survivability issues which precluded our analysis. Further efforts should be put to optimize and perform these experiments for a better assessment.

5.5 Concluding remarks

Axon guidance is a highly critical developmental event that underlies the formation of precise connections for building a properly functioning nervous system. Ever since the first attempt was put towards understanding the mechanism of axon guidance by Cajal and others, we now know many elements of this process, from the cues guiding axons to their targets, to more intricate intracellular effectors generating this directional movement. The aim of this thesis in that regard was to identify and explore a potential component of this machinery.

In this thesis, we characterized an unexplored function for microtubule associated protein TACC3 in neuronal growth cones during embryonic development. We, for the first time, showed that TACC3 tracks plus-ends of microtubules and regulates its growth dynamics in the vertebrate growth cone. Plus-end tracking proteins are becoming increasingly important to understand the growth dynamics of microtubules in various contexts. The hub that they create at the tip of the microtubule needs to become better understood, both in terms of +TIP interaction with microtubules but also with one another.

The easily accessible *Xenopus laevis* nervous system and the large growth cones of its neurons, combined with high resolution imaging techniques, allow us to monitor cytoskeletal dynamics. With the advent of high-resolution imaging techniques and reconstitution assays, additional novel functions are being identified for individual +TIPs, other than their conventional roles and here, we have defined new roles for a +TIP not only in regulating microtubule dynamics but also highlight a possible role for it in the crosstalk between microtubules and actin.

Appendix

A.1 Chapter 2 – Supplemental Movie Figure Legends

Supplemental Movie 1

Time lapse live images of cultured *Xenopus laevis* growth cones of control, TACC3 KD and TACC3 OE expressing mKate2-EB1. Images were acquired for 1min with 2 sec intervals. Scale bar, 5μm.

Supplemental Movie 2

Time lapse live images of cultured *Xenopus laevis* growth cone expressing mKate2-tubulin (red) and GFP-TACC3 (green). Images were acquired for 1min with 2 sec intervals. Scale bar, 1μm.

Supplemental Movie 3 - 4

Time lapse live images of cultured *Xenopus laevis* neural crest cell expressing mKate2-tubulin (red) and GFP-TACC3 (green). (Movie 3). Magnified time-lapse montage of boxed regions in G'-I' (Movie 4). Images were acquired for 1min with 2 sec intervals. Scale bar, 1μm.

Supplemental movie 5-6

Time lapse live images of cultured *Xenopus laevis* nonneuronal embryonic cell expressing mKate2-tubulin (red) and GFP-TACC3 (green) (Movie 5). Magnified time-lapse image of boxed regions in C (Movie 6). Images were acquired for 1min with 2 sec intervals. Scale bar, 1μm.

Supplemental Movie 7 - 11

Time lapse live images of cultured *Xenopus laevis* growth cones of GFP-TACC3 full-length (Movie 7), GFP-TACC3 N-term deletion (Movie 8), GFP-TACC3 C-terminal deletion (Movie 9), GFP-TACC3 TACC domain only (CC1/2) (Movie 10), TACC3-GFP (Movie 11). Growth cones are expressing mKate2-EB1 (red) and GFP-TACC3 (green). Images were acquired for 1min with 2 sec intervals. Scale bar, 5μm

A.2 Chapter 4 – Supplemental Movie Figure Legends

Supplemental Movie 12 – 17

Time lapse live images of cultured *Xenopus laevis* growth cones of GFP-TACC3 wild-type (Movie 12), GFP-TACC3 phospho-null mutants with tyrosine to alanine mutation of tyrosine residues; 608 (Movie 13), 628 (Movie 14), 759 (Movie 15), 762 (Movie 16) and combination of

all four tyrosine residues (Y4A, Movie 17). Growth cones are expressing mKate2-MACF43 (magenta) and GFP-TACC3 (green). Images were acquired for 1min with 2 sec intervals. Scale bar, 2μm.

Supplemental Movie 18 -19

Time lapse live images of cultured *Xenopus laevis* growth cones of GFP-TACC domain only wild-type (Movie 18) and GFP-TACC domain phospho-null mutant with all tyrosine residues are mutated into phenylalanine (6xYF, Movie 19). Growth cones are expressing mKate2-tubulin (magenta) and GFP-TACC3 (green). Images were acquired for 1min with 2 sec intervals. Scale bar, 2μm.

Supplemental Movie 20 -22

Time lapse live images of cultured *Xenopus laevis* growth cones of control (Movie 20), TACC domain only wild-type (Movie 21) and TACC domain phospho-null mutant (6xYF, Movie 22). Montages showing GFP-MACF43 on the left and microtubule growth tracks generated by *plusTipTracker* (shown in red) on the right panel. Growth cones are expressing GFP-MACF and Flag-TACC domain constructs. Images were acquired for 1min with 2 sec intervals. Scale bar, 5μm.

Supplemental Movie 23

Representative phase contrast time-lapse image of a neural tube explant recorded for 4 h with 5 min intervals. Scale bar, 10μm.

Supplemental Movie 24

Representative phase contrast time-lapse image of a single axon showing the growth track generated by Fiji, Manual Tracking plugin. Tracking data is used to calculate the growth velocity and directionality shown in Figures 4.7 B and F. Image is acquired for 4 h with 5 min intervals. Scale bar, 10μm.

Supplemental Movie 25

Representative phase contrast time-lapse image of a single axon showing axon pause and retraction. Time-lapse montage of this video is shown in Figure 4.7 C and quantification of the frequency of axon pause and retraction is shown in Figure 4.7 D. Image is acquired for 4 h with 5 min intervals. Scale bar, 10μm.

References

Akhmanova, A., and C.C. Hoogenraad. 2005. Microtubule plus-end-tracking proteins: mechanisms and functions. *Curr Opin Cell Biol*. 17:47-54.

Akhmanova, A., and M.O. Steinmetz. 2008. Tracking the ends: a dynamic protein network controls the fate of microtubule tips. *Nature Reviews Molecular Cell Biology*. 9:309-322.

Akhmanova, A., and M.O. Steinmetz. 2010. Microtubule +TIPs at a glance. *J Cell Sci*. 123:3415-3419.

Applegate, K.T., S. Besson, A. Matov, M.H. Bagonis, K. Jaqaman, and G. Danuser. 2011. plusTipTracker: Quantitative image analysis software for the measurement of microtubule dynamics. *J Struct Biol*. 176:168-184.

Barros, T.P., K. Kinoshita, A.A. Hyman, and J.W. Raff. 2005. Aurora A activates D-TACC-Msps complexes exclusively at centrosomes to stabilize centrosomal microtubules. *J Cell Biol*. 170:1039-1046.

Bearce, E.A., B. Erdogan, and L.A. Lowery. 2015. TIPsy tour guides: how microtubule plus-end tracking proteins (+TIPs) facilitate axon guidance. *Front Cell Neurosci*. 9:241.

Bellanger, J.M., and P. Gonczy. 2003. TAC-1 and ZYG-9 form a complex that promotes microtubule assembly in C. elegans embryos. *Current biology : CB*. 13:1488-1498.

Bentley, D., and A. Toroian-Raymond. 1986. Disoriented pathfinding by pioneer neurone growth cones deprived of filopodia by cytochalasin treatment. *Nature*. 323:712-715.

Bestman, J.E., R.C. Ewald, S.L. Chiu, and H.T. Cline. 2006. In vivo single-cell electroporation for transfer of DNA and macromolecules. *Nat Protoc*. 1:1267-1272.

Blum, M., E.M. De Robertis, J.B. Wallingford, and C. Niehrs. 2015. Morpholinos: Antisense and Sensibility. *Dev Cell*. 35:145-149.

Brouhard, G.J., J.H. Stear, T.L. Noetzel, J. Al-Bassam, K. Kinoshita, S.C. Harrison, J. Howard, and A.A. Hyman. 2008. XMAP215 is a processive microtubule polymerase. *Cell*. 132:79-88.

Buck, K.B., and J.Q. Zheng. 2002. Growth cone turning induced by direct local modification of microtubule dynamics. *J Neurosci*. 22:9358-9367.

Burnette, D.T., A.W. Schaefer, L. Ji, G. Danuser, and P. Forscher. 2007. Filopodial actin bundles are not necessary for microtubule advance into the peripheral domain of Aplysia neuronal growth cones. *Nat Cell Biol*. 9:1360-1369.

Byun, J., B.T. Kim, Y.T. Kim, Z. Jiao, E.M. Hur, and F.Q. Zhou. 2012. Slit2 inactivates GSK3β to signal neurite outgrowth inhibition. *PLoS One*. 7:e51895.

Cammarata, G.M., E.A. Bearce, and L.A. Lowery. 2016. Cytoskeletal social networking in the growth cone: How +TIPs mediate microtubule-actin cross-linking to drive axon outgrowth and guidance. *Cytoskeleton (Hoboken)*. 73:461-476.

Challacombe, J.F., D.M. Snow, and P.C. Letourneau. 1996. Actin filament bundles are required for microtubule reorientation during growth cone turning to avoid an inhibitory guidance cue. *J Cell Sci*. 109 (Pt 8):2031-2040.

Challacombe, J.F., D.M. Snow, and P.C. Letourneau. 1997. Dynamic microtubule ends are required for growth cone turning to avoid an inhibitory guidance cue. *J Neurosci*. 17:3085-3095.

Chen, L., M. Chuang, T. Koorman, M. Boxem, Y. Jin, and A.D. Chisholm. 2015. Axon injury triggers EFA-6 mediated destabilization of axonal microtubules via TACC and doublecortin like kinase. *eLife*. 4.

Dent, E.W., J.L. Callaway, G. Szebenyi, P.W. Baas, and K. Kalil. 1999. Reorganization and movement of microtubules in axonal growth cones and developing interstitial branches. *J Neurosci*. 19:8894-8908.

Dent, E.W., S.L. Gupton, and F.B. Gertler. 2011. The growth cone cytoskeleton in axon outgrowth and guidance. *Cold Spring Harb Perspect Biol*. 3.

Dickson, B.J. 2002. Molecular mechanisms of axon guidance. *Science*. 298:1959-1964.

Eide, F.F., S.R. Eisenberg, and T.A. Sanders. 2000. Electroporation-mediated gene transfer in free-swimming embryonic Xenopus laevis. *FEBS Lett*. 486:29-32.

Eisen, J.S., and J.C. Smith. 2008. Controlling morpholino experiments: don't stop making antisense. *Development*. 135:1735-1743.

Erdogan, B., G.M. Cammarata, E.J. Lee, B.C. Pratt, A.F. Francl, E.L. Rutherford, and L.A. Lowery. 2017. The microtubule plus-end-tracking protein TACC3 promotes persistent axon outgrowth and mediates responses to axon guidance signals during development. *Neural Dev*. 12:3.

Erdogan, B., P.T. Ebbert, and L.A. Lowery. 2016. Using Xenopus laevis retinal and spinal neurons to study mechanisms of axon guidance in vivo and in vitro. *Semin Cell Dev Biol*. 51:64-72.

Falk, J., J. Drinjakovic, K.M. Leung, A. Dwivedy, A.G. Regan, M. Piper, and C.E. Holt. 2007. Electroporation of cDNA/Morpholinos to targeted areas of embryonic CNS in Xenopus. *BMC Dev Biol*. 7:107.

Forscher, P., and S.J. Smith. 1988. Actions of cytochalasins on the organization of actin filaments and microtubules in a neuronal growth cone. *J Cell Biol*. 107:1505-1516.

Fraser, S.E., and R.K. Hunt. 1980. Retinotectal specificity: models and experiments in search of a mapping function. *Annu Rev Neurosci*. 3:319-352.

Gard, D.L., B.E. Becker, and S. Josh Romney. 2004. MAPping the eukaryotic tree of life: structure, function, and evolution of the MAP215/Dis1 family of microtubule-associated proteins. *Int Rev Cytol*. 239:179-272.

Gard, D.L., and M.W. Kirschner. 1987. A microtubule-associated protein from Xenopus eggs that specifically promotes assembly at the plus-end. *J Cell Biol*. 105:2203-2215.

Gergely, F., C. Karlsson, I. Still, J. Cowell, J. Kilmartin, and J.W. Raff. 2000a. The TACC domain identifies a family of centrosomal proteins that can interact with microtubules. *Proceedings of the National Academy of Sciences of the United States of America*. 97:14352-14357.

Gergely, F., D. Kidd, K. Jeffers, J.G. Wakefield, and J.W. Raff. 2000b. D-TACC: a novel centrosomal protein required for normal spindle function in the early Drosophila embryo. *The EMBO journal*. 19:241-252.

Gomez, T.M., and P.C. Letourneau. 2014. Actin dynamics in growth cone motility and navigation. *J Neurochem*. 129:221-234.

Groisman, I., Y.S. Huang, R. Mendez, Q. Cao, W. Theurkauf, and J.D. Richter. 2000. CPEB, maskin, and cyclin B1 mRNA at the mitotic apparatus: implications for local translational control of cell division. *Cell*. 103:435-447.

Haas, K., K. Jensen, W.C. Sin, L. Foa, and H.T. Cline. 2002. Targeted electroporation in Xenopus tadpoles in vivo--from single cells to the entire brain. *Differentiation*. 70:148-154.

HARRISON, R.G. 1959. The outgrowth of the nerve fiber as a mode of protoplasmic movement. *J Exp Zool*. 142:5-73.

Heasman, J., M. Kofron, and C. Wylie. 2000. Beta-catenin signaling activity dissected in the early Xenopus embryo: a novel antisense approach. *Dev Biol*. 222:124-134.

Hellsten, U., R.M. Harland, M.J. Gilchrist, D. Hendrix, J. Jurka, V. Kapitonov, I. Ovcharenko, N.H. Putnam, S. Shu, L. Taher, I.L. Blitz, B. Blumberg, D.S. Dichmann, I. Dubchak, E. Amaya, J.C. Detter, R. Fletcher, D.S. Gerhard, D. Goodstein, T. Graves, I.V. Grigoriev, J. Grimwood, T. Kawashima, E. Lindquist, S.M. Lucas, P.E. Mead, T. Mitros, H. Ogino, Y. Ohta, A.V. Poliakov, N. Pollet, J. Robert, A. Salamov, A.K. Sater, J. Schmutz, A. Terry, P.D. Vize, W.C. Warren, D. Wells, A. Wills, R.K. Wilson, L.B. Zimmerman, A.M. Zorn, R. Grainger, T. Grammer, M.K. Khokha, P.M. Richardson, and D.S. Rokhsar. 2010. The genome of the Western clawed frog Xenopus tropicalis. *Science*. 328:633-636.

Henty-Ridilla, J.L., A. Rankova, J.A. Eskin, K. Kenny, and B.L. Goode. 2016. Accelerated actin filament polymerization from microtubule plus ends. *Science*. 352:1004-1009.

Hong, K., L. Hinck, M. Nishiyama, M.M. Poo, M. Tessier-Lavigne, and E. Stein. 1999. A ligand-gated association between cytoplasmic domains of UNC5 and DCC family receptors converts netrin-induced growth cone attraction to repulsion. *Cell*. 97:927-941.

Huber, A.B., A.L. Kolodkin, D.D. Ginty, and J.F. Cloutier. 2003. Signaling at the growth cone: ligand-receptor complexes and the control of axon growth and guidance. *Annu Rev Neurosci*. 26:509-563.

Hubner, N.C., A.W. Bird, J. Cox, B. Splettstoesser, P. Bandilla, I. Poser, A. Hyman, and M. Mann. 2010. Quantitative proteomics combined with BAC TransgeneOmics reveals in vivo protein interactions. *J Cell Biol*. 189:739-754.

Hur, E.M., Saijilafu, B.D. Lee, S.J. Kim, W.L. Xu, and F.Q. Zhou. 2011. GSK3 controls axon growth via CLASP-mediated regulation of growth cone microtubules. *Genes Dev*. 25:1968-1981.

Iimori, M., K. Ozaki, Y. Chikashige, T. Habu, Y. Hiraoka, T. Maki, I. Hayashi, C. Obuse, and T. Matsumoto. 2012. A mutation of the fission yeast EB1 overcomes negative regulation by phosphorylation and stabilizes microtubules. *Exp Cell Res*. 318:262-275.

Kerstein, P.C., R.H. Nichol, and T.M. Gomez. 2015. Mechanochemical regulation of growth cone motility. *Front Cell Neurosci*. 9:244.

Kim, Y.T., E.M. Hur, W.D. Snider, and F.Q. Zhou. 2011. Role of GSK3 Signaling in Neuronal Morphogenesis. *Front Mol Neurosci*. 4:48.

Kinoshita, K., B. Habermann, and A.A. Hyman. 2002. XMAP215: a key component of the dynamic microtubule cytoskeleton. *Trends Cell Biol*. 12:267-273.

Kinoshita, K., T.L. Noetzel, L. Pelletier, K. Mechtler, D.N. Drechsel, A. Schwager, M. Lee, J.W. Raff, and A.A. Hyman. 2005. Aurora A phosphorylation of TACC3/maskin is required for centrosome-dependent microtubule assembly in mitosis. *The Journal of cell biology*. 170:1047-1055.

Kleele, T., P. Marinković, P.R. Williams, S. Stern, E.E. Weigand, P. Engerer, R. Naumann, J. Hartmann, R.M. Karl, F. Bradke, D. Bishop, J. Herms, A. Konnerth, M. Kerschensteiner, L. Godinho, and T. Misgeld. 2014. An assay to image neuronal microtubule dynamics in mice. *Nat Commun*. 5:4827.

Knöll, B., C. Weinl, A. Nordheim, and F. Bonhoeffer. 2007. Stripe assay to examine axonal guidance and cell migration. *Nat Protoc*. 2:1216-1224.

Koester, M.P., O. Müller, and G.E. Pollerberg. 2007. Adenomatous polyposis coli is differentially distributed in growth cones and modulates their steering. *J Neurosci*. 27:12590-12600.

Kolodkin, A.L., and M. Tessier-Lavigne. 2011. Mechanisms and molecules of neuronal wiring: a primer. *Cold Spring Harb Perspect Biol*. 3.

Kumar, P., M.S. Chimenti, H. Pemble, A. Schönichen, O. Thompson, M.P. Jacobson, and T. Wittmann. 2012. Multisite phosphorylation disrupts arginine-glutamate salt bridge networks required for binding of cytoplasmic linker-associated protein 2 (CLASP2) to end-binding protein 1 (EB1). *J Biol Chem*. 287:17050-17064.

Kumar, P., K.S. Lyle, S. Gierke, A. Matov, G. Danuser, and T. Wittmann. 2009. GSK3beta phosphorylation modulates CLASP-microtubule association and lamella microtubule attachment. *J Cell Biol*. 184:895-908.

Le Bot, N., M.C. Tsai, R.K. Andrews, and J. Ahringer. 2003. TAC-1, a regulator of microtubule length in the C. elegans embryo. *Current biology : CB*. 13:1499-1505.

Lee, H., U. Engel, J. Rusch, S. Scherrer, K. Sheard, and D. Van Vactor. 2004. The microtubule plus end tracking protein orbit/MAST/CLASP acts downstream of the tyrosine kinase Abl in mediating axon guidance. *Neuron*. 42:913-926.

Lee, M.J., F. Gergely, K. Jeffers, S.Y. Peak-Chew, and J.W. Raff. 2001. Msps/XMAP215 interacts with the centrosomal protein D-TACC to regulate microtubule behaviour. *Nature cell biology*. 3:643-649.

Lin, C.H., E.M. Espreafico, M.S. Mooseker, and P. Forscher. 1996. Myosin drives retrograde F-actin flow in neuronal growth cones. *Neuron*. 16:769-782.

Long, J.B., M. Bagonis, L.A. Lowery, H. Lee, G. Danuser, and D. Van Vactor. 2013. Multiparametric analysis of CLASP-interacting protein functions during interphase microtubule dynamics. *Mol Cell Biol*. 33:1528-1545.

Lowery, L.A., A.E. Faris, A. Stout, and D. Van Vactor. 2012. Neural Explant Cultures from Xenopus laevis. *J Vis Exp*:e4232.

Lowery, L.A., H. Lee, C. Lu, R. Murphy, R.A. Obar, B. Zhai, M. Schedl, D. Van Vactor, and Y. Zhan. 2010. Parallel genetic and proteomic screens identify Msps as a CLASP-Abl pathway interactor in Drosophila. *Genetics*. 185:1311-1325.

Lowery, L.A., A. Stout, A.E. Faris, L. Ding, M.A. Baird, M.W. Davidson, G. Danuser, and D. Van Vactor. 2013. Growth cone-specific functions of XMAP215 in restricting microtubule dynamics and promoting axonal outgrowth. *Neural Dev*. 8:22.

Lowery, L.A., and D. Van Vactor. 2009. The trip of the tip: understanding the growth cone machinery. *Nat Rev Mol Cell Biol*. 10:332-343.

Lucaj, C.M., M.F. Evans, B.U. Nwagbara, P.T. Ebbert, C.C. Baker, J.G. Volk, A.F. Francl, S.P. Ruvolo, and L.A. Lowery. 2015. Xenopus TACC1 is a microtubule plus-end tracking protein that can regulate microtubule dynamics during embryonic development. *Cytoskeleton (Hoboken)*. 72:225-234.

Marsh, L., and P.C. Letourneau. 1984. Growth of neurites without filopodial or lamellipodial activity in the presence of cytochalasin B. *J Cell Biol*. 99:2041-2047.

Marx, A., W.J. Godinez, V. Tsimashchuk, P. Bankhead, K. Rohr, and U. Engel. 2013. Xenopus cytoplasmic linker-associated protein 1 (XCLASP1) promotes axon elongation and advance of pioneer microtubules. *Molecular biology of the cell*. 24:1544-1558.

Maurer, S.P., F.J. Fourniol, G. Bohner, C.A. Moores, and T. Surrey. 2012. EBs recognize a nucleotide-dependent structural cap at growing microtubule ends. *Cell*. 149:371-382.

Medeiros, N.A., D.T. Burnette, and P. Forscher. 2006. Myosin II functions in actin-bundle turnover in neuronal growth cones. *Nat Cell Biol*. 8:215-226.
Mimori-Kiyosue, Y., I. Grigoriev, G. Lansbergen, H. Sasaki, C. Matsui, F. Severin, N. Galjart, F. Grosveld, I. Vorobjev, S. Tsukita, and A. Akhmanova. 2005. CLASP1 and CLASP2 bind to EB1 and regulate microtubule plus-end dynamics at the cell cortex. *J Cell Biol*. 168:141-153.
Ming, G.L., H.J. Song, B. Berninger, C.E. Holt, M. Tessier-Lavigne, and M.M. Poo. 1997. cAMP-dependent growth cone guidance by netrin-1. *Neuron*. 19:1225-1235.
Ming, G.L., S.T. Wong, J. Henley, X.B. Yuan, H.J. Song, N.C. Spitzer, and M.M. Poo. 2002. Adaptation in the chemotactic guidance of nerve growth cones. *Nature*. 417:411-418.
Mitchison, T., and M. Kirschner. 1984. Dynamic instability of microtubule growth. *Nature*. 312:237-242.
Mitchison, T., and M. Kirschner. 1988. Cytoskeletal dynamics and nerve growth. *Neuron*. 1:761-772.
Moody, S.A. 1987a. Fates of the blastomeres of the 16-cell stage Xenopus embryo. *Dev Biol*. 119:560-578.
Moody, S.A. 1987b. Fates of the blastomeres of the 32-cell-stage Xenopus embryo. *Dev Biol*. 122:300-319.
Mortuza, G.B., T. Cavazza, M.F. Garcia-Mayoral, D. Hermida, I. Peset, J.G. Pedrero, N. Merino, F.J. Blanco, J. Lyngso, M. Bruix, J.S. Pedersen, I. Vernos, and G. Montoya. 2014. XTACC3-XMAP215 association reveals an asymmetric interaction promoting microtubule elongation. *Nat Commun*. 5:5072.
Myers, J.P., E. Robles, A. Ducharme-Smith, and T.M. Gomez. 2012. Focal adhesion kinase modulates Cdc42 activity downstream of positive and negative axon guidance cues. *J Cell Sci*. 125:2918-2929.
Myers, J.P., M. Santiago-Medina, and T.M. Gomez. 2011. Regulation of axonal outgrowth and pathfinding by integrin-ECM interactions. *Dev Neurobiol*. 71:901-923.
Nwagbara, B.U., A.E. Faris, E.A. Bearce, B. Erdogan, P.T. Ebbert, M.F. Evans, E.L. Rutherford, T.B. Enzenbacher, and L.A. Lowery. 2014. TACC3 is a microtubule plus end-tracking protein that promotes axon elongation and also regulates microtubule plus end dynamics in multiple embryonic cell types. *Molecular biology of the cell*. 25:3350-3362.
O'Brien, L.L., A.J. Albee, L. Liu, W. Tao, P. Dobrzyn, S.B. Lizarraga, and C. Wiese. 2005. The Xenopus TACC homologue, maskin, functions in mitotic spindle assembly. *Molecular biology of the cell*. 16:2836-2847.
Peset, I., J. Seiler, T. Sardon, L.A. Bejarano, S. Rybina, and I. Vernos. 2005. Function and regulation of Maskin, a TACC family protein, in microtubule growth during mitosis. *The Journal of cell biology*. 170:1057-1066.
Peset, I., and I. Vernos. 2008. The TACC proteins: TACC-ling microtubule dynamics and centrosome function. *Trends in cell biology*. 18:379-388.
Pierre, P., J. Scheel, J.E. Rickard, and T.E. Kreis. 1992. CLIP-170 links endocytic vesicles to microtubules. *Cell*. 70:887-900.
Piper, M., R. Anderson, A. Dwivedy, C. Weinl, F. van Horck, K.M. Leung, E. Cogill, and C. Holt. 2006. Signaling mechanisms underlying Slit2-induced collapse of Xenopus retinal growth cones. *Neuron*. 49:215-228.
Ren, Y., and D.M. Suter. 2016. Increase in Growth Cone Size Correlates with Decrease in Neurite Growth Rate. *Neural Plast*. 2016:3497901.

Robles, E., and T.M. Gomez. 2006. Focal adhesion kinase signaling at sites of integrin-mediated adhesion controls axon pathfinding. *Nat Neurosci*. 9:1274-1283.
Rutherford, E.L., L. Carandang, P.T. Ebbert, A.N. Mills, J.T. Bowers, and L.A. Lowery. 2016. Xenopus TACC2 is a microtubule plus end-tracking protein that can promote microtubule polymerization during embryonic development. *Mol Biol Cell*. 27:3013-3020.
Sabry, J.H., T.P. O'Connor, L. Evans, A. Toroian-Raymond, M. Kirschner, and D. Bentley. 1991. Microtubule behavior during guidance of pioneer neuron growth cones in situ. *J Cell Biol*. 115:381-395.
Sadek, C.M., M. Pelto-Huikko, M. Tujague, K.R. Steffensen, M. Wennerholm, and J.A. Gustafsson. 2003. TACC3 expression is tightly regulated during early differentiation. *Gene expression patterns : GEP*. 3:203-211.
Schaefer, A.W., N. Kabir, and P. Forscher. 2002. Filopodia and actin arcs guide the assembly and transport of two populations of microtubules with unique dynamic parameters in neuronal growth cones. *J Cell Biol*. 158:139-152.
Schaefer, A.W., V.T. Schoonderwoert, L. Ji, N. Mederios, G. Danuser, and P. Forscher. 2008. Coordination of actin filament and microtubule dynamics during neurite outgrowth. *Dev Cell*. 15:146-162.
Slater, P.G., G.M. Cammarata, A.G. Samuelson, A. Magee, Y. Hu, and L.A. Lowery. 2019. XMAP215 promotes microtubule-F-actin interactions to regulate growth cone microtubules during axon guidance in. *J Cell Sci*. 132.
Slater, P.G., L. Hayrapetian, and L.A. Lowery. 2017. Xenopus laevis as a model system to study cytoskeletal dynamics during axon pathfinding. *Genesis*.
Song, H., G. Ming, Z. He, M. Lehmann, L. McKerracher, M. Tessier-Lavigne, and M. Poo. 1998. Conversion of neuronal growth cone responses from repulsion to attraction by cyclic nucleotides. *Science*. 281:1515-1518.
Song, H.J., G.L. Ming, and M.M. Poo. 1997. cAMP-induced switching in turning direction of nerve growth cones. *Nature*. 388:275-279.
SPERRY, R.W. 1963. CHEMOAFFINITY IN THE ORDERLY GROWTH OF NERVE FIBER PATTERNS AND CONNECTIONS. *Proc Natl Acad Sci U S A*. 50:703-710.
Srayko, M., S. Quintin, A. Schwager, and A.A. Hyman. 2003. Caenorhabditis elegans TAC-1 and ZYG-9 form a complex that is essential for long astral and spindle microtubules. *Current biology : CB*. 13:1506-1511.
Stehbens, S., and T. Wittmann. 2012. Targeting and transport: How microtubules control focal adhesion dynamics. *Journal of Cell Biology*. 198:481-489.
Stehbens, S.J., M. Paszek, H. Pemble, A. Ettinger, S. Gierke, and T. Wittmann. 2014. CLASPs link focal-adhesion-associated microtubule capture to localized exocytosis and adhesion site turnover. *Nat Cell Biol*. 16:561-573.
Stein, E., and M. Tessier-Lavigne. 2001. Hierarchical organization of guidance receptors: Silencing of netrin attraction by slit through a Robo/DCC receptor complex. *Science*. 291:1928-1938.
Stepanova, T., J. Slemmer, C.C. Hoogenraad, G. Lansbergen, B. Dortland, C.I. De Zeeuw, F. Grosveld, G. van Cappellen, A. Akhmanova, and N. Galjart. 2003. Visualization of microtubule growth in cultured neurons via the use of EB3-GFP (end-binding protein 3-green fluorescent protein). *J Neurosci*. 23:2655-2664.

Stout, A., S. D'Amico, T. Enzenbacher, P. Ebbert, and L.A. Lowery. 2014. Using plusTipTracker software to measure microtubule dynamics in Xenopus laevis growth cones. *J Vis Exp*:e52138.

Suter, D.M., and P. Forscher. 1998. An emerging link between cytoskeletal dynamics and cell adhesion molecules in growth cone guidance. *Curr Opin Neurobiol*. 8:106-116.

Suter, D.M., and P. Forscher. 2000. Substrate-cytoskeletal coupling as a mechanism for the regulation of growth cone motility and guidance. *J Neurobiol*. 44:97-113.

Tanaka, E., T. Ho, and M.W. Kirschner. 1995. The role of microtubule dynamics in growth cone motility and axonal growth. *The Journal of cell biology*. 128:139-155.

Tanaka, E., and M.W. Kirschner. 1995. The Role of Microtubules in Growth Cone Turning at Substrate Boundaries. *J Cell Biol*. 128:127-137.

Tanaka, E.M., and M.W. Kirschner. 1991. Microtubule behavior in the growth cones of living neurons during axon elongation. *J Cell Biol*. 115:345-363.

Tessmar, K., F. Loosli, and J. Wittbrodt. 2002. A screen for co-factors of Six3. *Mechanisms of development*. 117:103-113.

Thakur, H.C., M. Singh, L. Nagel-Steger, J. Kremer, D. Prumbaum, E.K. Fansa, H. Ezzahoini, K. Nouri, L. Gremer, A. Abts, L. Schmitt, S. Raunser, M.R. Ahmadian, and R.P. Piekorz. 2014. The centrosomal adaptor TACC3 and the microtubule polymerase chTOG interact via defined C-terminal subdomains in an Aurora-A kinase-independent manner. *J Biol Chem*. 289:74-88.

Tojima, T., J.H. Hines, J.R. Henley, and H. Kamiguchi. 2011. Second messengers and membrane trafficking direct and organize growth cone steering. *Nat Rev Neurosci*. 12:191-203.

Valetti, C., D.M. Wetzel, M. Schrader, M.J. Hasbani, S.R. Gill, T.E. Kreis, and T.A. Schroer. 1999. Role of dynactin in endocytic traffic: effects of dynamitin overexpression and colocalization with CLIP-170. *Mol Biol Cell*. 10:4107-4120.

van der Vaart, B., M.A. Franker, M. Kuijpers, S. Hua, B.P. Bouchet, K. Jiang, I. Grigoriev, C.C. Hoogenraad, and A. Akhmanova. 2012. Microtubule plus-end tracking proteins SLAIN1/2 and ch-TOG promote axonal development. *The Journal of neuroscience : the official journal of the Society for Neuroscience*. 32:14722-14728.

Watanabe, T., J. Noritake, M. Kakeno, T. Matsui, T. Harada, S. Wang, N. Itoh, K. Sato, K. Matsuzawa, A. Iwamatsu, N. Galjart, and K. Kaibuchi. 2009. Phosphorylation of CLASP2 by GSK-3beta regulates its interaction with IQGAP1, EB1 and microtubules. *J Cell Sci*. 122:2969-2979.

Watson, P., and D.J. Stephens. 2006. Microtubule plus-end loading of p150(Glued) is mediated by EB1 and CLIP-170 but is not required for intracellular membrane traffic in mammalian cells. *J Cell Sci*. 119:2758-2767.

Wen, Y., C.H. Eng, J. Schmoranzer, N. Cabrera-Poch, E.J. Morris, M. Chen, B.J. Wallar, A.S. Alberts, and G.G. Gundersen. 2004. EB1 and APC bind to mDia to stabilize microtubules downstream of Rho and promote cell migration. *Nat Cell Biol*. 6:820-830.

Widlund, P.O., J.H. Stear, A. Pozniakovsky, M. Zanic, S. Reber, G.J. Brouhard, A.A. Hyman, and J. Howard. 2011. XMAP215 polymerase activity is built by combining multiple tubulin-binding TOG domains and a basic lattice-binding region. *Proceedings of the National Academy of Sciences of the United States of America*. 108:2741-2746.

Williamson, T., P.R. GordonWeeks, M. Schachner, and J. Taylor. 1996. Microtubule reorganization is obligatory for growth cone turning. *P Natl Acad Sci USA*. 93:15221-15226.

Wittmann, T., and C.M. Waterman-Storer. 2005. Spatial regulation of CLASP affinity for microtubules by Rac1 and GSK3beta in migrating epithelial cells. *J Cell Biol*. 169:929-939.

Wu, X., Q.T. Shen, D.S. Oristian, C.P. Lu, Q. Zheng, H.W. Wang, and E. Fuchs. 2011. Skin stem cells orchestrate directional migration by regulating microtubule-ACF7 connections through GSK3β. *Cell*. 144:341-352.

Wurdak, H., S. Zhu, K.H. Min, L. Aimone, L.L. Lairson, J. Watson, G. Chopiuk, J. Demas, B. Charette, R. Halder, E. Weerapana, B.F. Cravatt, H.T. Cline, E.C. Peters, J. Zhang, J.R. Walker, C. Wu, J. Chang, T. Tuntland, C.Y. Cho, and P.G. Schultz. 2010. A small molecule accelerates neuronal differentiation in the adult rat. *Proc Natl Acad Sci U S A*. 107:16542-16547.

Xie, Z., L.Y. Moy, K. Sanada, Y. Zhou, J.J. Buchman, and L.H. Tsai. 2007. Cep120 and TACCs control interkinetic nuclear migration and the neural progenitor pool. *Neuron*. 56:79-93.

Yang, Y.T., C.L. Wang, and L. Van Aelst. 2012. DOCK7 interacts with TACC3 to regulate interkinetic nuclear migration and cortical neurogenesis. *Nature neuroscience*. 15:1201-1210.

Zhang, Y., Y. Luo, R. Lyu, J. Chen, R. Liu, D. Li, M. Liu, and J. Zhou. 2016. Proto-Oncogenic Src Phosphorylates EB1 to Regulate the Microtubule-Focal Adhesion Crosstalk and Stimulate Cell Migration. *Theranostics*. 6:2129-2140.

Zheng, J.Q., J.J. Wan, and M.M. Poo. 1996. Essential role of filopodia in chemotropic turning of nerve growth cone induced by a glutamate gradient. *J Neurosci*. 16:1140-1149.

Zhou, F.Q., C.M. Waterman-Storer, and C.S. Cohan. 2002. Focal loss of actin bundles causes microtubule redistribution and growth cone turning. *J Cell Biol*. 157:839-849.

Zhou, F.Q., J. Zhou, S. Dedhar, Y.H. Wu, and W.D. Snider. 2004. NGF-induced axon growth is mediated by localized inactivation of GSK-3beta and functions of the microtubule plus end binding protein APC. *Neuron*. 42:897-912.

Zicha, D., I.M. Dobbie, M.R. Holt, J. Monypenny, D.Y. Soong, C. Gray, and G.A. Dunn. 2003. Rapid actin transport during cell protrusion. *Science*. 300:142-145.

Zumbrunn, J., K. Kinoshita, A.A. Hyman, and I.S. Näthke. 2001. Binding of the adenomatous polyposis coli protein to microtubules increases microtubule stability and is regulated by GSK3 beta phosphorylation. *Curr Biol*. 11:44-49.